A modelling approach to carbon, water and energy feedbacks and interactions across the land-atmosphere interface.

Timothy C. Hill[1,2]

Doctor of Philosophy
University of Edinburgh
May 2007

[1]School of GeoSciences and NERC Centre for Terrestrial Carbon Dynamics, Crew Building, University of Edinburgh, EH9 3JN, UK
[2]NERC Centre for Terrestrial Carbon Dynamics, UK

Declaration

I declare that this thesis has been composed by myself and has not been submitted in any previous application for a degree. The work described is my own except where stated otherwise.

Timothy Hill

May 2007

Abstract

The climate is changing and the rate of this change is expected to increase. In the 20th century global surface temperatures rose by 0.6 (±0.2) K. Based on current model predictions, and economic forecasts, global temperature increases of 1.4 to 5.8 K are expected over the period 1990 – 2100. One of the main drivers for this temperature increase is the build up of CO_2 in the atmosphere which has been increasing since pre-industrial times. Pre-industrial concentrations of CO_2 were bounded between 180 ppm and 300 ppm, however the current concentrations of 380 ppm are far in excess of these bounds. Further more, forecasts indicates that a further doubling in the next century is a distinct possibility.

However making predictions about the future climate is difficult. Predicting the trajectory that the climate will take uses assumptions of economic growth, technological advances and ecological and physical processes. If we are to make informed decisions regarding the future of the planet, we have to account not only for future anthropogenic emissions and land use, but we also have to identify the response of the Earth system.

By its very nature the Earth is immensely complex; processes, interactions and feedbacks exist which operate on vastly different spatial and temporal scales. Each of these processes has an associated level of uncertainty. This uncertainty propagates through models and the processes and feedbacks they simulate. One of our jobs as environmental scientists is to quantify and then reduce these uncertainties. Consequently it is critical to quantify the interactions of the land-surface and the atmosphere.

The role of the land-surface is critical to the response of the Earth's climate. All general circulation models and regional scale models need representations of the land-surface. A lot of the work concerning the land-surface aims to determine the land-surface partitioning of energy, the evapotranspiration of water and if the land-surface is a sink or a source of CO_2. To do achieve this we need to understand (1) the underlying processes governing the response of the land-surface, (2) the response of these processes to perturbations from climate change and humans, (3) the temporal and spatial heterogeneity in these processes, and (4) the feedbacks that land-surface processes have with the climate.

In this thesis I use a coupled atmosphere-biosphere model to show current understanding of the carbon, water and energy dynamics of the biosphere and the atmosphere to be consistent with both PBL and stand-based measurements. I then use the CAB model to investigate the strength of different feedbacks between the atmosphere and biosphere. Finally the model is then used in a Monte Carlo Bayesian inversion scheme to invert atmospheric measurements to infer information about surface parameters.

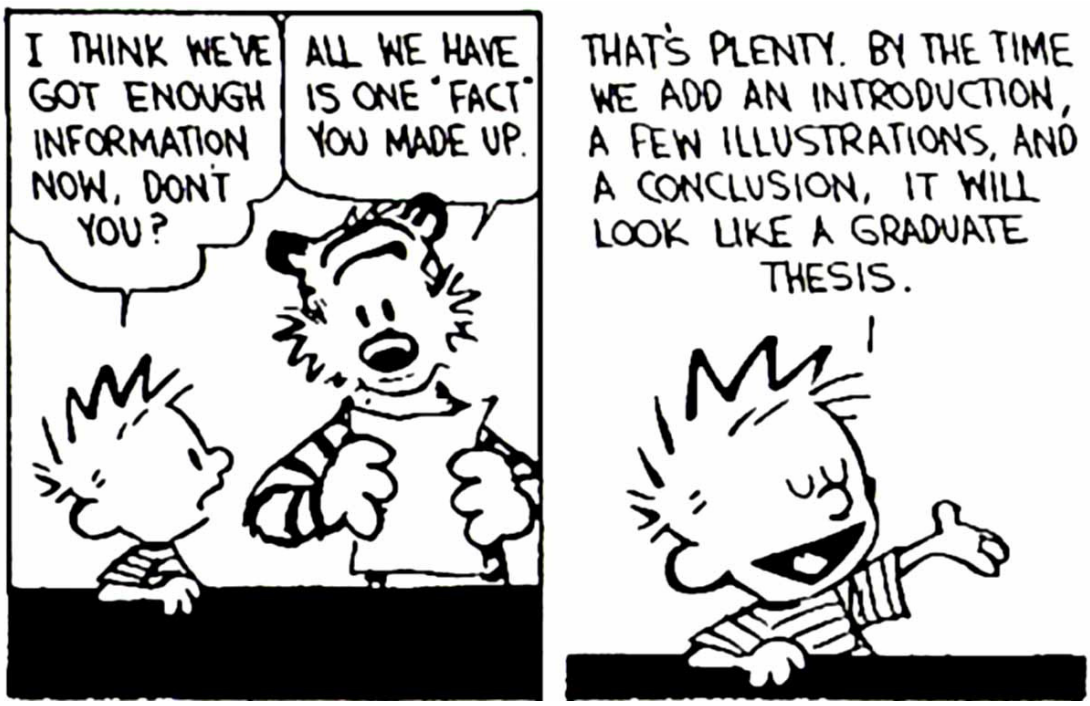

Acknowledgements

I would like to thank my supervisors Dr. Mat Williams, Prof. John Moncrieff and Prof. Ian Woodward for their help and support during my studies. I would also like to extend my thanks to family and friends for general support and encouragement, and in particular to Casey Ryan and Paul Parrish for proof reading.

Glossary

A/R	-	Accept/reject (criterion)
ACM	-	(the) Aggregated Canopy Model
AVHRR	-	(the) Advanced Very High Resolution Radiometer
BOREAS	-	(the) BOReal Ecosystem-Atmosphere Study
C	-	Carbon
CAB	-	(the) Coupled Atmosphere Biosphere (model)
Cf	-	Carbon in foliage (DALEC parameter)
C_{GPP}	-	Gross Primary Productivity (from the bayesian conceptual model)
Clit	-	Carbon in fresh foliar and fine root litter (DALEC parameter)
C_{NEE}	-	Net Ecosystem Exchange (from the bayesian conceptual model)
CO_2	-	Carbon dioxide
Cr	-	Carbon in fine roots (DALEC parameter)
Csom	-	Soil Organic Matter (DALEC parameter)
Cw	-	Carbon in wood (stems and coarse roots) (DALEC parameter)
DALEC	-	(the) Data Assimilation Linked ECosystem (model)
DGVM	-	Dynamic Global Vegetation Model
DoY	-	Day of Year
ECMWF	-	(the) European Centre for Medium-Range Weather Forecasts (' model)
EMIC	-	Earth-system Models of Intermediate Complexity
EPICA	-	European Project for Ice Coring in Antarctica
FACE	-	Free Atmosphere CO2 Enrichment
FIFE	-	(the) First ISLSCP Field Experiment
FN	-	Total Foliar Nitrogen
GCM	-	General Circulation Model
GPP	-	Gross Primary Productivity

HadCM3	-	(the) Hadley Centre Coupled Model, version 3 (model)
HAPEX	-	(the) Hydrologic Atmospheric Experiment for the Study of Water-Budget and Evaporation Flux at the Climatic Scale
ι	-	A water use efficiency parameter
i	-	Indices of model parameters
IBIS	-	(the) Integrated Biosphere Simulator (model)
IPCC	-	(the) Intergovernmental Panel on Climate Change
IRGA	-	Infra-Red Gas Analyser
ISLSCP	-	International Satellite Land Surface Climatology Project
j	-	*j*-th model step
Jmax	-	Maximal electron transport rate
L	-	Leaf area index (from the bayesian conceptual model)
L(m)	-	Likelihood estimator
LAI	-	Leaf Area Index
LAI_H	-	Hydraulically significant aspects of LAI
LAI_R	-	Radiatively significant aspects of LAI
LBA	-	(the) Large-Scale Biosphere-Atmosphere Experiment in Amazonia
LE	-	Latent Energy
LES	-	Large Eddy Simulations
LPJ	-	(the) Lund-Potsdam-Jena (model)
MAD	-	Mean Absolute Deviation
m^j	-	Model prediction for (*j*-th) model step
MM5	-	(the) PSU/NCAR's mesoscale model
MODIS	-	(the) MOderate Resolution Imaging Spectrometer
MOSES/MOSES2	-	(the) Met Office Surface Exchange Scheme
n	-	Number of parameters
N	-	Foliar nitrogen (from the bayesian conceptual model)
n	-	Frequency of occurance
NCAR	-	(the) National Center for Atmospheric Research
NDVI	-	Normalized Difference Vegetation Index
NEE+A57	-	Net Ecosystem Exchange
NIR	-	Near Infra-Red

NSA	-	Northern Study Area
NSA-OBS	-	Northern Study Area Old Black Spruce
NSA-OJP	-	Northern Study Area Old Jack Pine
obs	-	Observations
OCO	-	(the) Orbiting Carbon Observatory
OSU1DPBL	-	(the) Oregon State University One-Dimensional Planetary Boundary Layer (model)
P_{accept}	-	Probability of acceptance
PAR	-	Photosynthetically Active Radiation
PBL	-	Planetary Boundary Layer
P_i	-	Log-normalised parameter '*i*'
$\underline{P}_i$	-	Parameter value '*i*'
$\underline{P}_{i,0}$	-	*a prior* parameter value '*i*'
PSU	-	(the) Pennsylvania State University
Q_{10}	-	An exponential-temperature dependence
R	-	Respiration (from the bayesian conceptual model)
R^2	-	R-squared
RAD_{SW}	-	Shortwave radiation
RMSE	-	Root Mean Square Error
S	-	Function of m and obs
s^2	-	Variance of measurements
SDGVM	-	(the) Sheffield Dynamic Global Vegetation Model
SiB/SiB2	-	(the) Simple Biosphere model
SPA	-	(the) Soil-Plant-Atmosphere (model)
SRES	-	Special Report on Emissions Senarios
SSA	-	Southern Study Area
SSA-OBS	-	Southern Study Area Old Black Spruce
SVAT	-	Soil Vegetation Atmosphere Transport (model)
t1	-	Litter decomposition rate constant (DALEC parameter)
t2	-	Autotrophic repsiration (DALEC parameter)
t3	-	Fraction of net primary production allocated to foliage (DALEC parameter)
t4	-	Fraction of net primary production allocated

		to fine roots (DALEC parameter)
t5	-	Turnover rate of foliage (DALEC parameter)
t6	-	Turnover rate of woody matter (DALEC parameter)
t7	-	Turnover rate of fine roots (DALEC parameter)
t8	-	Mineralization rate of fresh litter (DALEC parameter)
t9	-	Mineralization rate of soil organic matter and woody debris (DALEC parameter)
TEM	-	Terrestrial Ecosystem Model
Tresponse	-	Heterotrophic temperature response function
u	-	Component of the horizontal wind
UTC	-	Coordinated Universal Time
v	-	Component of the horizontal wind
Vcmax	-	Maximal velocity of carboxylation
VPD	-	vapour pressure deficit
Zo	-	Roughness length
λE	-	Latent energy (from the bayesian conceptual model)

Contents

Thesis introduction

1 Background

It is now widely accepted that the climate is changing. According to the previous (2001) IPCC report, global surface temperatures rose by 0.6 K (±0.2) during the 20th century (Figure 1a) [*Jones and Moberg*, 2003]. The current rate of global mean sea-land temperature increase is the greatest seen in the last millennia (Figure 1b) [*Mann, et al.*, 1999]. However this rate of temperature increase is not constant and is expected to accelerate throughout the next century. The magnitude of this acceleration is relatively uncertain, with model predictions suggesting global temperature increases of 1.4 to 5.8 K over the period 1990 – 2100 (Figure 2) [*Houghton*, 2001].

The Vostok and EPICA Dome C ice cores show a strong correlation between atmospheric CO_2 concentrations and inferred air temperature over the last 740 kyrs [*Augustin, et al.*, 2004; *Petit, et al.*, 1999] (Figure 3). CO_2 concentrations can be measured directly from the gas bubbles trapped in the ice, whilst temperature records are inferred from the Antarctic temperature proxy (deuterium/hydrogen ratio and the $\delta^{18}O$ of oxygen). From these records we can see that over the past 740 kyr, CO_2 concentrations were bounded between 180 ppm and 300 ppm. Current CO_2 concentrations are far in excess of the past range from the ice cores and the global mean atmospheric CO_2 measured at Mauna Loa, Hawai'i, is currently 380 ppm.

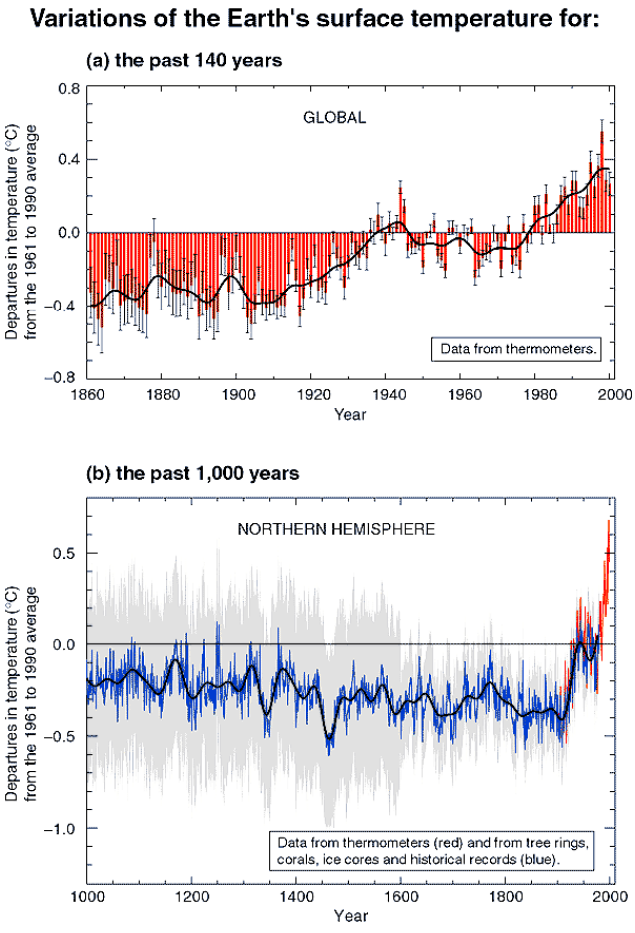

Figure 1: Global surface temperature anomalies over the last 140 years and millennium, source: [*Jones and Moberg*, 2003; *Mann, et al.*, 1999].

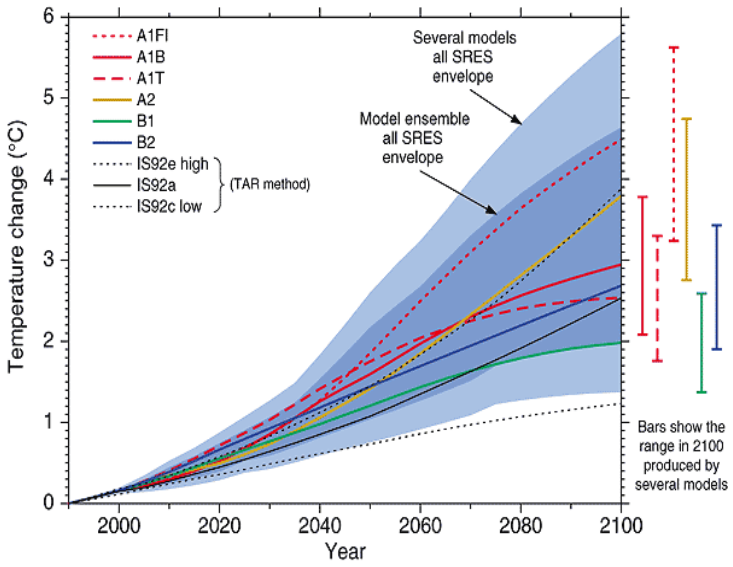

Figure 2: Model uncertainty and Special Report on Emissions Senarios (SRES) uncertainty, source: [*Houghton*, 2001].

The primary driver of recent surface temperature increase is the atmospheric concentration of CO_2. Increased CO_2 levels result in a greater proportion of the energy incident on the Earth being retained by the Earth and its atmosphere. This pushes the Earth further out of thermodynamic equilibrium, resulting in heating of the Earth. The concept of global warming is not a new one, in the 1820's Joseph Fourier calculated that gases in the atmosphere could trap energy from the Sun. However it was not until the late 19th century that the effect of CO_2 on the surface temperature of the Earth was calculated empirically. Svante Arrhenius (in his paper titled *"On the Influence of Carbonic Acid in the Air upon the Temperature of the Ground"*) calculated that doubling the concentration of CO_2 (which Arrhenius referred to as Carbonic Acid) would force the mean surface temperature to rise by 5 K [*Arrhenius*, 1896]. This is recognised as the first scientific work to predict that anthropogenic emissions of CO_2 could result in a warming of the Earth. However Arrhenius predicted that this increase would take over ~1000 years; whilst it is now expected that a doubling of CO_2 will take ~100 years (depending on future emissions scenarios).

It was not until 1960 when Charles Keeling produced data from the Mauna Loa Observatory showing CO_2 levels to be steadily rising (Figure 4) [*Keeling*, 1960] that people took the prospect of global warming seriously. Since measurements commenced at the Mauna Loa observatory in the 1950's, CO_2 levels have been rising steadily at ~1.5ppm/yr [*Keeling, et al.*, 1976]. 2005 concentrations of CO_2 were at 380 ppmv, and it is a distinct possibility that the concentration at the end of the century will be twice the levels of the year 2000.

In the 2001 IPCC report stated that *"There is new and stronger evidence that most of the warming over the last 50 years is attributable to human activities"*. In the most recent (2007)

IPCC report this statement was strengthened to state *"Most of the observed increase in globally averaged temperatures since the mid-20th century is very likely due to the observed increase in anthropogenic greenhouse gas concentrations"* [Alley, et al., 2007]. However whilst collective human activities are responsible for global warming, this responsibility is not equally distributed among countries or individuals. Furthermore, while the impacts of climate change are not uniformly bad, the expected increases may be more severe, with damaging consequences for much of the World. Unfortunately, it is likely that a correlation exists between the wealth of the region and the impact that climate change is expected to have. Wealthier countries, and individuals, have the resources to mitigate some of the impacts of global warming, an option that will not always be possible for poorer regions and individuals. Those that cannot adapt still suffer the effects of climate change, and so they have the potential to be the hardest hit.

Due to the nature of the Earth-Atmosphere system, with its tightly coupled feedbacks and interactions with humanity, it is exceptionally hard to quantify the effects and causes of climate change. Changes in the climate are complex and can have many subsequent impacts on the Earth, mainly through changing weather patterns, which impact everything from the timing of budburst and plant productivity to extremes in weather and sea level. However there is an environmental and moral obligation to try and improve our knowledge about the causes of climate change and the climate system in general. Improving our knowledge and reducing this uncertainty is critical if policy makers and the public are to make informed decisions about

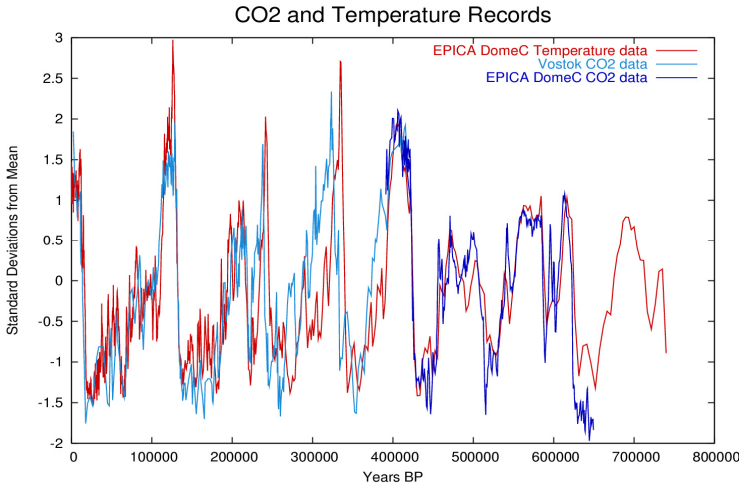

(Image reproduced courtesy of Leland McInnes).

Figure 3: Correlation between the CO_2 and temperature variations based on Antarctic ice cores.

(red) EPICA DomeC temperature data:

ftp://ftp.ncdc.noaa.gov/pub/data/paleo/icecore/antarctica/epica_domec/edc_dd.txt

(blue) EPICA DomeC CO_2 data:

ftp://ftp.ncdc.noaa.gov/pub/data/paleo/icecore/antarctica/epica_domec/edc-CO2-650k-390k.txt

(light blue) Vostok CO_2 data:

http://cdiac.ornl.gov/ftp/trends/CO2/vostok.icecore.CO2

how best to avoid, mitigate or adapt to future climate scenarios.

2 Uncertainties in understanding the climate

Predictions of the trajectory that the climate will take are based on assumptions of economic growth, technological advances and physical/biogeochemical processes. If we are to make informed decisions regarding the future of the planet, we have to account not only for future anthropogenic emissions and land use change, but we also have to quantify the response of the Earth system. By its very nature the Earth is immensely complex. Processes, interactions and feedbacks exist which operate on different spatial and temporal scales, and although we have been aware of these feedbacks since the 1970's [*Charney, et al.*, 1975], our understanding of these processes still has an appreciable level of uncertainty. The magnitude of uncertainty associated with land-atmosphere interactions is large, equating to approximately 1.5 °C over the next century [*Meir, et al.*, 2006]. This uncertainty propagates through models and the processes and feedbacks they simulate into the predictions that policy makers rely on. Our job as environmental scientists is to quantify and then reduce these uncertainties.

Attempts at quantifying climate uncertainties using models are primarily performed using general circulation models (GCMs) linked to dynamic global vegetation models (DGVMs). A range of models and measurements are used to study and test the processes that are simulated in these global models. We shall discuss this hierarchy of model/measurement scales later.

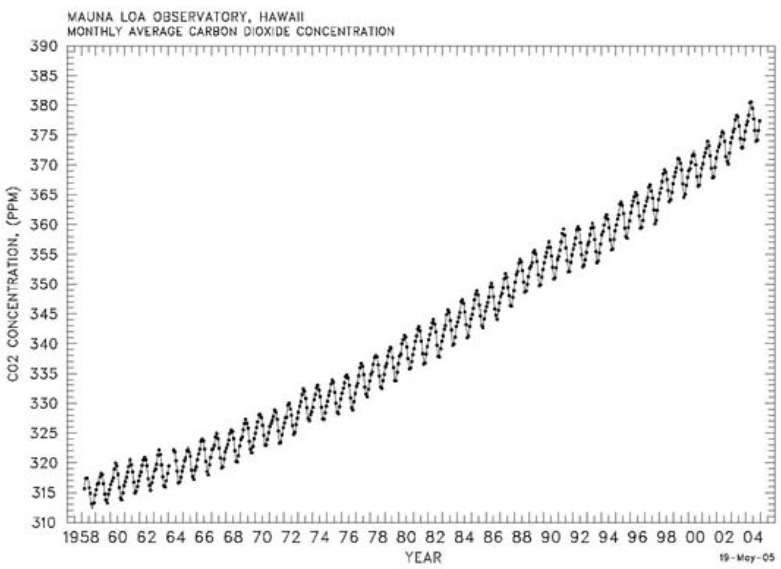

(Image reproduced from the Scripps Institution of Oceanography)

Figure 4: Mauna Loa atmospheric CO_2 concentration curve, source: [*Keeling, et al.*, 2001].

3 Land surface exchanges

The role of the land surface is a critical component in our understanding of the climate's response to

anthropogenic forcing. All GCMs and regional scale models need representations of land-atmosphere exchange. Much of the work performed aims to determine the exact nature of the land surface partitioning of energy, the evapotranspiration of water and the land surface flux of CO_2. To achieve this we need to understand (1) the underlying biogeochemical and biogeophysical processes governing the response of the land surface, (2) the response of these processes to perturbations from climate change and humans, (3) the temporal and spatial heterogeneity in these processes, and (4) land-atmosphere feedbacks.

To quantify land-atmosphere processes, both observations and modelling approaches are employed in conjunction with each other. Observations range from measurements of rates of biochemical reactions, to the characterisation of complete ecosystems (such as BOREAS) and even the whole Earth. Additionally, manipulation experiments are also possible, where systems are perturbed to investigate the impact of future climate change. Modelling is used to provide a framework for testing and corroborating our knowledge of physical processes, often in ways that cannot be physically achieved (e.g. running models into the future).

Unfortunately, our ability to make the required measurements is hampered by the complexity of the interactions at (and the spatial and temporal heterogeneity of) the land surface. We do not have enough observations to fully capture the heterogeneity of the land surface models are hampered by an incomplete knowledge of the Earth system, or they have computational limits. To tackle these problems a hierarchy of models and measurements has developed.

4 Model/Measurement hierarchy

Many approaches have been taken to the quantification of the climate system. These approaches range in scale spatial scales from focussed investigations of stomata to those that encompass the whole Earth, and across temporal scales ranging from the seconds to hundreds of thousands of years. Both measurement and modelling methods have been used to quantify the climate processes, and serious efforts are being made to combine these approaches using large collaborative projects. There is often considerable overlap between models and measurements which can be represented figuratively (Figures 5 and 6). We summarise these approaches to provide a context for the body of work contained in this thesis. However this review of models and measurements is not

meant to be exhaustive, but rather is intended to be a summary of the important model and measurement scales. Additionally it should be noted that this is not a unique synopsis, and similar summaries have been performed albeit with different perspectives [*Robinson and Ek*, 2000; *Running, et al.*, 1999; *Shuttleworth*, 1991].

5 The model hierarchy

5.1 Terrestrial ecosystem models/Soil vegetation atmosphere transport models

Terrestrial ecosystem models (TEM) and Soil vegetation atmosphere transport (SVAT) models are essentially land surface exchange schemes, incorporating the fundamentals of bioecophysiology. These are adaptable models used to simulate processes occurring on scales up to the stand level over time periods of decades, whilst also resolving responses down to a few minutes (Figure 5). There is a broad range of these TEMs, ranging in complexity from models which deal solely with the surface exchange of water and energy, to complex models which simulate the photosynthesis, growth, mortality and regeneration of vegetation within the system. The applications of these models are varied, ranging from inclusion as the land surface exchange schemes in larger atmospheric models to the diagnosis of eddy covariance observations.

Despite the diversity of the models, there are a several features that they have in common: (1) A representation of canopy/leaf elements (can be a single 'big leaf' or multiple canopy layers). (2) Soil hydrology and thermal properties. (3) Response to atmospheric conditions air temperature, humidity, radiation and precipitation. (4) Transpiration is commonly implemented by using the Penman-Monteith equation [*Jones*, 1992; *Monteith*, 1965]. The Penman-Monteith equation and other relations attempt to mechanistically estimate the rates of transpiration based (partially) on stomatal conductance [*Jarvis and Mcnaughton*, 1986; *Leuning*, 1995; *Mcnaughton and Jarvis*, 1991]. (5) These models have mechanistic predictions of photosynthetic rates [*Farquhar and Craemmerer*, 1982], however other models exist based on empirical relationships [*Dewar*, 1995]. Some of these schemes attempt to link stomatal dynamics to rates of photosynthesis [*Collatz, et al.*, 1991; *Leuning*, 1995; *Williams, et al.*, 1996].

The simplest TEM/SVAT models are often classed as 'big leaf' models, where the vegetation is approximated as a single large leaf. These approximations have been applied to modelling studies looking at the responses of even large areas, such as the

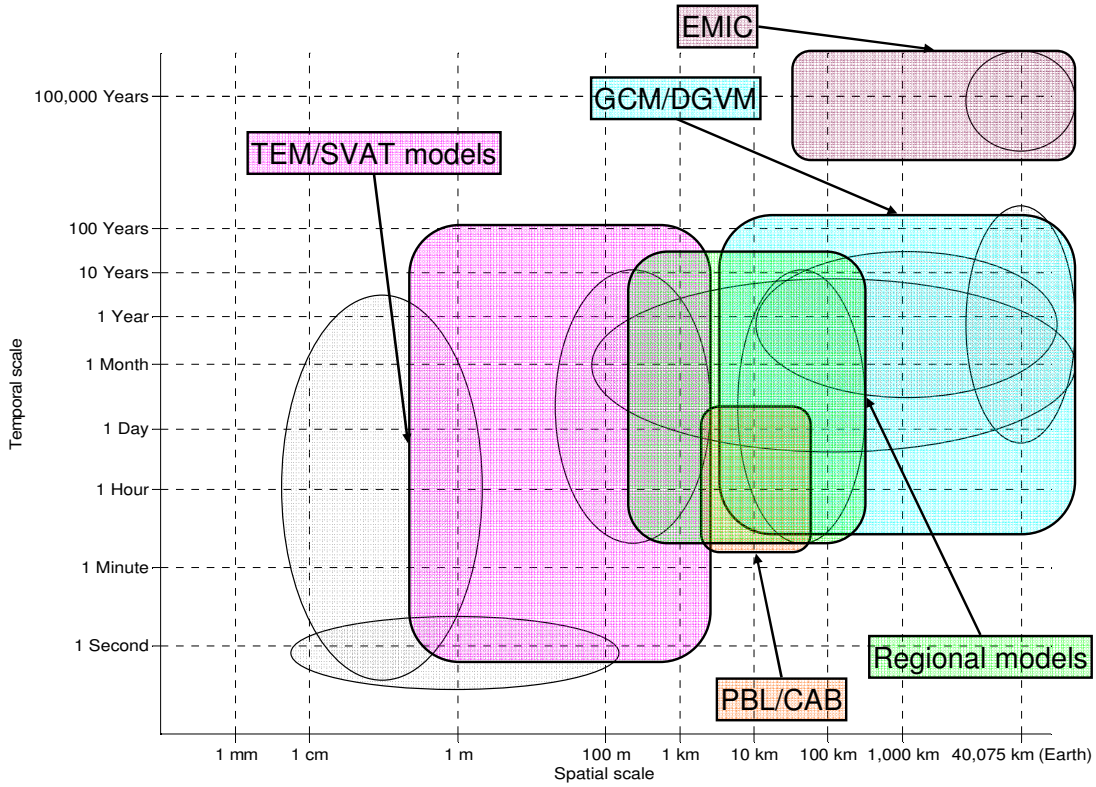

Figure 5: Hierarchy of models, from the short time/spatial scales to the long time/spatial scales: e.g. Terrestrial Ecosystem Models (TEM) and Soil Vegetation Atmosphere Transport (SVAT) models: Planetary Boundary Layer (PBL) models and the Coupled Atmosphere Biosphere (CAB) model; Regional models; General Circulation Models (GCM) and Dynamic Global Vegetation Models (DGVM); Earth-system Models of Intermediate Complexity (EMIC). The greyed out hierarchy of measurements is shown for comparison purposes (Figure 6).

Amazon [*Lloyd, et al.*, 1995]. More complex models deal with the interactions of multiple soil and canopy layers, modelling the detailed radiative and energy balance of each layer, e.g the Soil Plant Atmosphere model [*Williams, et al.*, 1996]. These high resolution schemes are intended to mesh closely with stand-based measurements and eddy covariance datasets (e.g. *Lloyd, et al.* (2001)), and allow in-depth studies into ecosystem processes.

Some schemes are specifically designed for inclusion in larger scale atmospheric models (e.g. the Simple Biosphere model (SiB/SiB2) [*Sellers, et al.*, 1996a; *Sellers, et al.*, 1986; *Sellers, et al.*, 1996b] and the Met Office Surface Exchange Scheme (MOSES/MOSES2) [*Cox, et al.*, 1999; *Richard Essery*, 2001]). The complexity of these schemes is limited by the need for computational efficiency and the requirements to reduce parameters to those that are globally available. Possible alternative to these

models exist that mimic the responses of the detailed SVATs using empirical representations e.g. the Aggregated Canopy Model (ACM) [*Williams, et al.*, 1997].

5.2 Planetary boundary layer models (PBL) [+ the Coupled Atmosphere-Biosphere (CAB) model]

The planetary boundary layer (PBL) is the lowest layer of the atmosphere, and is in constant contact with the land surface (Figure 5). As a result of this interaction with the land surface the dynamics of the PBL are closely tied to processes in the biosphere. This results in strong feedbacks which need to be captured by PBL models; turbulence in the PBL is determined (in part) by the energy partitioning of the land surface, and the properties of the PBL strongly impact the response of the vegetation at the land surface.

The processes in this region are simulated by a range of models from single column models [*Ayotte, et al.*, 1996; *Blackader*, 1976; *Cuxart, et al.*, 2006; *Garratt, et al.*, 1996; *Troen and Mahrt*, 1986] to Large Eddy Simulations (LES) [*Beare, et al.*, 2006; *Denning, et al.*, 2003]. The single column models calculate turbulence using ensemble averages, whereas the LES schemes only parameterise sub-grid turbulence (an approach that is more generally applicable though at considerably higher computational cost).

The Coupled-Atmosphere-Biosphere (CAB) model that is described, tested and implemented in this thesis is an example of a single column PBL model coupled to a SVAT model (see previous section). Consequently the CAB model inherits the various temporal and spatial scales of these two different types of models.

5.3 Regional atmospheric models

Regional models provide the intermediate scale between GCM (see next section) and smaller scale models such as LES and single column PBL models. Since the scale over which regional models operate is much reduced from the globe, these models can resolve finer scale meteorological processes than GCMs (Figure 5). These regions are approximately country sized, and regional models are often 'nested' within GCMs to obtain the boundary conditions required. Regional models (such as the Pennsylvania State University / National Center for Atmospheric Research (PSU/NCAR) numerical mesoscale model (MM5) [*Haagenson, et al.*, 1994]) generally include TEMs/SVATs of moderate complexity and simulate mesoscale atmospheric circulation.

5.4 General circulation models

GCMs simulate the dynamics of the global atmosphere (and its coupling to the ocean) by solving the fluid dynamic equations of the system (Figure 5). GCMs can be employed for two purposes; making short-term weather predictions, and making climate predictions. It is the second application that is of particular interest in this thesis, and models that are used for this purpose require additional components to model important processes e.g. evapotranspiration, sea ice and the carbon cycle. Notably GCMs include the Hadley Centre Coupled Model, version 3 (HadCM3) [*Cox, et al.*, 2000] which is coupled to the TRIFFID DGVM, and the European Centre for Medium-Range Weather Forecasts (ECMWF) model (http://www.ecmwf.int/).

5.5 Dynamic global vegetation models

DGVMs simulate the response of vegetation to species competition, climate change and other perturbations, e.g. fire and land use change (Figure 5). The models are typically complex and coupled to GCMs to allow climate predictions to be made. This coupling can be performed online (the DGVM is fully coupled to the GCM) or offline (the DGVM uses previous runs of the GCM). Several DGVMs exist such as the Top-down Representation of Interactive Foliage and Flora Including Dynamics (TRIFFID) [*Cox*, 2001], the Lund-Potsdam-Jena (LPJ) [*Sitch, et al.*, 2003], the Integrated Biosphere Simulator (IBIS) [*Foley, et al.*, 1996; *Kucharik, et al.*, 2000] and the Sheffield Dynamic Global Vegetation Model (SDGVM) [*Woodward, et al.*, 1995].

A comparison of 11 coupled global vegetation-atmosphere models found that future climate change will reduce the redundancy in the climate system (e.g. the ability of the Earth system to absorb effects of land use change) and a wide range of predicted CO_2 concentration by the year 2100 [*Friedlingstein, et al.*, 2006].

5.6 Earth system models of intermediate complexity (EMIC)

Earth system models of intermediate complexity (EMIC) bridge the gap between the extremely simple conceptual models of the atmospheric and Earth system processes and the highly complex GCMs (Figure 5). They include processes most critical on long timescales e.g. atmospheric circulation, land surface processes, ocean processes and sea ice. Due to the nature of these models they are suitable for extremely long global model runs on the order of 100,000 years [*Claussen, et al.*, 2002].

6 The measurement hierarchy

6.1 Biophysical measurements

At the site level, a range of measurements can be performed to measure the physical structure and composition of an ecosystem (Figure 6). These are important observations that need to be made before even simple processes can be described. These measurements range from the allometric and optical measurement of leaf area index (LAI) [*Gower and Norman*, 1991], to determining soil composition and soil characteristics. The range of these measurements is vast, and most techniques are not automated, and so can provide information at only one instance in time.

6.2 Branch bag/Chamber measurements/FACE

Branch bag, chamber measurements and Free Atmosphere CO_2 Enrichment studies (FACE) are also site specific techniques looking at the response of individual leaves, branchs and plots (Figure 6). Most of these techniques are automated and feasible for extended periods of time. [*Saugier, et al.*, 1997]

Measurements of sap flow are critical to determining the detailed process response of the vegetation. Whilst eddy covariance methods can be used to determine the water use of whole forest stands, and branch bags can be used to measure the response of individual branches, sap flow measurements allow a direct measure of the transpiration rate of an individual tree [*Saugier, et al.*, 1997]. Sap flow measurements can be used to complement these other methods by partitioning fluxes of individual trees/branches, or evapotranspiration into evaporation and transpiration. Sap flow measurements can also provide measures of transpiration when the terrain is unsuitable for eddy covariance [*Granier*, 1987; *Granier, et al.*, 1996; *Smith and Allen*, 1996]. There are several variations of the method, which generally rely on measuring the spread of heat from a continuous or pulsed heat source.

Branch bags and leaf cuvettes allow detailed flux measurements of (but not exclusively) water and CO_2. In order to make these measurements, the leaf, or branch is enclosed in a chamber. The chamber can be designed have particular optical properties; i.e. to allow the dark response (respiration) of the leaf/branch to be observed. Additionally the internal climate of the chambers can be controlled to maintain a certain temperature, humidity or CO_2 concentration level [*Dufrene, et al.*, 1993].

FACE studies focus on plants and ecosystems exposed to ambient atmospheric conditions and elevated atmospheric CO_2 concentration levels. The studies attempt to quantify the effect of elevated CO_2 on vegetation. In response to elevations in CO_2, stomatal conductance is expected to reduce, resulting in greater water use efficiency and consequently lower latent energy fluxes. Whilst at the same time the elevated CO_2 could increase the productivity of vegetation by 'fertilization'. To quantify these changes, FACE studies expose otherwise naturally grown plants in the open-air to elevated levels of CO_2. To elevate the CO_2, FACE studies use arrays of outlets to vent CO_2 into the up-wind air. However the response to elevated CO_2 appears to be species specific, with large variability in the responses. Additionally, there maybe methodological issues relating to the (possible) acclimatisation of the internal leaf CO_2 concentrations, to the higher atmospheric concentrations; these may not be evident in some experiments due to the cessation of CO_2 elevations at night due to technical difficulties and to reduce the cost of the experiment.

Soil/root respiration is an important component of the carbon cycle. It is has the potential to be one of the largest feedbacks between the carbon cycle and climate change. Soils store the majority of land surface carbon and if the Q_{10} exponential-temperature dependence of soil respiration holds true, then massive increases in soil respiration can be expected to accompany any warming of the soils. However, while there is a labile fraction of soil that exhibits temperature dependant respiration rates, temperature relations in other fractions are obscured by other factors (e.g. droughts, floods, freezing and chemical inhibitors) [*Davidson and Janssens*, 2006]. These differing responses of soil fractions make the interpretation of soil respiration measurements difficult.

Soil chambers are the traditional method of measuring these fluxes. The basic soil chamber uses a collar inserted into the ground and a infra-red gas analyser [*Kanemasu, et al.*, 1974]. Soil chambers can be setup to include or exclude roots to further partition the respiration fluxes into autotrophic and heterotrophic components. Additionally there are many other methods of partitioning the fluxes of carbon (e.g. tree girdling, shading, root cuvettes, isotopic discrimination) [*Kuzyakov*, 2006]. Isotopic discrimination is of particular interest as it can be used in eddy covariance towers, and is also used in atmospheric measurements. Isotopic discrimination uses the fractionation

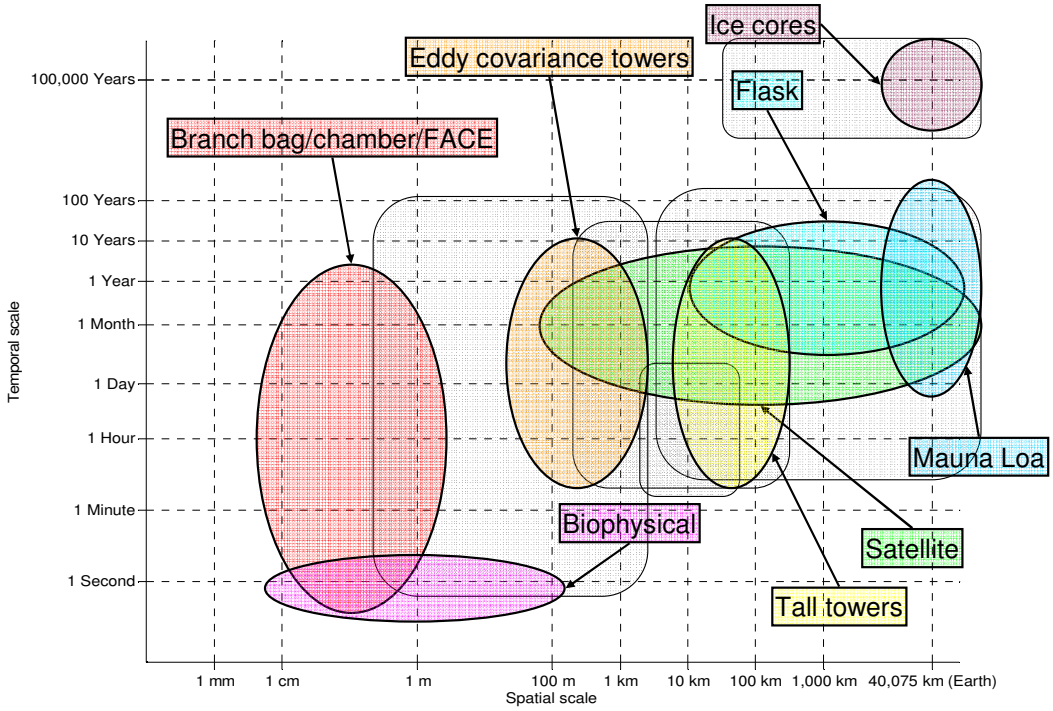

Figure 6: Hierarchy of measurements, from the short time/spatial scales to the long time/spatial scales:: e.g. Biophysical; Branch bag, chamber measurements and Free Air CO_2 Enrichment (FACE) experiments; Eddy covariance; Tall tower: Satellite; Flask; Mauna Loa; Ice cores. The greyed out hierarchy of models is shown for comparison purposes (Figure 5).

of $\delta^{13}C$ by plant processes, and is a powerful means of performing the partitioning [*Ehleringer, et al.*, 2000].

6.3 Eddy covariance

Eddy covariance techniques provide long term, direct measurements of ecosystem water vapour and CO_2 fluxes [*Baldocchi and Vogel*, 1996; *Moncrieff, et al.*, 1997; *Moore*, 1986] (Figure 6). The method uses sonic anemometers to measure the vertical wind speed at high sampling rates. An infra-red gas analyser (IRGA) is used to measure the concentrations of water vapour and CO_2 in the atmosphere. This gas analyser can be a closed path or an open path gas analyser [*Auble and Meyers*, 1992]. In either setup, the sample point is at approximately the same location as the sonic anemometer; positioned on a tower above the ecosystem giving a footprint on the order of several meters to several kilometres (depending on atmospheric stability) [*Schmid*, 1994].

Each flux tower is capable of providing high resolution, long term monitoring of the fluxes at an individual site. However, since eddy covariance towers are (normally) fixed, there is considerable difficulty in using eddy covariance measurements to calculate

the fluxes for larger regions. In order to tackle this difficulty there are a number of collaborations involving large numbers of eddy covariance monitoring systems. The most notable of these are; EUROFLUX [*Aubinet, et al.*, 2000] (latter absorbed into CARBOEUROPE [*Dolman, et al.*, 2006]), FLUXNET [*Baldocchi, et al.*, 2001]. These groups are collecting a rich dataset of long term ecosystem flux measurements.

Despite the benefits of eddy covariance, a number of uncertainties exist which are particular to the method. Katabatic flows can arise during stable (normally nocturnal) conditions. These flows are setup by slight topographical gradients at the measurement sites, and allow CO_2 to flow out of the system unmeasured below the level of the flux system. Pressure differences between weather systems can also setup drainage flows somewhat similar to the katabatic flows. There are additional systematic and random uncertainties to the measurement techniques and systems and, a large effort is underway to quantify and reduce these uncertainties [*Goulden, et al.*, 1996; *Hollinger and Richardson*, 2005; *Moncrieff, et al.*, 1996; *Richardson, et al.*, 2006].

6.4 Tall towers/Aircraft/Radiosondes

Quantifying the carbon budget of an extended region requires measurements with a much larger footprint than conventional eddy covariance systems (Figure 6). These measurements can be made from a number of platforms; tall towers, aircraft and radiosonde. Each of these has its own benefits: Tall towers provide excellent temporal resolution and extent, but the number of suitable towers is limited [*Baknin, et al.*, 1998; *Berger, et al.*, 2001; *Haszpra, et al.*, 2005; *Richardson, et al.*, 2006; *Wang, et al.*, 2006]: Aircraft provide a very flexible platform that can be used in a number of modes [*Crawford, et al.*, 1996; *Desjardins, et al.*, 1997; *Levy, et al.*, 1999], but the running costs are high: Radiosondes provide excellent profile measurements, but can be expensive to instrument [*Barr and Betts*, 1997].

6.5 Flask sampling

Flask sampling of composition of the atmosphere started in the 1960's. Flask networks can be large international collaborations such as GLOBALVIEW [*NOAA*, 2006]. These global dataset have been used in assessing the carbon sink strength of the Northern and Southern Hemispheres [*Denning, et al.*, 1999] and global inversions [*Gurney, et al.*, 2002; *Gurney, et al.*, 2003] (Figure 6).

6.6 Mauna Loa

The Mauna Loa Observatory is an atmospheric recording station 3397 m above sea level on the Mauna Loa volcano, Big Island, Hawaii. The observatory started atmospheric measurements of CO_2 during the 1950's [*Keeling*, 1960] and since then has kept continuous records of CO_2 [*Keeling, et al.*, 1995]. Mauna Loa is located in the middle of the Pacific Ocean and this allows the station to record the global mean background CO_2 concentration levels in the atmosphere (Figure 6).

6.7 Satellite

At the largest spatial scale satellites provide the most comprehensive direct land surface coverage of any observation, although they can only measure the spectral properties of the land-cover (Figure 6). The temporal coverage of satellites varies from geostationary satellites that continuously monitor the same location, to satellites that have return times of a few days or more. MODIS, the MOderate Resolution Imaging Spectrometer has a two day global coverage with 64 spectral bands ranging from 400 nm to 1040 nm [*Salomonson, et al.*, 1989]. From these bands, 'products' such as LAI can be retrieved which describe the spatial distribution of land surface parameters. Landsat (http://landsat.gsfc.nasa.gov/) provides high resolution photography (30 m resolution) of the land surface. The Advanced Very High Resolution Radiometer (AVHRR) provides 1.1 km resolution mapping in the infra red and visible regions of the spectrum (http://noaasis.noaa.gov/NOAASIS/ml/avhrr.html) to provide estimations of meteorological properties such as surface temperature and phenological indicators such as the Normalized Difference Vegetation Index (NDVI) e.g. [*Czajkowski, et al.*, 1997; *Sellers, et al.*, 1996a]. The Orbiting Carbon Observatory (OCO) is designed to retrieve atmospheric column measurements with a precision of 1 ppm [*Crisp, et al.*, 2004; *Crisp and Johnson*, 2005]. If successful this satellite will provide much improved constraints on the inversions of atmospheric CO_2.

6.8 Ice cores

Antarctic ice cores have allowed the determination of gas concentrations going back 740 kyrs (Figures 3 & 6). Reconstructed temperature and CO_2 records from these ice cores show strong co-variations of greenhouse gases and Antarctic temperatures. In particular, CO_2 can be seen to closely follow the temperature changes, with the glacial-interglacial temperature increases preceding the rise in CO_2 [*Caillon, et al.*, 2003; *Monnin, et al.*, 2001].

This indicates that temperatures precipitate the increase in CO_2 concentrations (but does not rule out the CO_2 concentration increase amplifying the temperature rise). Primarily these records come from the Vostok ice core (420 kyr) and the Dome C ice core (740 kyrs) [*Augustin, et al.*, 2004; *Dansgaard, et al.*, 1993; *Petit, et al.*, 1999]. Gas is trapped in the ice when the firn (an intermediate stage between snow and glacier ice) is compressed and fused into glacier ice. Gases are trapped in bubbles which can be sampled, and dated using seasonal variability. These ice-core measurements have been linked up to the Mauna Loa record [*Neftel, et al.*, 1985], confirming that the recent rising trend in CO_2 is anthropogenic.

7 Multi-scale projects

Many projects exist which attempt to quantify whole ecosystem dynamics of carbon and water (and fire). These are large interdisciplinary projects, incorporating most if not all of the above measurement and modelling techniques. The extent of the datasets collected allows these projects to provide some of the closest links between the different measurement scales and modelling techniques. The goals of the First International Satellite Land Surface Climatology Project (ISLSCP) Field Experiment (FIFE) were the improvement of understanding about land-atmosphere processes involving energy, heat and mass, and the scaling up of these processes to the regional and global scale. The project focused on a 15 × 15 km grass site in the USA [*Hall and Sellers*, 1995; *Sellers, et al.*, 1988]. The Hydrologic Atmospheric Experiment for the Study of Water-Budget and Evaporation Flux at the Climatic Scale (HAPEX) [*Andre, et al.*, 1986] aimed to link GCMs to the sub-grid scale hydrology and energy balance at a 100 × 100 km site in southwest France. The Boreal Ecosystem-Atmosphere Study (BOREAS) focused on a 1000 × 1000 km region of the boreal forest in Canada, in 1994 & 1996. BOREAS attempted to consolidate the local scale (e.g. biophysical, chamber, eddy covariance measurements) with the regional scale (e.g. satellite, aircraft/radiosondes observations), and improve understanding of atmospheric and land-atmosphere interactions [*Betts, et al.*, 2001; *Gamon, et al.*, 2004; *Hall*, 1999; *Ryan*, 2000; *Sellers, et al.*, 1997]. The Large-Scale Biosphere-Atmosphere Experiment in Amazonia (LBA) focused on how the ecology and biology of Amazonia will be impacted by changing land-use and climate [*Avissar, et al.*, 2002; *Avissar and Nobre*, 2002]. These projects (in particular BOREAS) have provided valuable multi-scale data to use as a test bed for work in this thesis.

8 Context of thesis

Interactions and feedbacks between the atmosphere and land surface occur on multiple spatial and temporal scales [*Otter, et al.*, 2002; *Swap, et al.*, 2002a; *Swap, et al.*, 2002b]. As a result, atmospheric and land surface observations can be hard to reconcile. The land surface directly interacts with the atmosphere in a region of the atmosphere known as the planetary boundary layer (PBL). Mixing within the planetary boundary layer is governed by turbulence resulting from solar radiation and land surface boundary conditions. Land-atmosphere boundary conditions are the result of ecological processes, and their response to local meteorology. Controls on ecological processes vary from the physical leaf area available for light interception, transpiration and photosynthesis, to the biophysical response of stomata. Forced by local meteorology and soil conditions, the biosphere determines energy partitioning into sensible and latent heat fluxes, and thus a significant proportion of the PBL forcing.

The ecological and atmospheric modelling communities take interest in each other's work due to the mutual interdependence of the systems that they model. Despite this interest, there remain gaps in the range of models which draw on the expertise already held in both fields. To date there has been a focus on large-scale, global modelling which tends to be a compromise between computational cost and model detail. Models drawing together the biosphere and atmosphere tend to be either simple schemes at a low spatial resolution, or incur significant computational costs. To study the effects of feedbacks, these models attempt to incorporate the basic atmosphere-biosphere interactions. However, due to the simplified nature of the biosphere schemes used, and/or their parameterisation (it is likely that) GCMs are not capturing most of the critical feedbacks present between the atmosphere and biosphere [*Betts, et al.*, 1996; *Foley, et al.*, 2000].

9 Thesis objectives

Broadly speaking, the aim of this thesis is improving the quantification of feedbacks and interactions at the land-atmosphere interface. This task is approached from a modelling perspective, by developing and implementing a coupled-atmosphere-biosphere (CAB) model. The motivations for the CAB model are numerous, as the CAB model provides a bridge across the land atmosphere interface. In this thesis, several applications of the model (site specific studies, sensitivity analysis and inversion studies) are demonstrated

and future applications of the model are discussed. Finally, the limitations of the approach are discussed, as are alternatives.

The thesis is structured as a series of papers intended for publication. The outline of the thesis is as follows:

Chapter 2 (Paper 1): Interactions between a boreal forest stand and the planetary boundary layer

The atmosphere and biosphere meet at the land surface. Strong interactions and feedbacks occur at the land surface between the biosphere and the PBL. On short timescales, the response of the land cover is determined by meteorological conditions. Feedbacks occur because the land cover modifies the atmosphere in the PBL. Quantifying these interactions will allow better scaling between observations at the stand-scale and those at larger scales, e.g. airborne measurements or satellites.

A coupling between a processed based biosphere model (SPA), and the PBL model (OSU1DPBL) is demonstrated. These models are coupled together in consistent manner to form the Coupled-Atmosphere-Biosphere (CAB) model. The CAB model is applied to a boreal forest site, and verified with above ground, below ground and airborne measurements. The interactions of the planetary boundary layer and the vegetation are discussed and shown to be consistent with observations.

Using the coupled model is used to show that negative feedbacks at the black spruce site have strong moderating effects; the feedbacks reduce the impact of LAI changes on the atmosphere by 22%, 37% and 27% for latent energy flux, air temperature and water mixing ratio respectively. We show that both radiative and hydraulic limitations imposed by the plant structure strongly affect the coupling within the atmosphere-biosphere system, whilst the effect of the mechanical impact of plant structure is weak.

Chapter 3 (Paper 2): Exchanges of carbon, water and energy between a boreal forest and the planetary boundary layer.

The role of the feedbacks and processes between the biosphere and PBL are critical for quantifying the future carbon cycle. In this chapter the work done in chapter 3 is built upon by including carbon dynamics. Biogeochemical and biogeophysical feedbacks between the biosphere and atmosphere are expected to play a critical role in the future carbon (C) cycle. Attempts at quantifying these interactions use both top-down (global

inversions) and bottom-up (site or species specific) approaches. Combining both measurements and models of the PBL provides one possible method of drawing the two approaches together.

In this chapter it is demonstrated that the C dynamics of the biosphere and the atmosphere can be captured by a coupled model. The coupled atmosphere-biosphere model is shown to be consistent with both atmospheric PBL observations and stand-based land surface measurements, both of which came from the Boreal Ecosystem-Atmosphere Study (BOREAS). The CAB model is used to show the strength of different feedbacks between the atmosphere and biosphere: (1) Atmospheric CO_2 concentrations at the land surface have a strong diurnal signal, driven by the net ecosystem exchange (NEE) and the rectifier effect. Diurnal changes in CO_2 concentration initiate feedbacks between the daytime uptake of CO_2 by the vegetation, and the concentration of atmospheric CO_2. However, the diurnal feedback involving the atmospheric CO_2 concentration is weak, reducing gross primary productivity (GPP) by less than 0.3%. (2) Hydrological feedbacks between the atmosphere and biosphere are strong, with impacts on the latent energy (LE) heat flux and GPP reaching 5% and 2% respectively. The feedbacks occur due to changes in transpiration and energy partitioning at the land surface, and the modification of PBL dynamics.

Chapter 4 (Paper 3): A simple inverse modelling approach using Monte Carlo sampling, applied to a terrestrial ecosystem and planetary boundary layer model.

Quantifying the C, water and energy dynamics of the land surface is critical for improving predictions of climate change. The spatial heterogeneity of C, water and energy fluxes causes difficulties when attempting to relate top-down (spatially averaged) and bottom-up (site/species specific) approaches. The PBL provides a potential stepping stone between the two approaches. The PBL is in direct contact with the land-surface, and dynamics within this atmospheric region are driven by ecosystem processes. Modelling the interaction between the PBL and the land surface provides a particularly powerful approach by simulating processes independent of scale.

In this study a simple Monte Carlo inversion scheme and a coupled atmosphere-biosphere model are used to investigate the interactions of the atmospheric (spatially averaged) and biosphere (site specific) systems. The inversions of atmospheric and/or

eddy covariance observations are shown to have the potential to give good estimates of ecosystem parameters such as leaf area index and the respiration rate. However, the observations contain less information about foliar nitrogen, plant hydraulic conductance and albedo, and no information on the surface roughness. Inverting both atmospheric and eddy covariance data improves the performance of the inversions by reducing the average uncertainty on the posterior distributions by 84% (compared to eddy covariance data only) and 74% (compared to atmospheric profile data only). Unbiased uncertainty is shown to have has little impact on the inversions, unlike biases which influence the inversions strongly.

Chapter 5: Discussion

The CAB model has been applied and corroborated in a number of studies (Chapters 2, 3 and 4). In the light of these three studies, the capabilities of the model are discussed and the applications of the model summarised. Model limitations discussed, and possible solutions are suggested. I also propose further applications for the CAB model.

Appendix A: Treatment of random errors

A discussion of the treatment of the random errors on eddy covariance fluxes.

Appendix B: CAB manual: Description of the Coupled-Atmosphere-Biosphere model

The CAB manual is intended as a comprehensive guide to the methodology behind the CAB model and covers 1) the fundamentals of the two models, such that someone unfamiliar with the subject can grasp the basic principles involved, 2) the coupling between the models, 3) the modifications made to the individual models to make them suitable for coupling. The manual is also intended as a user guide to provide users with a reference manual allowing easy implementation of the CAB model.

10 References

Alley, R., et al. (2007), *Climate Change 2007: The Physical Science Basis, Summary for Policymakers*, 18 pp.

Andre, J. C., et al. (1986), Hapex-Mobilhy - a Hydrologic Atmospheric Experiment for the Study of Water-Budget and Evaporation Flux at the Climatic Scale, *Bulletin of the American Meteorological Society*, *67*, 138-144.

Arrhenius, S. (1896), On the Influence of Carbonic Acid in the Air upon the Temperature of the Ground, *Journal of Science (fifth series)*, *41*, 237-275.

Aubinet, M., et al. (2000), Estimates of the annual net carbon and water exchange of forests: The EUROFLUX methodology, *Advances in Ecological Research, Vol 30*, *30*, 113-175.

Auble, D. L., and T. P. Meyers (1992), An Open Path, Fast Response Infrared-Absorption Gas Analyzer for H2o and Co2, *Boundary-Layer Meteorology*, *59*, 243-256.

Augustin, L., et al. (2004), Eight glacial cycles from an Antarctic ice core, *Nature*, *429*, 623-628.

Avissar, R., et al. (2002), The Large-Scale Biosphere-atmosphere Experiment in Amazonia (LBA): Insights and future research needs, *Journal of Geophysical Research-Atmospheres*, *107*, 1-6.

Avissar, R., and C. A. Nobre (2002), Preface to special issue on the Large-Scale Biosphere-Atmosphere Experiment in Amazonia (LBA), *Journal of Geophysical Research-Atmospheres*, *107*, 1-2.

Ayotte, K. W., et al. (1996), An evaluation of neutral and convective planetary boundary-layer parameterizations relative to large eddy simulations, *Boundary-Layer Meteorology*, *79*, 131-175.

Bakwin, P. S., et al. (1998), Measurements of carbon dioxide on very tall towers: results of the NOAA/CMDL program, *Tellus Series B-Chemical and Physical Meteorology*, *50*, 401-415.

Baldocchi, D., et al. (2001), FLUXNET: A new tool to study the temporal and spatial variability of ecosystem-scale carbon dioxide, water vapor, and energy flux densities, *Bulletin of the American Meteorological Society*, *82*, 2415-2434.

Baldocchi, D. D., and C. A. Vogel (1996), Energy and CO2 flux densities above and below a temperate broad-leaved forest and a boreal pine forest, *Tree Physiology*, *16*, 5-16.

Barr, A. G., and A. K. Betts (1997), Radiosonde boundary layer budgets above a boreal forest, *Journal of Geophysical Research-Atmospheres*, *102*, 29205-29212.

Beare, R. J., et al. (2006), An intercomparison of large-eddy simulations of the stable boundary layer, *Boundary-Layer Meteorology*, *118*, 247-272.

Berger, B. W., et al. (2001), Long-term carbon dioxide fluxes from a very tall tower in a northern forest: Flux measurement methodology, *Journal of Atmospheric and Oceanic Technology*, *18*, 529-542.

Betts, A. K., et al. (1996), The land surface-atmosphere interaction: A review based on observational and global modeling perspectives, *Journal of Geophysical Research-Atmospheres*, *101*, 7209-7225.

Betts, A. K., et al. (2001), Impact of BOREAS on the ECMWF forecast model, *Journal of Geophysical Research-Atmospheres*, *106*, 33593-33604.

Blackader, A. K. (1976), Modeling the Nocturnal Boundary Layer, paper presented at 3rd Symposium on the Atmospheric Turbulence, Diffusion and Air Quality, Raleigh, Oct 9-12.

Caillon, N., et al. (2003), Timing of atmospheric CO2 and Antarctic temperature changes across termination III, *Science*, *299*, 1728-1731.

Charney, J., et al. (1975), Drought in Sahara - Biogeophysical Feedback Mechanism, *Science*, *187*, 434-435.

Claussen, M., et al. (2002), Earth system models of intermediate complexity: closing the gap in the spectrum of climate system models, *Climate Dynamics*, *18*, 579-586.

Collatz, G. J., et al. (1991), Physiological and Environmental-Regulation of Stomatal Conductance, Photosynthesis and Transpiration - a Model That Includes a Laminar Boundary-Layer, *Agricultural and Forest Meteorology*, *54*, 107-136.

Cox, P. (2001), Description of the "TRIFFID" Dynamic Global Vegetation Model, Hadley Centre technical note 24.

Cox, P. M., et al. (1999), The impact of new land surface physics on the GCM simulation of climate and climate sensitivity, *Climate Dynamics*, *15*, 183-203.

Cox, P. M., et al. (2000), Acceleration of global warming due to carbon-cycle feedbacks in a coupled climate model, *Nature*, *408*, 184-187.

Crawford, T. L., et al. (1996), Air-surface exchange measurement in heterogeneous regions: Extending tower observations with spatial structure observed from small aircraft, *Global Change Biology*, *2*, 275-285.

Crisp, D., et al. (2004), The orbiting carbon observatory (OCO) mission, *Trace Constituents in the Troposphere and Lower Stratosphere*, *34*, 700-709.

Crisp, D., and C. Johnson (2005), The orbiting carbon observatory mission, *Acta Astronautica*, *56*, 193-197.

Cuxart, J., et al. (2006), Single-column model intercomparison for a stably stratified atmospheric boundary layer, *Boundary-Layer Meteorology*, *118*, 273-303.

Czajkowski, K. P., et al. (1997), Biospheric environmental monitoring at BOREAS with AVHRR observations, *Journal of Geophysical Research-Atmospheres*, *102*, 29651-29662.

Dansgaard, W., et al. (1993), Evidence for General Instability of Past Climate from a 250-Kyr Ice-Core Record, *Nature*, *364*, 218-220.

Davidson, E. A., and I. A. Janssens (2006), Temperature sensitivity of soil carbon decomposition and feedbacks to climate change, *Nature*, *440*, 165-173.

Denning, A. S., et al. (2003), Simulated variations in atmospheric CO2 over a Wisconsin forest using a coupled ecosystem-atmosphere model, *Global Change Biology*, *9*, 1241-1250.

Denning, A. S., et al. (1999), Can a strong atmospheric CO2 rectifier effect be reconciled with a "reasonable" carbon budget?, *Tellus Series B-Chemical and Physical Meteorology*, *51*, 249-253.

Desjardins, R. L., et al. (1997), Scaling up flux measurements for the boreal forest using aircraft-tower combinations, *Journal of Geophysical Research-Atmospheres*, *102*, 29125-29133.

Dewar, R. C. (1995), Interpretation of an Empirical-Model for Stomatal Conductance in Terms of Guard-Cell Function, *Plant Cell and Environment*, *18*, 365-372.

Dolman, A. J., et al. (2006), The CarboEurope regional experiment strategy, *Bulletin of the American Meteorological Society*, *87*, 1367-+.

Dufrene, E., et al. (1993), A Branch Bag Technique for Simultaneous Co2 Enrichment and Assimilation Measurements on Beech (Fagus-Sylvatica L), *Plant Cell and Environment*, *16*, 1131-1138.

Ehleringer, J. R., et al. (2000), Carbon isotope ratios in belowground carbon cycle processes, *Ecological Applications*, *10*, 412-422.

Farquhar, G. D., and S. Craemmerer (1982), Modelling of photosynthetic response to the environment., in *Physiological plant ecology II* edited by O. L. Lange, et al., pp. 549-587, Springer-Verlag, Berlin ; New York.

Foley, J. A., et al. (2000), Incorporating dynamic vegetation cover within global climate models, *Ecological Applications*, *10*, 1620-1632.

Foley, J. A., et al. (1996), An integrated biosphere model of land surface processes, terrestrial carbon balance, and vegetation dynamics, *Global Biogeochemical Cycles*, *10*, 603-628.

Friedlingstein, P., et al. (2006), Climate-carbon cycle feedback analysis: Results from the (CMIP)-M-4 model intercomparison, *Journal of Climate*, *19*, 3337-3353.

Gamon, J. A., et al. (2004), Remote sensing in BOREAS: Lessons learned, *Remote Sensing of Environment*, *89*, 139-162.

Garratt, J. R., et al. (1996), The atmospheric boundary layer - Advances in knowledge and application, *Boundary-Layer Meteorology*, *78*, 9-37.

Goulden, M. L., et al. (1996), Measurements of carbon sequestration by long-term eddy covariance: Methods and a critical evaluation of accuracy, *Global Change Biology*, *2*, 169-182.

Gower, S. T., and J. M. Norman (1991), Rapid Estimation of Leaf-Area Index in Conifer and Broad-Leaf Plantations, *Ecology*, *72*, 1896-1900.

Granier, A. (1987), Evaluation of Transpiration in a Douglas-Fir Stand by Means of Sap Flow Measurements, *Tree Physiology*, *3*, 309-319.

Granier, A., et al. (1996), Transpiration of trees and forest stands: Short and longterm monitoring using sapflow methods, *Global Change Biology*, *2*, 265-274.

Gurney, K. R., et al. (2002), Towards robust regional estimates of CO2 sources and sinks using atmospheric transport models, *Nature*, *415*, 626-630.

Gurney, K. R., et al. (2003), TransCom 3 CO2 inversion intercomparison: 1. Annual mean control results and sensitivity to transport and prior flux information, *Tellus Series B-Chemical and Physical Meteorology*, *55*, 555-579.

Haagenson, P. L., et al. (1994), The Penn State/NCAR Mesoscale Model (MM5)
Source Code Documentation, in *NCAR Technical Note*, edited, Mesoscale and Microscale Meterorology Division.

Hall, F. G. (1999), Introduction to special section: BOREAS in 1999: Experiment and science overview, *Journal of Geophysical Research-Atmospheres*, *104*, 27627-27639.

Hall, F. G., and P. J. Sellers (1995), First International Satellite Land Surface Climatology Project (ISLSCP) Field Experiment (FIFE) in 1995, *Journal of Geophysical Research-Atmospheres*, *100*, 25383-25395.

Haszpra, L., et al. (2005), Long-term tall tower carbon dioxide flux monitoring over an area of mixed vegetation, *Agricultural and Forest Meteorology*, *132*, 58-77.

Hollinger, D. Y., and A. D. Richardson (2005), Uncertainty in eddy covariance measurements and its application to physiological models, *Tree Physiology*, *25*, 873-885.

Houghton, J. T. (2001), Climate change 2001 : the scientific basis, x, 881 p.

Jarvis, P. G., and K. G. Mcnaughton (1986), Stomatal Control of Transpiration - Scaling up from Leaf to Region, *Advances in Ecological Research*, *15*, 1-49.

Jones, H. G. (1992), *Plants and microclimate : a quantitative approach to environmental plant physiology*, 2nd ed., xxiv, 428 p. pp., Cambridge University Press, Cambridge [England] ; New York.

Jones, P. D., and A. Moberg (2003), Hemispheric and large-scale surface air temperature variations: An extensive revision and an update to 2001, *Journal of Climate*, *16*, 206-223.

Kanemasu, E. T., et al. (1974), Field Chamber Measurements of Co2 Flux from Soil Surface, *Soil Science*, *118*, 233-237.

Keeling, C. D. (1960), The Concentration and Isotopic Abundances of Carbon Dioxide in the Atmosphere, *Tellus*, *12*, 200-203.

Keeling, C. D., et al. (1976), Atmospheric Carbon-Dioxide Variations at Mauna-Loa Observatory, Hawaii, *Tellus*, *28*, 538-551.

Keeling, C. D., et al. (2001), Exchanges of atmospheric CO2 and 13CO2 with the terrestrial biosphere and oceans from 1978 to 2000. I. Global aspects., 1-28 pp, Scripps Institution of Oceanography.

Keeling, C. D., et al. (1995), Interannual Extremes in the Rate of Rise of Atmospheric Carbon-Dioxide since 1980, *Nature*, *375*, 666-670.

Kucharik, C. J., et al. (2000), Testing the performance of a Dynamic Global Ecosystem Model: Water balance, carbon balance, and vegetation structure, *Global Biogeochemical Cycles*, *14*, 795-825.

Kuzyakov, Y. (2006), Sources of CO2 efflux from soil and review of partitioning methods, *Soil Biology & Biochemistry*, *38*, 425-448.

Leuning, R. (1995), A Critical-Appraisal of a Combined Stomatal-Photosynthesis Model for C-3 Plants, *Plant Cell and Environment*, *18*, 339-355.

Levy, P. E., et al. (1999), Regional-scale CO2 fluxes over central Sweden by a boundary layer budget method, *Agricultural and Forest Meteorology*, *98-9*, 169-180.

Lloyd, C. R., et al. (2001), Surface fluxes of heat and water vapour from sites in the European Arctic, *Theoretical and Applied Climatology*, *70*, 19-33.

Lloyd, J., et al. (1995), A Simple Calibrated Model of Amazon Rain-Forest Productivity Based on Leaf Biochemical-Properties, *Plant Cell and Environment*, *18*, 1129-1145.

Mann, M. E., et al. (1999), Northern hemisphere temperatures during the past millennium: Inferences, uncertainties, and limitations, *Geophysical Research Letters*, *26*, 759-762.

Mcnaughton, K. G., and P. G. Jarvis (1991), Effects of Spatial Scale on Stomatal Control of Transpiration, *Agricultural and Forest Meteorology*, *54*, 279-302.

Meir, P., et al. (2006), The influence of terrestrial ecosystems on climate, *Trends in Ecology & Evolution*, *21*, 254-260.

Moncrieff, J. B., et al. (1996), The propagation of errors in long-term measurements of land-atmosphere fluxes of carbon and water, *Global Change Biology*, *2*, 231-240.

Moncrieff, J. B., et al. (1997), A system to measure surface fluxes of momentum, sensible heat, water vapour and carbon dioxide, *Journal of Hydrology*, *189*, 589-611.

Monnin, E., et al. (2001), Atmospheric CO2 concentrations over the last glacial termination, *Science*, *291*, 112-114.

Monteith, J. L. (1965), Evaporation and Environment, in *Symposia of the Society for Experimental Biology ; no.19*, edited, pp. 205-234, University Press, Cambridge.

Moore, C. J. (1986), Frequency-Response Corrections for Eddy-Correlation Systems, *Boundary-Layer Meteorology*, *37*, 17-35.

Neftel, A., et al. (1985), Evidence from Polar Ice Cores for the Increase in Atmospheric Co2 in the Past 2 Centuries, *Nature*, *315*, 45-47.

NOAA (2006), GLOBALVIEW: Cooperative Atmospheric Data Integration Project, edited.

Otter, L. B., et al. (2002), The Southern African Regional Science Initiative (SAFARI 2000): wet season campaigns, *South African Journal of Science*, *98*, 131-137.

Petit, J. R., et al. (1999), Climate and atmospheric history of the past 420,000 years from the Vostok ice core, Antarctica, *Nature*, *399*, 429-436.

Richard Essery, M. B., Peter Cox (2001), MOSES 2.2 Technical Documentation, in *Hadley Centre technical*, edited.

Richardson, A. D., et al. (2006), A multi-site analysis of random error in tower-based measurements of carbon and energy fluxes, *Agricultural and Forest Meteorology*, *136*, 1-18.

Robinson, A. P., and A. R. Ek (2000), The consequences of hierarchy for modeling in forest ecosystems, *Canadian Journal of Forest Research*, *30*, 1837-1846.

Running, S. W., et al. (1999), A global terrestrial monitoring network integrating tower fluxes, flask sampling, ecosystem modeling and EOS satellite data, *Remote Sensing of Environment*, *70*, 108-127.

Ryan, M. G. (2000), Introduction to BOREAS special issue, *Tree Physiology*, *20*, 709-711.

Salomonson, V. V., et al. (1989), Modis - Advanced Facility Instrument for Studies of the Earth as a System, *Ieee Transactions on Geoscience and Remote Sensing*, *27*, 145-153.

Saugier, B., et al. (1997), Transpiration of a boreal pine forest measured by branch bag, sap flow and micrometeorological methods, *Tree Physiology*, *17*, 511-519.

Schmid, H. P. (1994), Source Areas for Scalars and Scalar Fluxes, *Boundary-Layer Meteorology*, *67*, 293-318.

Sellers, P. J., et al. (1988), The 1st Islscp Field Experiment (Fife), *Bulletin of the American Meteorological Society*, *69*, 22-27.

Sellers, P. J., et al. (1997), BOREAS in 1997: Experiment overview, scientific results, and future directions, *Journal of Geophysical Research-Atmospheres*, *102*, 28731-28769.

Sellers, P. J., et al. (1996a), A revised land surface parameterization (SiB2) for atmospheric GCMs .2. The generation of global fields of terrestrial biophysical parameters from satellite data, *Journal of Climate*, *9*, 706-737.

Sellers, P. J., et al. (1986), A Simple Biosphere Model (Sib) for Use within General-Circulation Models, *Journal of the Atmospheric Sciences*, *43*, 505-531.

Sellers, P. J., et al. (1996b), A revised land surface parameterization (SiB2) for atmospheric GCMs .1. Model formulation, *Journal of Climate*, *9*, 676-705.

Shuttleworth, W. J. (1991), Insight from Large-Scale Observational Studies of Land Atmosphere Interactions, *Surveys in Geophysics*, *12*, 3-30.

Sitch, S., et al. (2003), Evaluation of ecosystem dynamics, plant geography and terrestrial carbon cycling in the LPJ dynamic global vegetation model, *Global Change Biology*, *9*, 161-185.

Smith, D. M., and S. J. Allen (1996), Measurement of sap flow in plant stems, *Journal of Experimental Botany*, *47*, 1833-1844.

Swap, R. J., et al. (2002a), Southern African Regional Science Initiative (SAFARI 2000): summary of science plan, *South African Journal of Science*, *98*, 119-124.

Swap, R. J., et al. (2002b), The Southern African Regional Science Initiative (SAFARI 2000): overview of the dry season field campaign, *South African Journal of Science*, *98*, 125-130.

Troen, I., and L. Mahrt (1986), A Simple-Model of the Atmospheric Boundary-Layer - Sensitivity to Surface Evaporation, *Boundary-Layer Meteorology*, *37*, 129-148.

Wang, W. G., et al. (2006), Decomposing CO2 fluxes measured over a mixed ecosystem at a tall tower and extending to a region: A case study, *Journal of Geophysical Research-Biogeosciences*, *111*, -.

Williams, M., et al. (1997), Predicting gross primary productivity in terrestrial ecosystems, *Ecological Applications*, *7*, 882-894.

Williams, M., et al. (1996), Modelling the soil-plant-atmosphere continuum in a Quercus-Acer stand at Harvard forest: The regulation of stomatal conductance by light, nitrogen and soil/plant hydraulic properties, *Plant Cell and Environment*, *19*, 911-927.

Woodward, F. I., et al. (1995), A Global Land Primary Productivity and Phytogeography Model, *Global Biogeochemical Cycles*, *9*, 471-490.

Paper 1: Interactions between a boreal forest stand and the planetary boundary layer

T.C. Hill[1,2], M. Williams[1,2] and J. B. Moncrieff[1,2]

[1]School of GeoSciences and NERC Centre for Terrestrial Carbon Dynamics, Crew Building, University of Edinburgh, EH9 3JN, UK

[2]NERC Centre for Terrestrial Carbon Dynamics, UK

(Intended for submission to the Journal of Geophysical Research)

Abstract

The atmosphere and biosphere interact strongly with each other in the planetary boundary layer. Understanding both these interactions and their ecological controls on the coupled system will allow improved scaling between observations at the stand-scale and those at larger scales, e.g. airborne measurements or satellites. In addition, the successful simulation of the joint atmosphere-biosphere system will allow the study of feedbacks occurring within the coupled system. In this paper two well-tested models, one a process-based biosphere model (SPA) and the other, a planetary boundary layer model (OSU1DPBL), are coupled together. The coupled model is designed to capture the feedbacks and interactions that occur on minute, hour and daily timescales. We show that the biosphere model, which is already tested at multiple sites globally, can be validated at a boreal black spruce site. Verification of the biosphere model utilises a wide range of data from a 120 day period during the 1994 BOREAS field campaign. The coupled model is tested with radiosonde data above the black spruce site, demonstrating that atmosphere and biosphere models can be coherently combined. Using the coupled model we show that negative feedbacks at the black spruce site have strong moderating effects; the feedbacks reduce the impact of LAI changes on the atmosphere by 22%, 37% and 27% for latent energy flux, air temperature and water mixing ratio respectively. We show that both radiative and hydraulic limitations imposed by the plant structure strongly affect the coupling within the atmosphere-biosphere system, whilst the effect of the mechanical impact of plant structure is weak.

Introduction

The climate is changing; model predictions suggest that the climate will warm by 1.4 to 5.8 K over the period 1990 – 2100 [*Houghton*, 2001]. These predictions were generated by an ensemble of future global scenarios and climate models. The uncertainty associated with this model ensemble was large, with an inter-model standard deviation of 0.8 K. Parameterisation of land surface schemes, and their interaction with the climate system causes significant uncertainty in the predictions of global climate models, particularly when the changing climate is considered [*Crossley, et al.*, 2000; *Desborough, et al.*, 2001; *Essery, et al.*, 2003].

Many approaches have been taken in order to quantify how vegetation will respond to perturbations in the climate [*Cox, et al.*, 2000; *Foley, et al.*, 2000; *Jacobs and de Bruin*, 1997; *Ryan*, 2000]. However these approaches exclude some of the complex interactions occurring at the land surface. Atmospheric processes are intrinsically linked to the biosphere through the surface energy balance, and water transport and exchange. The response of terrestrial ecosystems to perturbations will initiate feedbacks between atmospheric and land surface processes. To better quantify uncertainties in climate change predictions, atmosphere-biosphere feedbacks need to be better understood.

The interaction of the land surface with the global climate is generally simulated using General Circulations Models (GCMs). GCMs tend to use simplified biosphere schemes to reduce computational costs. Such simplifications (e.g. empirical models of stomatal conductance) make model testing difficult, as many parameters may remain which are either not measured, or have little physical basis. More recently, Large Eddy Simulations (LES) have been performed for atmosphere-land surface interactions over small regions, on the order of ~10 km. The use of LES models in conjunction with realistic vegetation models avoids many of the issues that GCMs face. Two dimensional LES schemes have been shown to have good agreement with tall tower observations [*Denning, et al.*, 2003]. However, LES models suffer from some limitations; due to their detail they are still incur large computational overheads, and their initialisation requires reanalysis data and thus reliance on other models. A role now exists for detailed, focused modelling studies which are robust, and which can be quickly and easily run to inform large scale models of critical processes. Such a model would also lend itself to data assimilation, inversion studies and other computationally intensive techniques.

We couple two well tested models; the soil-plant-atmosphere (SPA) biosphere model, and, the Oregon State University one dimensional planetary boundary layer (OSU1DPBL) atmospheric model (see later chapters for descriptions of the models and their coupling). The coupled atmosphere-biosphere (CAB) model simulates energy, water and heat exchanges within the atmosphere-biosphere system, and operates at a spatial and temporal scale relevant to both ecological and atmospheric processes and measurements. The model formulation was designed to be; (1) easily implemented and modified, (2) run with minimal computational cost, making its use in data assimilation and bayesian studies feasible, (3) parameterised using observations which are independent of those used in testing. The model was designed to be tested against both stand-based flux measurements (eddy covariance estimates of surface fluxes) and atmospheric profile measurements (aircraft/radiosonde measurements in the planetary boundary layer (PBL)). Verification and parameterisation data came from the Boreal Ecosystems Atmosphere Study (BOREAS) [*Ryan*, 2000]. BOREAS was chosen because of the comprehensive simultaneous datasets available, and the importance of atmosphere-biosphere interactions in the boreal region, which covers 11% of the terrestrial land surface [*Bonan and Shugart*, 1989].

Objectives: Once verified, we shall use the CAB model as part of a sensitivity analysis to answer several questions: (1) Can we identify feedbacks between the PBL and the biosphere, and what are their impacts on vegetation and PBL responses? We know high air temperatures and low humidity can stress the hydraulics system of the vegetation, forcing plants to close stomata to avoid damaging vital infrastructure [*Jones*, 1992; *Williams, et al.*, 2001]. This defensive response of vegetation can reduce transpiration, resulting in further drying and heating of the atmosphere. However, at the same time, the resulting water vapour pressure deficit (VPD) will be higher, increasing the atmospheric demand for water and further stressing the plant hydraulics. Can we assess the importance of feedbacks such as these and distinguish them from a simple driving force? (2) What is the relative importance to the coupled system of changes to in the hydraulic, mechanical, and radiative properties of the biosphere? Simple variations within the biosphere, such as the height of a forest stand, may have complex impacts on the coupled system, e.g. growth of forests changes the mechanical roughness of the canopy, as seen by the atmosphere. Increasing canopy cover also alters both the albedo and self shading of the canopy. Changes to the canopy will also have strong impacts on

the hydraulic capacity of the stand. Due to the feedbacks involved, the effects of these changes on the coupled system are likely to be complex and nonlinear. We aimed to disentangle the contributions to atmosphere-biosphere feedbacks, from the plants interaction with radiation, the plants hydrology and the mechanical interaction of the plant and atmosphere.

In this atmosphere-biosphere coupling virtually all model parameters come from previous studies, and biogeochemical and biophysical processes are modelled mechanistically. The model draws together leaf, soil and eddy-flux measurements at a single site, and corroborates these with radiosonde measurements above the same region. Model results were not "tuned" using flux measurements, and this allows greater confidence to be placed on the model's prognostic abilities. We suggest that the CAB model is suitable for data assimilation, tracer experiments and inversion studies, and later we discuss these applications further.

Data description

Model runs were compared to a wide range of measurements within the southern study area (SSA), located in Saskatchewan, Canada (53.9°N, 105.1°W), during the 1994 BOREAS field campaign. The launch site for the radiosondes was Candle Lake (53.7°N 105.3°W, 503 m). The radiosondes provided the atmospheric profile measurements of temperature, water mixing ratio and windspeed used to initialise and verify the atmospheric sub-model (Table 1). To the North East of Candle Lake, black spruce (*Picea mariana*) was the dominant tree species. Consequently we assumed that black spruce dominated the daytime forcing of the boundary layer [*Betts, et al.*, 2001; *Jarvis, et al.*, 1997]. At the stand-level, eddy-flux and other companion data sets from the southern study area old black spruce (SSA-OBS) eddy-flux tower site were used to drive and test the biosphere sub-model.

Stand-based data

As far as possible the biosphere model is parameterised using measurements from the SSA-OBS site, or other local old black spruce sites (Table 1). Plant capacitance and a water use efficiency parameter (ι) were the only parameters not to be explicitly measured, or inferred from measurements. Values for these parameters came from expected ranges of previous studies [*Williams*, 2005].

The results of the biosphere model are compared to half-hourly eddy-flux measurements from the SSA-OBS site [*Jarvis, et al.*, 1997; *Jarvis and Moncrieff*, 2000; *Newcomer, et al.*, 2000]. Measurements were made for 120 days throughout the 1994

Parameter/variable	Value/range	Units	Comments	Source
Site information				
Lattitude	53.99	^{o} N	-	Jarvis et al. (1997)
Longditude	-105.12	^{o} E	-	Jarvis et al. (1997)
Altitude	628.94	m	-	Newcomer et al. (2000)
Biosphere parameters				
Leaf Area Index (LAI)	4.4	$m^2 m^{-2}$ *ground area*	-	Chen et al. (1997)
Total Foliar Nitrogen (FN)	5.54 / 7.40	g m-2 *leaf area*	-	Rayment et al. (2002)
Maximal velocity of carboxylation (Vc_{max})	11	µmol CO_2 m^{-2} s^{-1}	Calibrated on DOY 160	Rayment et al. (2002)
Maximal electron transport rate (J_{max})	31.31	µmol e^- m^{-2} s^{-1}	Calibrated on DOY 160	Rayment et al. (2002)
Plant hydraulic conductance	10	mmol m^{-1} s^{-1} MPa^{-1}	Calibrated using the hydraulic conductance per leaf area (KL)	Ewers et al. (2005)
Minimum Leaf Water Potential	-1.5	Mpa	-	Ewers et al. (2005)
Leaf capacitance	2000	mmol m^{-2} s^{-1}	-	Williams (2005)
Water use efficiency (Iota)	1.01	-	-	Williams (2005)
Root Resistance	100	MPa s g $mmol^{-1}$	Calibrated using KL	Ewers et al. (2005)
Tower Height	27	m	-	Jarvis et al. (1997)
PAR leaf reflectance	0.11	-	Tuned	Betts et al. (1997), Baldocchi et al. (2000)
PAR leaf transmission	0.16	-	Tuned	Betts et al. (1997), Baldocchi et al. (2000)
PAR soil reflectance	0.08	-	-	Miller et al. (1997)
NIR leaf reflectance	0.43	-	Tuned	Betts et al. (1997), Baldocchi et al. (2000)
NIR leaf transmission	0.26	-	Tuned	Betts et al. (1997), Baldocchi et al. (2000)
NIR soil reflectance	0.37	-	-	Miller et al. (1997)
Below ground distributions				
Organic Fraction	0.0 / 0.5	-	-	Anderson et al (2000), Saxton et al. (1986)
Mineral Fraction	0.0 / 0.5	-	-	Anderson et al (2000), Saxton et al. (1986)
Water/Ice Fraction	0.02 / 0.75	-	-	Cuenca et al. (1997), Cuenca et al. (2000)
Soil Temperature	-0.2 / 29.4	^{o}C	-	Jarvis et al. (1997), Jarvis et al. (2000)
Fine root distribution	0.0 / 0.3	m	-	Steele et al. (1997)
Fine Root Biomass	591	g m^{-2}	-	Steele et al. (1997)
Sand fraction	0.65 / 0.90	-	-	Anderson et al (2000)
Clay fraction	0.10 / 0.15	-	-	Anderson et al (2000)
Silt fraction	0.00 / 0.26	-	-	Anderson et al (2000)
Atmospheric parameters				
Air Temperature (above canopy)	1.1 / 28.4	^{o}C	-	Jarvis et al. (1997), Jarvis et al. (2000)
VPD (above canopy)	0.0 / 2.77	kPa	-	Jarvis et al. (1997), Jarvis et al. (2000)
PAR (above canopy)	0 / 1936	µmol m-2 s^{-1}	-	Jarvis et al. (1997), Jarvis et al. (2000)
Wind Speed (above canopy)	0.0 / 8.8	m s^{-1}	-	Jarvis et al. (1997), Jarvis et al. (2000)
Precipitation	0 / 28	mm d^{-1}	-	Jarvis et al. (1997), Jarvis et al. (2000)
Roughness length (Zo)	1	m	-	Holtslag et al. (1983)
Albedo	0.093	-	-	Betts et al. (1997), Baldocchi et al. (2000)
Fractional cloud cover	0 / 0.5	-	-	Jarvis et al. (1997), Jarvis et al. (2000)
Horzontal Wind Speed (u & v)	0.0 / 5.8 (DoY 167)	m s^{-1}	-	Barr et al. (2000), Barr et al. (2000), Barr et al. (1997)
	0.0 / 8.8 (DoY 250)	m s^{-1}	-	Barr et al. (2000), Barr et al. (2000), Barr et al. (1997)
Potential temperature (0 - 3000m)	282.1 / 294.1 (DoY 167)	K	-	Barr et al. (2000), Barr et al. (2000), Barr et al. (1997)
	286.7 / 302.1 (DoY 250)	K	-	Barr et al. (2000), Barr et al. (2000), Barr et al. (1997)
Mixing Ratio (0 - 3000m)	1.0 / 5.4 (DoY 167)	g kg^{-1}	-	Barr et al. (2000), Barr et al. (2000), Barr et al. (1997)
	4.7 / 6.9 (DoY 250)	g kg^{-1}	-	Barr et al. (2000), Barr et al. (2000), Barr et al. (1997)

Table 1: Model parameters and corroborative data; all parameters are either directly from the literature or have been calibrated using literature. The exceptions are leaf capacitance and ι which are taken from within the range suggested in the SPA model's manual [*Williams*, 2005]. The roughness length is taken as the commonly accepted value for continuous canopy cover.

growing period (late-May to early-September). At the start of the study period, the soil was frozen to a depth of 0.4 m, and snow had recently fallen. The study period extended throughout the summer and continued till the first frosts of the autumn.

The eddy-flux system utilised a sonic anemometer, mounted on a tower 27 m above ground level. Black spruce extended from the tower at least 1200 m in all directions. Energy closure for the study period was very good with energy balance residuals for the period of 3%. The tower was positioned in an extensive area of black spruce, with ~10 % tamarack (*Larix Laricina*). The SSA-OBS stand was 10-11 m in height and had an average LAI of 4.4 [*Chen, et al.*, 1997].

Despite the moderately high LAI, thin crowns resulted in significant gaps in the canopy. Under the canopy there was a sparse undergrowth of shrubs. In wetter areas *Sphagnum* is present, giving way to feather mosses and lichens in drier areas. The site was flat with a height variation of less than 1 m.

We calculated random errors for latent energy (LE) using half-hourly eddy flux data according to the method outlined in Hollinger [*Hollinger and Richardson*, 2005], *see Appendix A*. Hollinger suggests that errors on flux measurements follow a Laplace distribution, not a normal distribution. So instead of the standard deviation, the mean absolute deviation (MAD) is calculated. In addition, a uniform systematic error of 20% was assumed, [*Goulden, et al.*, 1996].

At the SSA, detailed soil profiles had been taken, recording soil mineral and organic composition [*Anderson*, 2000; *Newcomer, et al.*, 2000]. Surface soil layers were organic (i.e. no mineral content); this necessitated some updates to the SPA model's soil routines, which are discussed later in the description of the modelling scheme. In addition to the soil profiles, several companion data sets exist which ran in parallel with the eddy-flux tower. Profiles of soil temperature [*Jarvis, et al.*, 1997; *Jarvis and Moncrieff*, 2000; *Newcomer, et al.*, 2000] and volumetric water content [*Cuenca*, 2000; *Cuenca, et al.*, 1997; *Newcomer, et al.*, 2000] were recorded at the site. Soil temperatures at depths of 0.025, 0.05, 0.1, 0.2, 0.5 m were measured every half hour using thermocouples, with a reference temperature probe at a depth of 1 m. Manual volumetric water content measurements were taken periodically throughout the study period; on average every 4 days. The measurements were taken using a Moisture Point, Manual time domain reflectometer.

Atmospheric data

Atmospheric profile data was taken from serial radiosonde releases from Candle Lake [*Barr and Hrynkiw*, 2000; *Barr*, 2000; *Barr, et al.*, 1997; *Newcomer, et al.*, 2000]. Radiosonde releases were performed during the three BOREAS Intensive Field Campaigns of 1994. Radiosondes were available on 56 days throughout the 120 day study period. Release times from the Candle Lake site were typically 1115, 1515, 1715, 1915, 2115 and 2315 hours UTC, correcting for local time sets these times back 7 hours. The site is situated 1.5 km south of Candle Lake which is 17 km long and, at widest, is 12 km wide; maps are shown in *Barr, et al.* (1997). The release site was a clearing 200 m wide surrounded by a mixed forest 12-15 m. To the north east of the release site the vegetation is dominated by black spruce.

Test days

The coupled atmosphere-biosphere (CAB) model was corroborated on two test days. These test days were selected from the 120 day study period using a number of criteria:

1. A minimum of 2 morning and 2 afternoon radiosonde profiles must be available for the day in question. The first profile should be as close to dawn as possible.
2. The radiosonde flight paths must remain over black spruce dominated forest for the first 3500 m of their accent.
3. Radiosonde flight paths must not diverge by more than a total of 45^{o} for the first 3500 m of their accent.
4. Eddy flux data should exist for the day, with no more than 15% of the half-hourly measurements missing.
5. Days should be chosen to be within periods of stable synoptic weather conditions, in order to avoid fronts disturbing the boundary layer profiles.
6. Ideally, test days should cover the range of ecological conditions captured during the study period, i.e. a good distribution throughout the study period.

The suitable days based on these criteria were days 167, 211, 250 and 260. Only results from days 167 and 250 shall be shown in this paper due to the limited number of suitable radiosonde profiles, and to limit the verbosity of the results section. However, model-measurement agreement for the other two days is similarly good. There are no such data availability issues with the eddy covariance observations, and the full study period is shown as daily averages.

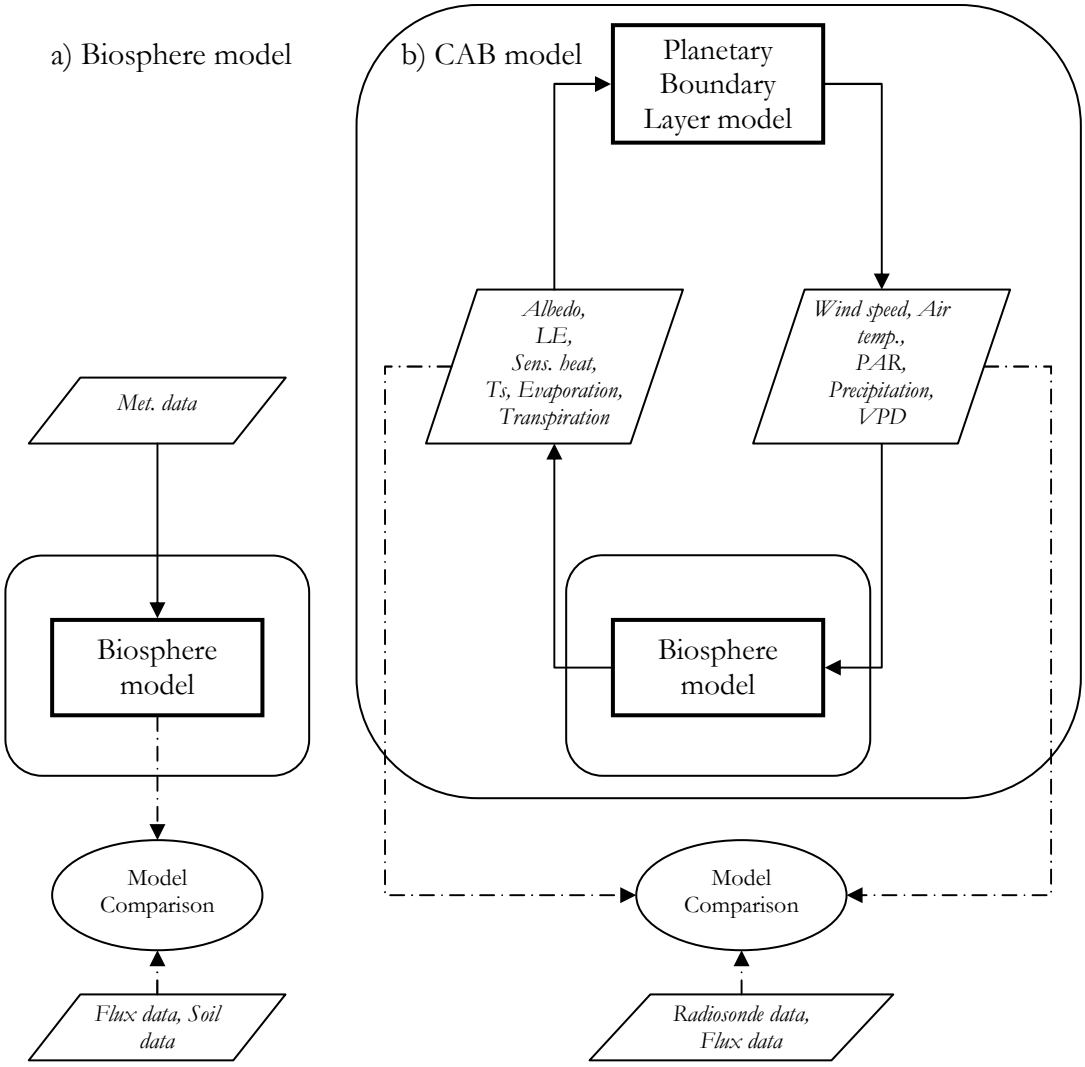

Figure 1: a) Initially, the biosphere model is run independently of the atmospheric model. The model is driven by meteorological data, and verified by stand-based data. b) The CAB model then incorporates the corroborated biosphere with an atmospheric model. The CAB model is initialised with atmospheric profile data and initial biosphere conditions; it then runs in a prognostic mode. Meteorological conditions are updated by the PBL model. Responding to these updates, the biosphere model calculates new surface boundary conditions and fluxes. CAB model predictions are corroborated with atmospheric profile data and surface fluxes and meteorology

Model Structure

The CAB model is based on two existing models (Figure 1). Biosphere processes and planetary boundary layer processes are simulated in separate, well tested models. The biosphere component partitions the surface energy balance, calculating surface

evaporation, transpiration and albedo. Based on these parameters the atmospheric component determines the evolution of the boundary layer. The atmospheric component then predicts the required meteorological drivers: temperature, VPD, down-welling radiation and wind speed, which are then passed back to the biosphere model. Meteorological drivers are taken from the first atmospheric model layer above the forest canopy. Shortwave radiation is used to estimate the photosynthetically active radiation (PAR). The base time-step for the CAB model is set at 1 minute.

Ecosystem Sub-model

The Soil-Plant-Atmosphere ecosystem model is a high resolution process based model (10 canopy layers and 20 soil layers), in this study it was modified to run on a continuously variable time-step. A full description of the model can be found [*Williams*, 2005; *Williams, et al.*, 2001; *Williams, et al.*, 1996]. Its design function was the modelling of leaf and canopy level eco-physiological processes, to allow the diagnosis of eddy flux data. The model has been used in a number of different applications and shown to perform well in all studies for a range of vegetation covers and latitudes [*Engel, et al.*, 2002; *Fisher, et al.*, 2006; *Schwarz, et al.*, 2004; *Van Wijk, et al.*, 2003; *Williams, et al.*, 2000; *Williams, et al.*, 1997; *Williams, et al.*, 1996].

In this study, the model scales up from leaf level processes and measurements to canopy scales, in order to provide the surface fluxes and surface partitioning of energy. A brief description of some of the key features of the model is presented here.

The SPA model contains a detailed radiative transfer scheme which accounts for shaded and sunlit fractions of the canopy; modelling the absorption, transmission and reflectance of near infra-red (NIR), direct and diffuse PAR and long-wave radiation. Albedo is calculated on the basis of the reflectance and transmission in the PAR and NIR wavelengths of the soil and canopy elements. Canopy reflectance and transmission is tuned to NIR and PAR under-story reflectance [*Miller, et al.*, 1997] and above canopy albedos [*Betts and Ball*, 1997]. Wind speed profile throughout the canopy is modelled with as an exponential reduction, which decreases with height [*Cionco*, 1985].

The Farquhar model of leaf level photosynthesis [*Farquhar and Craemmerer*, 1982] and the Penman-Monteith model of leaf transpiration [*Jones*, 1992; *Monteith*, 1965; *Penman*, 1948] are linked in the SPA model. Within the limitations set by plant hydraulics, stomatal conductance is varied to optimize the carbon gain per unit of leaf

nitrogen. This optimization is set by the water use efficiency parameter, ι [*Williams, et al.*, 1996].

Plants regulate stomatal conductance to maintain the minimum leaf water potential at a safe threshold and avoid excessive water stresses which can cause cavitations in the xylem. Plant hydraulic resistance is assumed to increase with height, increasing the water stress in the upper layers of the canopy.

Soil hydrology and temperature response is calculated by solving the soil surface energy balance and by the modelling of heat and moisture transport within 20 soil layers. Soil temperatures, water fractions and rooting profiles are initialised from measurements. The core soil temperature is set constant at a depth of 2 m, at the local 1994 annual mean air temperature of 0.7 °C [*Environment Canada*, 2004]. Heat flux between the soil layers is dynamically modelled, with each layer having its own prescribed soil composition of organic, mineral and silt matter. Roots preferentially extracted water from the layer with the highest available water content and non-zero root fraction.

The SSA-OBS site has some soil layers with very high organic fractions, reaching volumetric organic carbon fractions of 0.45. To run the biosphere model at the site, the SPA model's soil routines for calculating soil field capacity, were modified to calculate the field capacity of organic soils with equations from [*Nemati, et al.*, 2002]. These routines replace the *Saxton et al (1986)* equations for soil layers with no mineral content. The routine for calculating the thermal conductivity of the soil layers was also changed [*Wijk*, 1963].

Atmosphere Sub-model

The atmospheric component of the CAB model is represented by the Oregon State University one dimensional planetary boundary layer model [*Mahrt and Pan*, 1984; *Troen and Mahrt*, 1986], which has been extensively tested [*Guichard, et al.*, 2004; *Holtslag, et al.*, 1990; *Holtslag and Ek*, 1996; *Lee and Mahrt*, 2004; *Murthy, et al.*, 2004]. The OSU1DPBL model is capable of medium resolution modelling of the dynamics within the PBL, with low computational cost. The formulation of the PBL within OSU1DPBL is robust and can simulate transitions from unstable to stable PBL conditions. Within the model, turbulent diffusivity tends to zero at the top of the boundary layer. The model represents the first 10,000 m of the atmosphere using 68 atmospheric layers, with the

spatial resolution increasing closer to the land-surface. The original simple surface layer parameterisation used in the OSU1DPBL [*Louis*, 1979] is replaced by the more complex SPA model, allowing the model to be parameterised and tested with observations.

Originally the OSU1DPBL used a cloud formation routine. The routine placed clouds at the atmospheric layer with the highest relative humidity. However, the routine was found to produce unrealistic cloud cover. To avoid the complication of unrealistic boundary layer cloud formation the routine was replaced by a constant fractional cloud cover. This constant could be determined from the down-welling radiation measurements.

Modelling Scheme

The model was run in two stages. (1) The off-line version of the biosphere model (SPA) was run in a diagnostic mode for the 120 day period. This run was used to evaluate the biosphere component of the model (Figure 1a). Soil and canopy layers were parameterised from the literature, and air temperature above the canopy, VPD, precipitation, wind speed and incoming radiation from the eddy covariance tower were used to drive the offline biosphere model. (2) The CAB model was run in a prognostic mode (Figure 1b). The atmospheric component of the CAB model was initialised at midnight using a profile based on the first pre-dawn radiosonde release (Table 1). Soil temperatures and moistures were initialised using the off-line model predictions from the biosphere model. The atmospheric model was then driven by land surface fluxes of energy and water, from the biosphere model. In turn, the atmospheric component provided the meteorological drivers to drive the biosphere model. In this second mode, the CAB model could be tested against eddy covariance and atmospheric measurements and also used for sensitivity analysis.

Sensitivity analysis

A sensitivity analysis was run to identify ecological processes initiating feedbacks within the coupled atmosphere-biosphere system, and to analyse these feedbacks in terms of their hydraulic, mechanical and radiative contributions. The first step in the sensitivity analysis was to generate the nominal meteorology by running the CAB model for the nominal parameterisations, those of day 250 (Table 1). We will refer to this as the nominal model run. Then the CAB model was run to investigate the sensitivity of the system to changes in LAI using two versions of the CAB model; (1) the standard

version of the CAB model, with the full coupling between the atmosphere and biosphere included, (2) a modified CAB model, with the atmospheric feedback onto the land surface bypassed. In this second case, the biosphere was driven by the nominal meteorology as predicted by the nominal model run. Despite the atmospheric feedback onto the land surface being bypassed, the PBL was allowed to develop, for comparison purposes. For both model versions the LAIs were varied from 1 to 6 to cover the expected extremes of a boreal forest stand. As the LAI of a forest stand changes (for example, through growth) the height and roughness length change as well. To approximate these additional effects of changing the canopy, the height of the stand was scaled with the LAI change. An allometric relationship between the height of the canopy and the LAI could have been used, but would have been unnecessary due to the synthetic nature of the analysis. Instead an arbitrarily relationship was chosen, with canopy height ranging from 6 m to 12 m (varying linearly with LAI). Roughness length was assumed to be $1/10^{th}$ the canopy height to fit in with roughness length estimates from *Stull* [1988]. For simplicity, the combined changes of LAI, height and roughness length are referred to as changes in 'combined LAI'.

The latent energy flux, canopy conductance, and atmospheric measures of potential temperature and water mixing ratio at 20 m above ground level were used to diagnose the state of the coupled system. Canopy conductance is the total conductance of all the canopy elements (leaves), and includes the response of the stomata. The diagnostics are presented relative to the nominal case, either as percentage changes or residuals. Measures of the latent energy, air temperature and mixing ratio of water were calculated from daily means. Canopy conductance was taken from early-afternoon, 2 pm (local time) to reduce the dependence on leaf water capacitance.

The variations in the range of combined LAI specified for the sensitivity analysis had the potential to impact several mechanisms in the coupled atmosphere-biosphere system. The changes were divided into three broad contributing factors (hydraulic, mechanical roughness and radiative) to assess their individual contribution. The range for each factor was determined by the corresponding range resulting from the variations in combined LAI:

1) *Hydraulic impacts, (1 to 6 hydraulic LAI and 6 to 12 m canopy height)*: plant hydraulic conductance determines the resistance to water transport within the plant, and thus the plants' ability to transpire. The hydraulic conductance is strongly affected by the

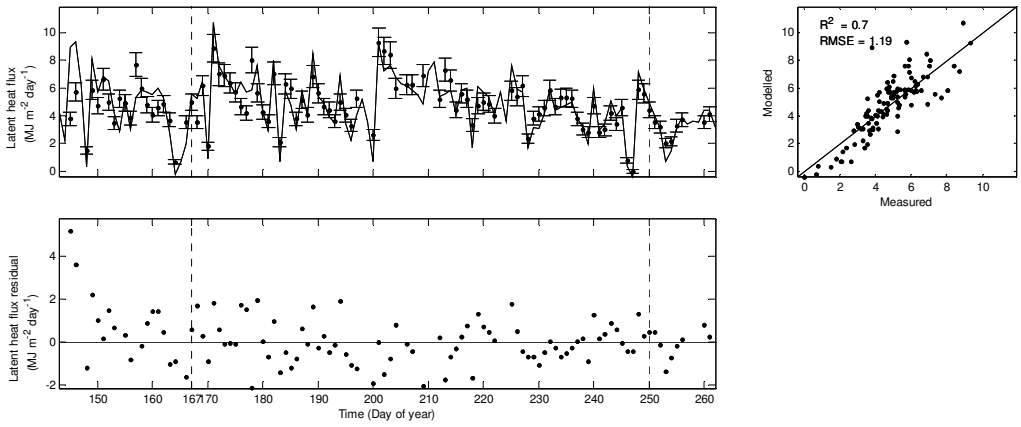

Figure 2: Modelled response of the biosphere model, and SSA-OBS eddy flux tower measurements during the 1994 study period. Comparisons of daily aggregated LE are shown. Days with less than 44 half hourly values are excluded from the measurement plots. The modelled LE is shown using a solid line and the measurements are shown using points (·····) with random errors. LE residuals (measured – modelled LE) are shown with a zero line for reference. A scatter plot showing the modelled and measured data is included: In addition to R^2 and RMSE values, a 1:1 is plotted. Vertical dashed lines (- - - -) indicate the two test days.

canopy height and the LAI. Canopy height is inversely proportional to the stem hydraulic conductance; the conductance between the canopy and the roots. In this analysis of the CAB model the canopy height and the hydraulic specific LAI were changed. The Hydraulic LAI (LAI_H) is the LAI directly affecting the plant hydraulics, through mechanisms such as total plant resistance. Other canopy characteristics, including the radiative effects of LAI, were preserved at the nominal levels.

2) *Mechanical roughness impacts, (0.6 m to 1.2 m roughness length)*: roughness length is a measure of the momentum flux of to the surface, seen as a frictional effect to the air flowing over the land surface. As the canopy height increases so does the roughness length, increasing the mechanical mixing in the boundary layer. In the sensitivity analysis, roughness length was set to $1/10^{th}$ the canopy height. Other canopy characteristics, including the canopy height for hydraulic purposes, were preserved at the nominal levels.
3) *Radiative impacts, (1 to 6 radiative LAI)*: the radiative LAI (LAI_R) of the canopy affects both the albedo of the stand and the shading of the canopy elements. Albedo controls the net absorption of radiation at the land surface and the fraction of PAR

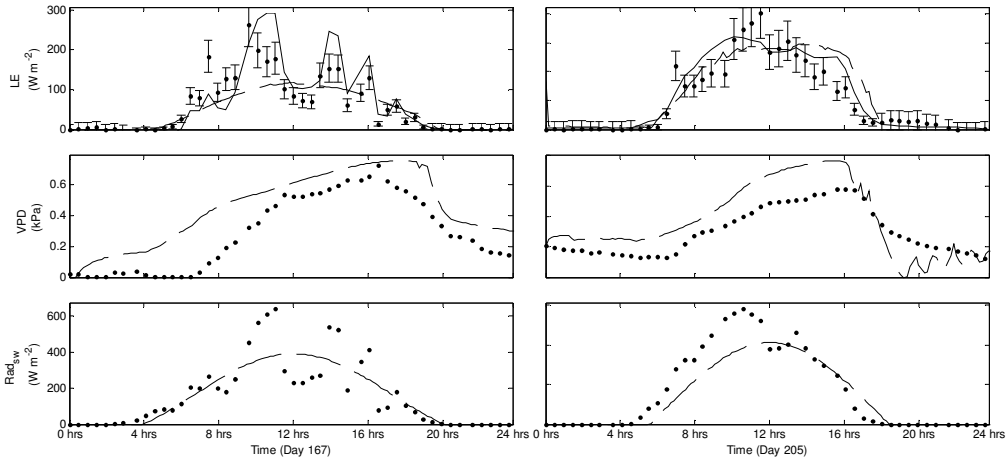

Figure 3: Half-hourly model estimates and measurements for the two study days, 167 and 250. Day 167 had 1.2 mm of precipitation before dawn. On Day 250 at 3 pm there was a 0.2 mm precipitation event. Measurements are shown as points (·····), random errors are estimated using the Hollinger approach [Hollinger and Richardson, 2005], systematic errors are set at 20% [Goulden, et al., 1996]. Biosphere model's estimate of LE is shown with a solid line (———). CAB model predictions of LE, VPD and RAD are indicated with a dashed line (— — —).

available for photosynthesis, while shading affects the balance between direct and diffuse radiation reaching the leaves. Both these effects have subsequent implications for the energy balance and evapotranspiration of the stand. Other canopy characteristics, including the LAI_H, were preserved at the nominal levels.

Model testing

Latent energy at the land-surface

The off-line biosphere model LE predictions were compared against measurements over a 120 day period from the 23rd of May to the 20th of September, 1994. Modelled daily LE compared favourably with the daily LE measurements from the SSA-OBS eddy-flux site (Figure 2). The R^2 value was 0.7 and the root mean square error (RMSE) was 1.19 MJ m^{-2} day^{-1}. The model captured the range and the dynamics of the measured LE, with the distribution of the residuals showing little structure. However, there was some correlation of LE and VPD (not shown); during periods of low VPD, simulated LE was lower than the measured (Figure 2's scatter plot). Low VPDs during the study period were often associated with precipitation, clouds and reduced PAR (not shown).

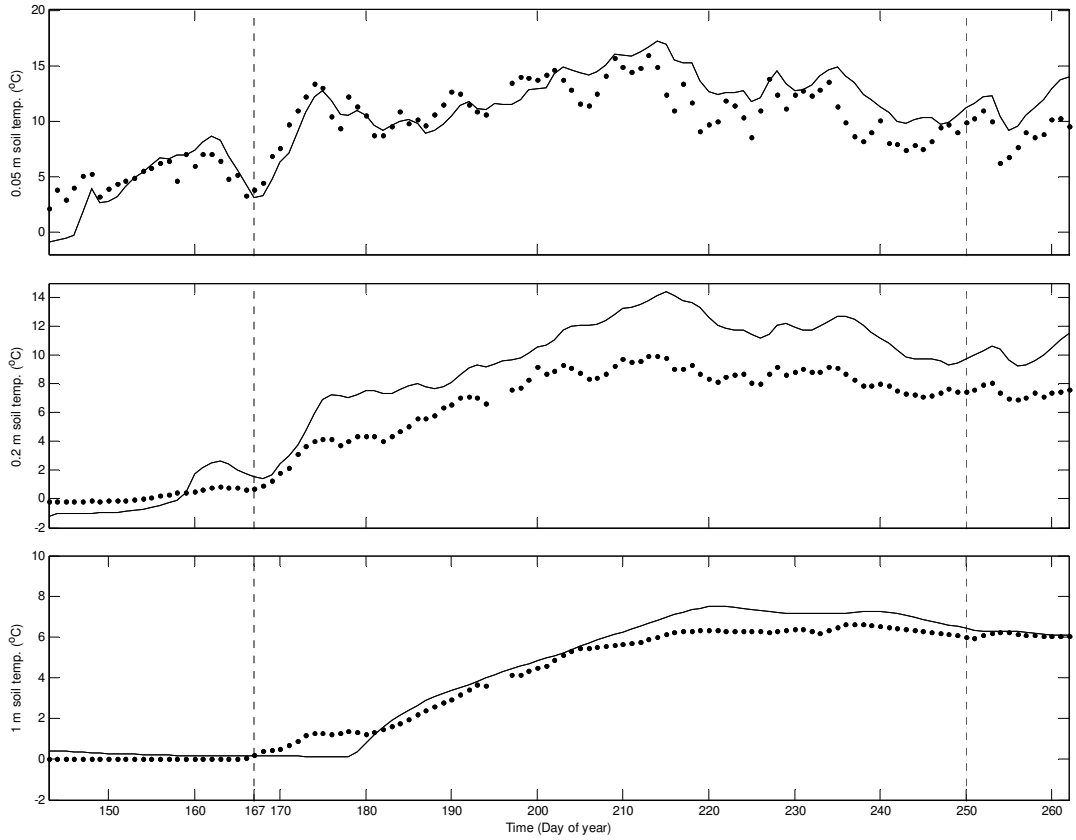

Figure 4: Modelled response of the off-line biosphere model (———) compared to the soil temperature measurements (·····) for the 1994 study period at the SSA-OBS site. Vertical dashed lines (- - - -) indicate the two test days.

Comparisons of the LE fluxes from both biosphere model and the eddy-flux measurements were performed on a half hourly time-step for days 167 and 250 (Figure 3). Modelled LE was compared to half-hourly LE measurements; the magnitudes of modelled and measured LE were in close agreement for both days. On day 167 the model captured the magnitude of fluctuations in measured LE, though there appeared to be a slight phase shift. Both days 167 and 250 showed a limited number of LE measurements which were greater than either the model, or surrounding measurements. Both days had a precipitation event; on day 167 the precipitation occurred pre-dawn, and on day 250 it occurred mid-afternoon. Radiation plots suggested intermittent clouds on both days, with day 167 having a greater frequency of cloudy periods.

Soil temperature

At the start of the study period, soils below the surface layer were at 0 °C (Figure 4). At the end of the study period, soil temperatures at a depth of 1 m had risen to 6 °C. Peak surface soil temperatures were in early August, with deepest layers lagging behind,

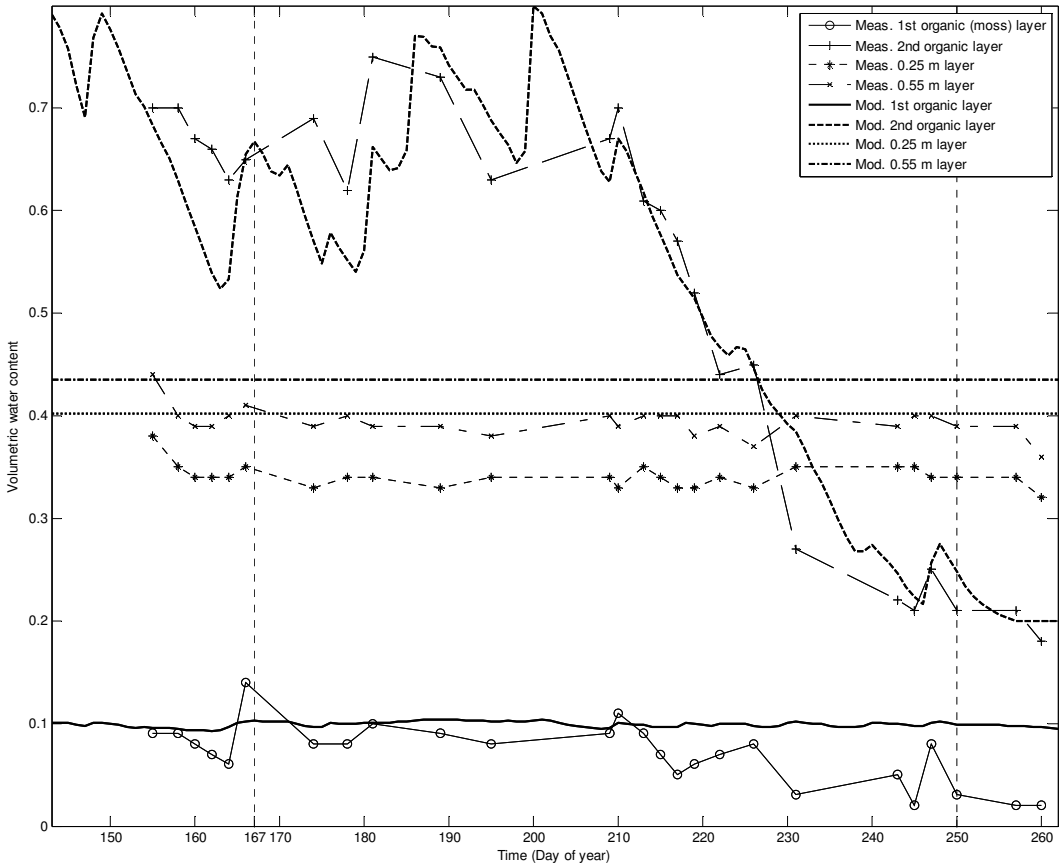

Figure 5: Modelled response of the off-line biosphere model, compared to the volumetric soil water measurements for the 1994 study period at the SSA-OBS site. Vertical dashed lines (- - - -) indicate the two test days.

reaching maximum temperatures by the end of August. Initially the modelled 0.05 m temperatures closely followed the measurements. After day 210, modelled 0.05 m soil temperatures were consistently higher than measured. 1 m temperature measurements agreed closely with the 1 m modelled soil layer. The greatest discrepancies were seen between the 0.2 m soil temperature measurements and the 0.2 m modelled layer, with the model consistently over-estimating soil temperature.

Soil moisture

The off-line biosphere model captured the general trends of the volumetric water content (Figure 5). Critically, the model captured the correct timing for the drying out of the organic layer. During the study period the soils below 0.2 m were largely saturated. Over the study, the model predicted consistently lower soil water content than the 0.25 m and 0.55 m soil layer measurements, and missed the slight drying observed in the surface layer.

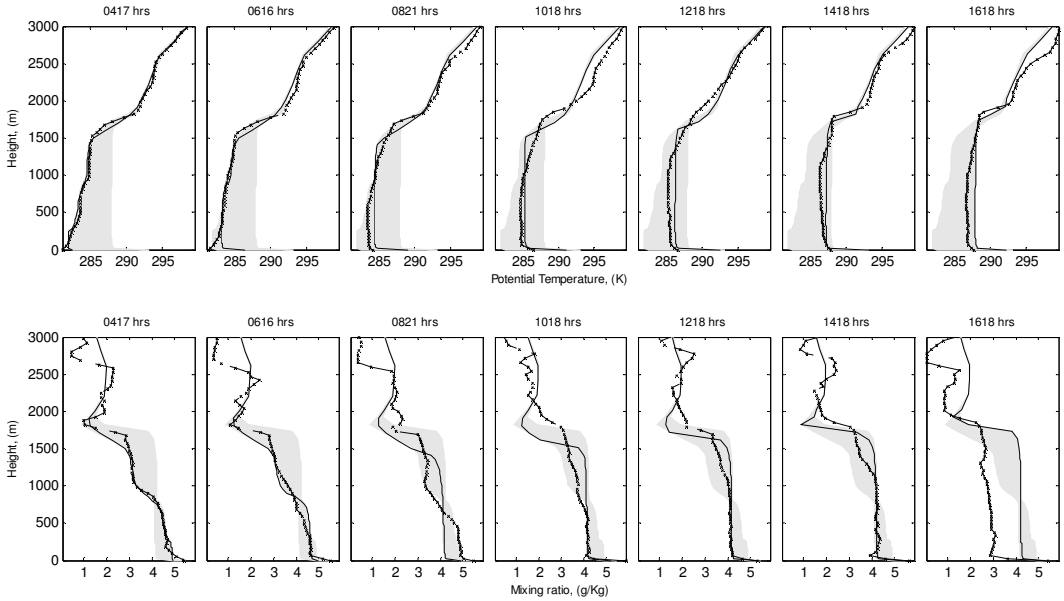

Figure 6: Modelled and measured boundary layer profiles of potential temperature and water mixing ratio for day 167, 1994. Radiosondes are released at approximately 2 hourly intervals during the each day; times are shown in local-time. The first profile in each day's measurement series is used to initialise the model. Measurements are shown as diagonal crosses and modelled data by solid lines. The grey shaded areas show the full area covered by the modelled profiles, and are presented here to provide a reference for the diurnal progression of the measured and modelled profiles.

Coupled atmosphere-biosphere model

CAB model simulations for days 167 and 250 compared well with data, with the exception of soil temperature at certain levels. The CAB model runs used parameterisations from the off-line SPA model, and were the tested above the canopy using surface fluxes of LE and above canopy measurements of VPD and radiation. CAB model predictions of atmospheric profiles were compared to radiosonde measurements of potential temperature and water mixing ratio (Figures 6 & 7).

At the land-surface, the CAB model explained the magnitude of the LE fluxes. Despite not capturing the short term variations in down welling radiation (on DoY 167), the CAB model simulated the daily mean radiation well. The model is a prognostic model, but is not designed to reproduce the periodicity of clouds, which cause variations in radiation on day 167. The diurnal profile of simulated LE flux responded to the radiation generated by the CAB model. Simulated VPD captured the diurnal trends, but was marginally higher than measured on both the test days. On day 250 there was an unexplained phase shift between modelled and measured radiation.

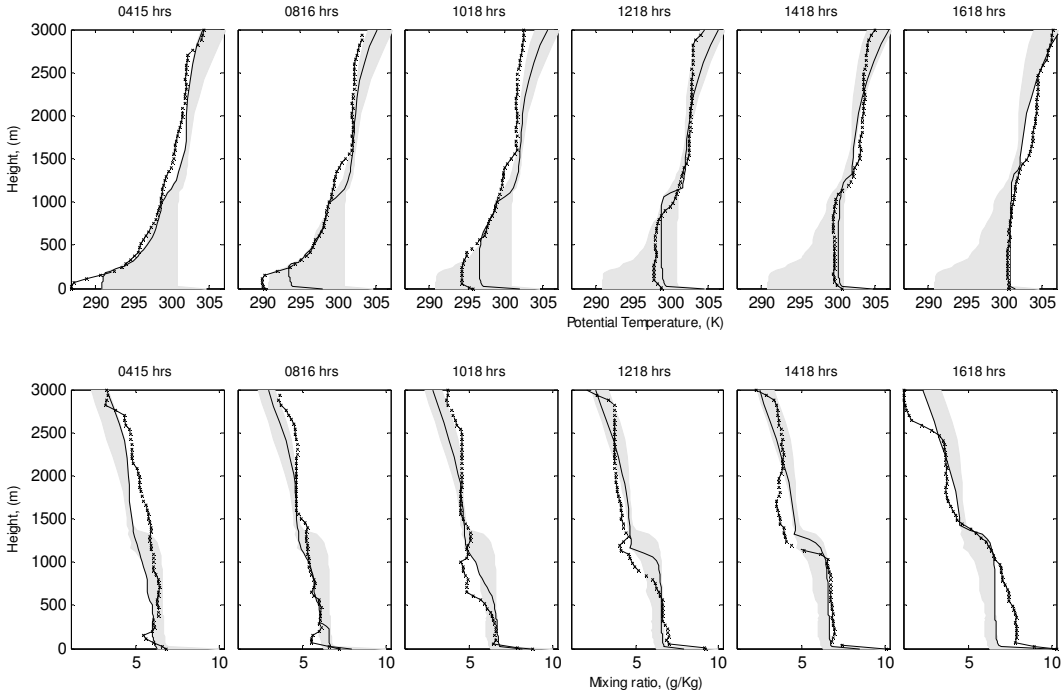

Figure 7: Modelled and measured boundary layer profiles of potential temperature and water mixing ratio for day 250, 1994. Radiosondes are released at approximately 2 hourly intervals during the each day; times are shown in local time. Note that there is no 6am radiosonde release. The first profile in each day's measurement series is used to initialise the model. Measurements are shown as diagonal crosses and modelled data by solid lines. The grey shaded areas show the full area covered by the modelled profiles and are presented here to provide a reference for the diurnal progression of the measured and modelled profiles.

Visual inspection of the simulated and measured profiles showed that the CAB model correctly evolved the boundary layer. The mixed layer potential temperature and water mixing ratios were also modelled accurately. The boundary layer top was correctly defined in the model, any errors between the model and the measured boundary layer depths were within the regional fluctuation shown by observation [*Davis, et al.*, 1997]. The 1600 hours profile of day 167 showed a uniform change in the mixing ratio of 1 g kg^{-1}, whilst also showing 0 g kg^{-1} at 2800 m. After an inspection of radiosonde data, local meteorological and synoptic weather conditions, nothing was found to explain the change in water mixing ratio, and so this profile was considered to be erroneous, and was excluded from the discussions. On day 250 the 0600 hours profile was not present due to computer failure at the time of launch.

Sensitivity Analysis

The coupled runs: With LAI reduced from 4.4 to 1, LE was reduced by 50%, the

atmosphere was 0.7 g kg^{-1} drier and 0.7 K warmer, and canopy conductance dropped 65%. Generally, the impact of decreasing LAI was greater than the impact of increasing LAI, which seemed to be tending toward an asymptote for infinite LAI. The response of the coupled system to LAI_H and LAI_R was similar to the system's response to combined LAI. However, changes to the mechanical roughness of the canopy had comparatively little impact on the system. If summed, the accumulated impact of the three components ($LAI_{H,}$ LAI_R and mechanical roughness) would have been greater than the impact of combined LAI.

The uncoupled runs: The uncoupled runs were generated by driving the biosphere model with the nominal meteorology, and showed very similar form but generally greater impacts than the coupled runs. The exception to this rule was the response of canopy conductance (for all but the LAI_H), where the uncoupled runs showed greater changes. The atmospheric temperature and water mixing ratio predicted by the uncoupled runs did not influence the model runs; rather they showed the meteorology that would have resulted from the forcing of the uncoupled vegetation. The difference between the uncoupled and coupled model runs is attributable to the feedbacks occurring between the atmosphere and biosphere.

Discussion

CAB offline and at the land surface

The CAB model has been corroborated at the land-surface, and throughout the boundary layer. The model demonstrated that it could coherently explain the coupled atmosphere-biosphere system, and ergo was suitable for investigating feedbacks in the coupled system. The biosphere model was entirely parameterised from measurement, with the exception of leaf capacitance and ι. Parameters were not tuned against eddy covariance data to obtain the best fit, allowing greater confidence to be placed in the model's ability to perform outside the range of measured parameters.

The offline biosphere model was tested against data from the full 120 day study period. Corroboration with daily flux data indicated that the biosphere model was capturing the majority of observations. However, at low LE fluxes the model was under predicting the LE flux, which we attribute to the moss under-story. At the SSA-OBS site, *Sphagnum* and feather moss made up a surface layer 0.1 m deep. Evaporation from mosses is not stomatally controlled, but rather is closer mechanistically to simple surface

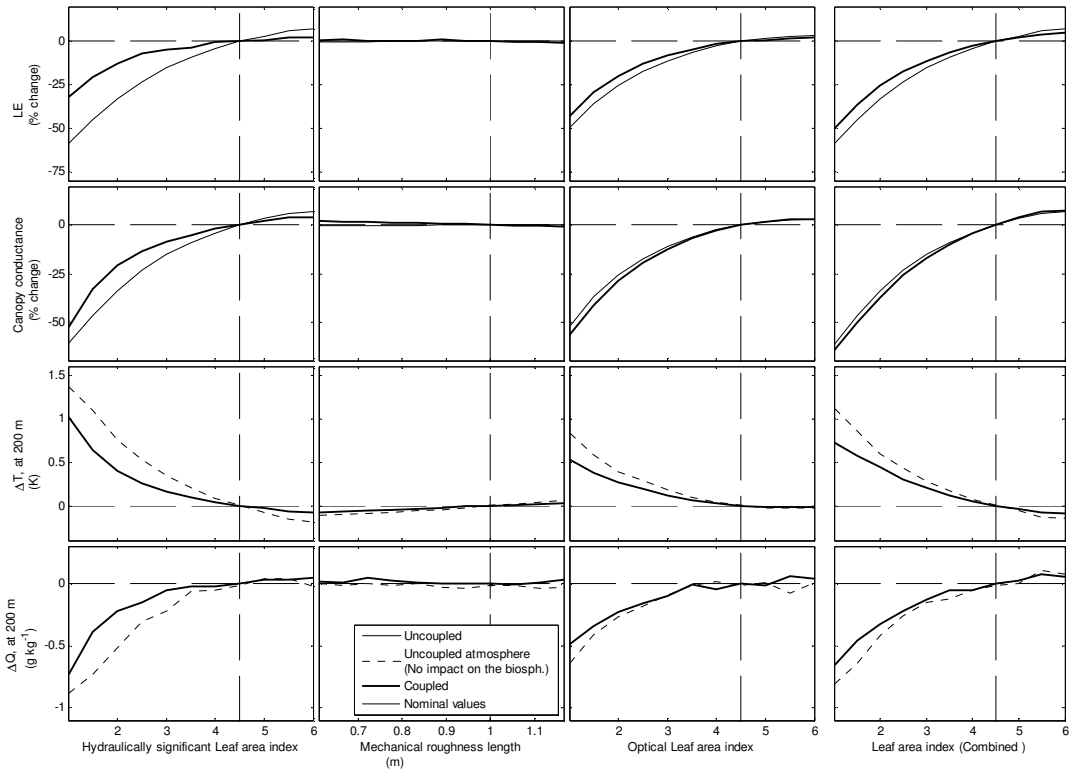

Figure 8: Sensitivity analysis showing the response of the coupled atmosphere-biosphere system to changes in LAI, for the two test days. Changes are shown as % or absolute differences from the nominal case. Physiological changes, resulting from combined LAI variations, have been split into the hydraulic, mechanical and radiative contributions. Combined LAI encompasses both radiative and hydraulic changes in LAI as well as changes in height and roughness length. The uncoupled runs are driven with the nominal meteorology, but for comparison purposes the uncoupled PBL is allowed to continue developing.

evaporation [*Betts, et al.*, 1999]. After precipitation, the moss layer acted as a large wetted surface from which evaporation could occur. However, the deviations of the biosphere model (at low LE fluxes) from the LE flux observations were not critical to the CAB model testing. The timing of the deviations was such that they did not occur when the criteria for suitable test days were fulfilled.

Soil moisture predictions were consistent with measurements over the whole study period (Figure 5). Differences in the modelled and measured volumetric water content at 0.25 m and 0.55 m depths were attributed to the approximate nature of the Saxton equations [*Saxton, et al.*, 1986], which were linked to soil sand, silt and clay percentages. These deviations were constant throughout the study period and, consequently the effect of these deviations was negligible on the LE fluxes.

Due to the increased simulated soil water content, and therefore soil thermal inertia, simulated soil temperatures might have been expected to increase more slowly than the measured soil temperatures. In fact the opposite was observed; the 0.2 m modelled soil temperatures increased more rapidly than the 0.2 m data. At some points, the measured 0.2 m soil temperature was more than 5 ^{o}C below the modelled 0.2 m layer. However, the soil energy balance can be seen to be adequate, as the off-line model was corroborated by the surface (0.05 m) and deep (1 m) soil temperature measurements.

Compared on a half-hourly time-step, the biosphere model reproduced all the essential detail in the LE flux measurements (Figure 5). Some individual flux measurements were not captured, but were viewed as perturbations from the main diurnal signal. Capturing all measurement spikes is not considered critical to the off-line model's ability to predict LE fluxes. We can be confident that with the local meteorology, we can adequately simulate LE fluxes at the SSA-OBS site for the purposes of the CAB model.

CAB at the atmosphere-biosphere interface

The CAB model simulations were broadly consistent with measurements at both the stand and PBL level (Figure 6 & 7). Some discrepancies existed between the model and the measurements during the transition between stable to unstable boundary conditions. In general these differences were small and/or expected. The area immediately surrounding the launch site was not representative of the rest of the region. The launch site, a 200 m wide grass clearing, was next to a small unnamed lake, beside Candle Lake. Low altitude radiosonde measurements were a reflection of the land cover at the radiosonde launch site, not the region as a whole.

In the CAB model the original OSU1DPBL model cloud routine was found to be unable to produce realistic cloud fractions, and was replaced with a fixed fraction for each day. As a result, the model was not expected to capture sporadic events such as cloud formation. Allowing for this, the CAB model was seen to reproduced the correct (albeit, smoothed) LE fluxes from the predicted radiation (Figure 3). From this we infer that the energy partitioning performed by SPA is adequate.

Can we identify feedbacks between the PBL and the biosphere, and what are their impacts on vegetation and PBL responses?

In order to identify feedbacks, we need to be able to distinguish between the response of coupled feedback systems, and uncoupled (driven) systems. We used a simple dual sensitivity analysis focusing on changes in combined LAI. The coupled runs (thick solid line, Figure 8) were compared to the uncoupled runs (thin lines). In the uncoupled runs, feedbacks were removed by driving the vegetation with a predetermined meteorology, from the nominal run. The result was that in the coupled runs, the vegetation at low combined LAIs responded to an atmosphere that was both drier and warmer than the nominal meteorology. Where as the uncoupled vegetation only ever saw the nominal meteorology. The differences between the two runs were due to the effects of feedbacks.

Comparing the coupled and uncoupled response to combined LAI showed that feedbacks between the atmosphere and biosphere have a moderating effect (i.e. a negative feedback, Figure 8). Changes to the LE, air temperature and mixing ratio of water were moderated by mean values of 22%, 37% and 27% respectively. The exception was canopy conductance, which the coupling increased by a mean of 7%. At low combined LAIs and in the uncoupled case, the biosphere was driven by the (relatively) cooler, more humid atmosphere of the nominal case. In the coupled case, the biosphere was responding to the warmer, drier atmosphere that was the result of reductions in combined LAI. The biosphere's response to the warmer, drier atmosphere was to constrict the spruce's stomata and reduce the canopy conductance. Despite the reduction in canopy conductance, the coupled biosphere actually transpired more, due to the higher atmospheric demand for water. This increase in transpiration was accompanied by higher LE fluxes and water mixing ratio, and a moderation of the impacts that LAI changes had on the coupled system.

What is the relative importance to the coupled system of changes to the hydraulic, mechanical, and radiative properties of the biosphere?

In the sensitivity analysis, the combined LAI was varied to investigate the impacts on the system. The analysis was then modified to separate the main contributing ecological factors.

1) *Hydraulic impacts:* LAI_H showed significant impacts on the coupled system (Figure 8). The uncoupled response was very similar to that of combined LAI. Low LAI_H restricted the vegetation's ability to transpire and resulted in a warming and drying of the atmosphere. The uncoupled runs 'saw' the nominal meteorology and did not respond to the atmospheric warming and drying. For the coupled runs, the high temperatures and drier air resulted in higher VPDs. Due to the high VPDs the latent energy flux increased, cooling and humidifying the atmosphere.

   LAI_H produced the only canopy conductance response that was more extreme for the uncoupled runs. The dynamic component of canopy conductance is largely determined the stomatal conductance. In the SPA model, the stomatal conductance is set at the highest level that increases the assimilation rate by over a certain threshold set by ι. In the case of the uncoupled runs, the system was not limited by light, or hydraulic conductance, but rather the atmospheric demand for water. Thus, increasing the stomatal conductance did not increase the assimilation rate and the stomatal conductance, and therefore the canopy conductance, was low. In the case of the coupled atmosphere the canopy conductance was higher because the atmospheric demand was greater. This allowed appreciable increases in carbon assimilation at higher values of stomatal conductance. Thus, the ι threshold was only reached at a higher stomatal conductance and the drop in stomatal conductance was less for the coupled run, than for the uncoupled run.

   Impacts of the LAI_H on the atmosphere were greater than for the combined LAI. This counter-intuitive result is accounted for by the mechanical roughness component. If the effects of roughness length are removed from the combined LAI, then the effect of changing the combined LAI is greater than that of just the LAI_H, as expected (not shown).

2) *Mechanical roughness impacts:* roughness length had the least impact on the coupled system (Figure 8). Impacts, although slight, were attributed to the effect of roughness length on turbulent mixing within the PBL. Greater roughness induced the surface layer to undergo more mixing with warmer, drier air from higher up in the PBL. It also caused the PBL to grow more, entraining the warm, dry air of the free atmosphere. The roughness length explained the higher impact of the LAI_H compared to the combined LAI, and so might be an important consideration, but only in certain circumstances.

3) *Radiative impacts:* LAI_R had strong impacts on the coupled system, initiating feedbacks between the atmosphere and the stomata (Figure 8). Responses to LAI_R were very similar in form and magnitude to the impact of combined LAI. The responses were due to altered absorption of radiation, resulting in lower LE fluxes, more sensible heating and greater atmospheric temperatures.

The response to both the LAI_H and LAI_R was very similar in magnitude to that of the combined LAI, and both have to be considered as important. This suggests that both LAI_H and LAI_R are independent and their effects are limiting under different conditions. Thus we would expect a severe drought to have a similar impact potential on the system to that of clear felling.

Conclusions

Our biosphere model was verified by long-term datasets and was shown to accurately simulate biosphere processes. Fluxes were correctly represented on both daily and half-hourly time scales. At the daily time step, days with low LE flues were underestimated by the model. These underestimations were attributed to the thick layer of moss at the study site, and the moisture representation in the model of the surface soil layer. These underestimations were not critical to the CAB model, as the test day criteria were not fulfilled for the low LE days. Soil moisture and temperature records also corroborated the model predictions. Flux data were not used to tune the SPA model and this added confidence in the model's prognostic abilities. The CAB model's deviations from the observed boundary layer inversions were less than the variation seen over the boreal forest.

We have shown that strong feedbacks occur between the atmosphere and biosphere. Predominately these occur via the response of the vegetation to atmospheric demands. The feedbacks tend to moderate the impacts that ecological changes have on the system. As expected, reductions in the vegetation cover tend to increase the partitioning into sensible heat, reducing the latent heat flux, drying and heating the atmosphere. Calculating these effects without accounting for the effect of the vegetation's response to the changing atmospheric conditions will lead to predictions that are too extreme.

This study has shown that the CAB model to be a suitable tool for investigating the coupled atmosphere-biosphere system on short timescales. However, there is

substantial room for improvement of the model. The CAB model does not capture the variability in meteorology due to cloud formation/dissipation, or the changing of synoptic weather conditions. Two possible routes are suggested to overcome these obstacles: (1) nest the CAB model within reanalyses of weather systems. (2) Implement a data assimilation routine to improve simulation of the PBL over longer periods of time. It should be noted that the two suggestions are not mutually exclusive. The model provides the framework for simulating other tracer gases in the lower atmosphere, such as CO_2, and stable isotopes. Finally, the model runs sufficiently quickly to allow implementation of numerically intensive modelling methods (e.g. inversions and data assimilation). In particular, Bayesian inversions of the model could provide a powerful means of investigating the interdependence of the model with its parameterisations and measurements.

References

Anderson, D. W. (2000), "General Soil Survey for Primary Sites in SSA (OA, OBS, OJP, YJP, Fen)." In Collected Data of The Boreal Ecosystem-Atmosphere Study., edited by J. Newcomer, et al.

Baldocchi, D., et al. (2000), Climate and vegetation controls on boreal zone energy exchange, *Global Change Biology*, *6*, 69-83.

Barr, A., and C. Hrynkiw (2000), BOREAS AFM-5 Level-1 Upper Air Network Data, Volume 8, NASA.

Barr, A. a. A. B. (2000), "Upper-Air Network (AFM-05) Boundary Layer Research For BOREAS (AFM-08)." In Collected Data of The Boreal Ecosystem-Atmosphere Study., edited by J. Newcomer, et al.

Barr, A. G., et al. (1997), Comparison of regional surface fluxes from boundary-layer budgets and aircraft measurements above boreal forest, *Journal of Geophysical Research-Atmospheres*, *102*, 29213-29218.

Betts, A. K., and J. H. Ball (1997), Albedo over the boreal forest, *Journal of Geophysical Research-Atmospheres*, *102*, 28901-28909.

Betts, A. K., et al. (2001), Near-surface climate in the boreal forest, *Journal of Geophysical Research-Atmospheres*, *106*, 33529-33541.

Betts, A. K., et al. (1999), Controls on evaporation in a boreal spruce forest, *Journal of Climate*, *12*, 1601-1618.

Bonan, G. B., and H. H. Shugart (1989), Environmental-Factors and Ecological Processes in Boreal Forests, *Annual Review of Ecology and Systematics*, *20*, 1-28.

Chen, J. M., et al. (1997), Leaf area index of boreal forests: Theory, techniques, and measurements, *Journal of Geophysical Research-Atmospheres*, *102*, 29429-29443.

Cionco, R. M. (1985), The forest-atmosphere interaction : Modeling windfields and surface layer wind profiles over complex terrain and within vegetative canopies., edited by B. A. Hutchison and B. B. Hicks, pp. 501-520, D. Reidel, Dordrecht.

Cox, P. M., et al. (2000), Acceleration of global warming due to carbon-cycle feedbacks in a coupled climate model (vol 408, pg 184, 2000), *Nature*, *408*, 750-750.

Crossley, J. F., et al. (2000), Uncertainties linked to land-surface processes in climate change simulations, *Climate Dynamics*, *16*, 949-961.

Cuenca, R. H. (2000), "Coupled Atmosphere-Forest Canopy-Soil Profile Monitoring and Simulation." In Collected Data of The Boreal Ecosystem-Atmosphere Study., edited by J. Newcomer, et al.

Cuenca, R. H., et al. (1997), Soil water balance in a boreal forest, *Journal of Geophysical Research-Atmospheres*, *102*, 29355-29365.

Davis, K. J., et al. (1997), Role of entrainment in surface-atmosphere interactions over the boreal forest, *Journal of Geophysical Research-Atmospheres*, *102*, 29219-29230.

Denning, A. S., et al. (2003), Simulated variations in atmospheric CO2 over a Wisconsin forest using a coupled ecosystem-atmosphere model, *Global Change Biology*, *9*, 1241-1250.

Desborough, C. E., et al. (2001), Surface energy balance complexity in GCM land surface models. Part II: coupled simulations, *Climate Dynamics*, *17*, 615-626.

Engel, V. C., et al. (2002), Forest canopy hydraulic properties and catchment water balance: observations and modeling, *Ecological Modelling*, *154*, 263-288.

Environment Canada (2004), Monthly Data Report for 1994, edited, Environment Canada.

Essery, R. L. H., et al. (2003), Explicit representation of subgrid heterogeneity in a GCM land surface scheme, *Journal of Hydrometeorology*, *4*, 530-543.

Ewers, B. E., et al. (2005), Effects of stand age and tree species on canopy transpiration and average stomatal conductance of boreal forests, *Plant Cell and Environment*, *28*, 660-678.

Farquhar, G. D., and S. Craemmerer (1982), Modelling of photosynthetic response to the environment., in *Physiological plant ecology II* edited by O. L. Lange, et al., pp. 549-587, Springer-Verlag, Berlin ; New York.

Fisher, R. A., et al. (2006), Evidence from Amazonian forests is consistent with isohydric control of leaf water potential, *Plant Cell and Environment*, *29*, 151-165.

Foley, J. A., et al. (2000), Incorporating dynamic vegetation cover within global climate models, *Ecological Applications*, *10*, 1620-1632.

Goulden, M. L., et al. (1996), Measurements of carbon sequestration by long-term eddy covariance: Methods and a critical evaluation of accuracy, *Global Change Biology*, *2*, 169-182.

Guichard, F., et al. (2004), Modelling the diurnal cycle of deep precipitating convection over land with cloud-resolving models and single-column models, *Quarterly Journal of the Royal Meteorological Society*, *130*, 3139-3172.

Hollinger, D. Y., and A. D. Richardson (2005), Uncertainty in eddy covariance measurements and its application to physiological models, *Tree Physiology*, *25*, 873-885.

Holtslag, A. A. M., et al. (1990), A High-Resolution Air-Mass Transformation Model for Short-Range Weather Forecasting, *Monthly Weather Review*, *118*, 1561-1575.

Holtslag, A. A. M., and M. Ek (1996), Simulation of surface fluxes and boundary layer development over the pine forest in HAPEX-MOBILHY, *Journal of Applied Meteorology*, *35*, 202-213.

Holtslag, A. A. M., and A. P. Vanulden (1983), A Simple Scheme for Daytime Estimates of the Surface Fluxes from Routine Weather Data, *Journal of Climate and Applied Meteorology*, *22*, 517-529.

Houghton, J. T. (2001), Climate change 2001 : the scientific basis, x, 881 p.

Jacobs, C. M. J., and H. A. R. de Bruin (1997), Predicting regional transpiration at elevated atmospheric CO2: Influence of the PBL-vegetation interaction, *Journal of Applied Meteorology*, *36*, 1663-1675.

Jarvis, P. G., et al. (1997), Seasonal variation of carbon dioxide, water vapor, and energy exchanges of a boreal black spruce forest, *Journal of Geophysical Research-Atmospheres*, *102*, 28953-28966.

Jarvis, P. G., and J. B. Moncrieff (2000), "The CO2 Exchanges of Boreal Black Spruce Forest." In Collected Data of The Boreal Ecosystem-Atmosphere Study., edited by J. Newcomer, et al.

Jones, H. G. (1992), *Plants and microclimate : a quantitative approach to environmental plant physiology*, 2nd ed., xxiv, 428 p. pp., Cambridge University Press, Cambridge [England] ; New York.

Lee, Y. H., and L. Mahrt (2004), Comparison of heat and moisture fluxes from a modified soil-plant-atmosphere model with observations from BOREAS, *Journal of Geophysical Research-Atmospheres*, *109*, -.

Louis, J. F. (1979), Parametric Model of Vertical Eddy Fluxes in the Atmosphere, *Boundary-Layer Meteorology*, *17*, 187-202.

Mahrt, L., and H. Pan (1984), A 2-Layer Model of Soil Hydrology, *Boundary-Layer Meteorology*, *29*, 1-20.

Miller, J. R., et al. (1997), Seasonal change in understory reflectance of boreal forests and influence on canopy vegetation indices, *Journal of Geophysical Research-Atmospheres*, *102*, 29475-29482.

Monteith, J. L. (1965), Evaporation and Environment, in *Symposia of the Society for Experimental Biology ; no.19*, edited, pp. 205-234, University Press, Cambridge.

Murthy, B. S., et al. (2004), Interactions of the land-surface with the atmospheric boundary layer: case studies from LASPEX, *Current Science*, *86*, 1128-1134.

Nemati, M. R., et al. (2002), Determining air entry value in peat substrates, *Soil Science Society of America Journal*, *66*, 367-373.

Newcomer, J., et al. (2000), Collected Data of The Boreal Ecosystem-Atmosphere Study. NASA., edited.

Penman, H. L. (1948), Natural Evaporation from Open Water, Bare Soil and Grass, *Proceedings of the Royal Society of London Series a-Mathematical and Physical Sciences*, *193*, 120-&.

Rayment, M. B., et al. (2002), Photosynthesis and respiration of black spruce at three organizational scales: shoot, branch and canopy, *Tree Physiology*, *22*, 219-229.

Ryan, M. G. (2000), Introduction to BOREAS special issue, *Tree Physiology*, *20*, 709-711.

Saxton, K. E., et al. (1986), Estimating Generalized Soil-Water Characteristics from Texture, *Soil Science Society of America Journal*, *50*, 1031-1036.

Schwarz, P. A., et al. (2004), Climatic versus biotic constraints on carbon and water fluxes in seasonally drought-affected ponderosa pine ecosystems, *Global Biogeochemical Cycles*, *18*, -.

Stull, R. B. (1988), *An introduction to boundary layer meteorology*, Kluwer Academic Publishers, Dordrecht ; Boston.

Troen, I., and L. Mahrt (1986), A Simple-Model of the Atmospheric Boundary-Layer - Sensitivity to Surface Evaporation, *Boundary-Layer Meteorology*, *37*, 129-148.

Van Wijk, M. T., et al. (2003), Interannual variability of plant phenology in tussock tundra: modelling interactions of plant productivity, plant phenology, snowmelt and soil thaw, *Global Change Biology*, *9*, 743-758.

Wijk, W. R. v. (1963), *Physics of plant environment*, xvi, 382 p pp., North-Holland Pub. Co., Amsterdam.

Williams, M. (2005), The Soil-Plant-Atmosphere model: Manual, version 1.2, April 2005, edited, p. 32, University of Edinburgh.

Williams, M., et al. (2000), The controls on net ecosystem productivity along an Arctic transect: a model comparison with flux measurements, *Global Change Biology*, *6*, 116-126.

Williams, M., et al. (2001), Use of a simulation model and ecosystem flux data to examine carbon-water interactions in ponderosa pine, *Tree Physiology*, *21*, 287-298.

Williams, M., et al. (1997), Predicting gross primary productivity in terrestrial ecosystems, *Ecological Applications*, *7*, 882-894.

Williams, M., et al. (1996), Modelling the soil-plant-atmosphere continuum in a Quercus-Acer stand at Harvard forest: The regulation of stomatal conductance by light, nitrogen and soil/plant hydraulic properties, *Plant Cell and Environment*, *19*, 911-927.

Paper 2: Testing the carbon, water and energy flux predictions of a coupled atmosphere-biosphere model above a boreal forest.

T.C. Hill[1,3], M. Williams[1,3], F. I. Woodward[1,2] and J. B. Moncrieff[1,3]

[1]School of GeoSciences and NERC Centre for Terrestrial C Dynamics, Crew Building, University of Edinburgh, EH9 3JN, UK

[2]Department of Animal & Plant Sciences, University of Sheffield, Sheffield, S10 2TN, UK

[3]NERC Centre for Terrestrial C Dynamics, UK

(Intended for submission to the Journal of Geophysical Research)

Abstract

Biogeochemical and biogeophysical feedbacks between the biosphere and atmosphere are expected to play a critical role in the future carbon cycle. Attempts at quantifying these interactions use both top-down (global inversions) and bottom-up (site or species specific) approaches. The two methods examine the same system, but on vastly different spatial and temporal scales. Consolidating these two approaches is a difficult, but important task. Combining both measurements and models of the planetary boundary layer provides one possible method of drawing the two approaches together. The planetary boundary layer has a footprint, and thus an integrating scale, which can be on the order of ~1-100 km. Investigating the planetary boundary layer and its interactions with the biosphere, potentially bridges the gap in scales between regional atmospheric and stand-based measurements.

In this paper we show how the carbon dynamics of the biosphere and the atmosphere can be captured by a coupled model. The coupled atmosphere-biosphere model is shown to be consistent with both planetary boundary layer observations and stand-based land surface measurements, both of which came from the Boreal Ecosystem-Atmosphere Study (BOREAS). We then use the coupled atmosphere-biosphere model to show the strength of different feedbacks between the atmosphere and biosphere: (1) atmospheric CO_2 concentrations at the land surface have a strong diurnal signal, driven by the net ecosystem exchange and the rectifier effect. Diurnal changes in CO_2 concentration initiate feedbacks between the daytime uptake of CO_2 by the vegetation, and the concentration of atmospheric CO_2. However, we show that the diurnal feedback involving the atmospheric CO_2 concentration is weak, reducing gross primary productivity by less than 0.3%. (2) Hydrological feedbacks between the atmosphere and biosphere are strong, with impacts on the latent energy heat flux and gross primary production reaching 5% and 2% respectively. The feedbacks occur due to changes in transpiration and energy partitioning at the land surface, and the modification of planetary boundary layer dynamics.

Introduction

Determining how climatic and anthropogenic forcings affect ecosystem processes is critical for predicting future changes in the carbon (C) cycle. Many different approaches are being used to constrain C flux estimates of ecosystems, and improve the understanding of the processes behind them [*Running, et al.*, 1999]. Generally, approaches are split into top-down and bottom-up methodologies. Top-down approaches, such as general circulation models (GCMs) and inversion models, are used to infer ecological impacts and responses on a global scale from satellite reflectance observations/products and flask data [*Lawrence and Slingo*, 2004]. Bottom-up approaches use physiological measurements, and networks of eddy covariance towers (such as FLUXNET [*Baldocchi, et al.*, 2001]) to study the ecological responses at the site or stand level (spatial scale <2 km) [*Baldocchi, et al.*, 2001; *Houghton*, 2003; *Schmid*, 1994].

Both the top-down and bottom-up techniques are powerful tools for improving knowledge about the C cycle. However, comparing the two approaches remains a difficult task, due to the mismatch in the spatial and temporal scales resolution of the methods. It is possible that the two methodologies will never be fully compatible due to fundamental differences between top-down and bottom-up approaches and the practical limitations to sampling [*Houghton*, 2003]. However, it remains an important task to try to unite the two approaches, as many uncertainties about the future climate result from the knowledge gap between the global and the fine-scale.

Measurements in the planetary boundary layer (PBL) can be used as an intermediary between the top-down and bottom-up approaches [*Shuttleworth*, 1991]. Strong daytime mixing within the PBL results in atmospheric PBL measurements integrating over a much larger land area than the footprint of a flux tower. Depending on the region and characteristics of the PBL, the region of integration can be on the order of ~1-100 km [*Kljun, et al.*, 2004]. The land surface and the PBL are a tightly coupled system, and relating atmospheric measurements to stand-based measurements requires a detailed knowledge of both systems and how they interact.

Understanding the interactions between the physical processes operating at the atmospheric-level, and processes at the ecosystem-level is nontrivial. PBL dynamics change rapidly, driven by solar radiation and land surface fluxes, but are also impacted by past events. Weather systems, and the fronts associated with them, force the PBL

into totally new states. Additionally, ecosystem processes occur on a wide range of temporal scales. Rates of photosynthesis respond almost instantaneously to changes in meteorological conditions, such as incident photosynthetically active radiation (PAR). The response of vegetation is also subject to seasonal changes in meteorology, soil water and plant physiology; dry soils may prompt drought responses in the vegetation. Additionally, photosynthesis is linked to the C cycle by the rates of carboxylation and diffusion, which are dependant on the atmospheric concentration of CO_2. Consequently, the limits placed on photosynthesis by these rates will likely change with future changes in CO_2 concentration.

To capture land-atmosphere feedbacks, a process-based modelling scheme needs to be implemented and systematically tested on scales applicable to both the systems. In particular it is vital to understand the feedbacks involving fluxes of water, energy and CO_2, as these fluxes provide the most dynamic links between the biosphere, atmosphere and climate.

Terrestrial ecosystem models (TEMs) have successfully modelled C cycling in the biosphere for several years, e.g. *Williams* [1996]. We show that these ecosystem models can be integrated into a coupled atmosphere-biosphere (CAB) model. The CAB model couples the process-based Soil-Plant-Atmosphere (SPA) model [*Williams, et al.*, 1996] and the Oregon State University One-Dimensional Planetary Boundary Layer (OSU1DPBL) model [*Mahrt and Pan*, 1984; *Troen and Mahrt*, 1986]. Respiration fluxes are dealt with separately in a simple C-pool model based on the box model within the data assimilation linked ecosystem model (DALEC), [*Williams, et al.*, 2005].

In a previous study it was demonstrated that the dynamics of the PBL could be coupled to a process-based vegetation model [*Hill, et al.*, 2007]. In this paper we aim to enhance this model, by including C cycling into the modelling framework. This addition will provide increased confidence in the model (more constraints on the system), and greater functionality (C modelling applications).

We parameterise and run the CAB model for the two sites used in the 1994 boreal ecosystems atmosphere study (BOREAS) project [*Sellers, et al.*, 1997]. CAB model results were verified using eddy covariance data and atmospheric measurements of mixing ratio, temperature and CO_2 concentration at and above these two sites. The sites were chosen on the basis of the good availability of above ground, below ground, eddy covariance and PBL datasets, and the importance of the boreal forest to the global C

cycle: Boreal forests cover 11% of the Earth's land surface [*Bonan and Shugart*, 1989], and thus are a significant component of the global C cycle.

Water transport and C uptake in plants are linked by mechanisms such as the regulation of photosynthesis and evapotranspiration by stomatal conductance. In this study, we aim to show that these aspects of the C cycle can be coherently included in the coupled atmosphere-biosphere framework. We use a set of model runs to test; (1) the importance of the diurnal CO_2 concentration cycle at the land surface, and (2) the overall impact of feedbacks between the atmosphere and ecosystem. How much do the atmospheric modifications resulting from the presence of vegetation, affect energy portioning and C uptake?

Finally, we suggest that a corroborated atmosphere-biosphere model capable of capturing C dynamics is suitable for use in a number of inversion and data assimilation applications.

Data description

The datasets used for the running and corroboration of the model were taken from/above two sites, both in Saskatchewan, Canada, which were part of the BOREAS field campaign of 1994. The two sites were approximately 500 km apart; mature black spruce (*Picea mariana*) was the dominant species at both sites. Sites were chosen due to the close proximity of flux towers to atmospheric profile measurements of the PBL. Eddy flux measurements were used to verify the land surface scheme, and aircraft measurements to corroborate the coupled model. The values and ranges used for the southern study area old black spruce (SSA-OBS) site can be found in paper 1 [*Hill, et al.*, 2007] and for the northern study area old black spruce (NSA-OBS) site in Table 1.

Eddy-flux data

The two sites, the SSA-OBS, and the NSA-OBS, both had eddy covariance flux systems, and extensive soil and ecological datasets. Key aspects of these datasets are described in paper 1 [*Hill, et al.*, 2007] and later in this paper. Flux data were chosen for periods when the black spruce was photosynthetically active and data availability was good.

For the SSA-OBS site, the chosen period covered 120 days from the 23rd of May (DoY 143) to the 19th of September (DoY 262). At the start of this period, soil was frozen between depths of 0.25 m and 0.40 m. Eddy covariance instrumentation was

mounted on a 27 m tower, with an effective fetch of approx 1200 m in all directions [*Jarvis, et al.*, 1997; *Jarvis and Moncrieff*, 2000; *Newcomer, et al.*, 2000]. Canopy height surrounding the tower was 10-11 m, with an average leaf area index (LAI) of 4.4 [*Chen, et al.*, 1997]. The surrounding canopy was dominated by black spruce, with the addition of ~10% tamarack (*Larix laricina*). Energy closure at the site was good, with residuals of 3% [*Jarvis, et al.*, 1997].

The chosen NSA-OBS study period was also 120 days long, from the 31st of May (DoY 151) till the 27th of September (DoY 270). Soil temperature data was not

Altitude	259	m	-	Newcomer et al. (2000)
Biosphere parameters				
Leaf Area Index (LAI)	5.3	$m^2 m^{-2}$ *ground area*	-	Chen et al. (1997)
Total Foliar Nitrogen (FN)	9.3	g m-2 *leaf area*	-	Rayment et al. (2002)
Maximal velocity of carboxylation (Vc_{max})	11	$\mu mol\ CO_2\ m^{-2}\ s^{-1}$	Calibrated on DOY 160	Rayment et al. (2002)
Maximal electron transport rate (J_{max})	31.3	$\mu mol\ e^-\ m^{-2}\ s^{-1}$	Calibrated on DOY 160	Rayment et al. (2002)
Plant hydraulic conductance	6	$mmol\ m^{-1}\ s^{-1}\ MPa^{-1}$	Calibrated using the hydraulic conductance per leaf area (KL)	Ewers et al. (2005)
Minimum Leaf Water Potential	-1.5	Mpa	-	Ewers et al. (2005)
Leaf capacitance	2000	$mmol\ m^{-2}\ s^{-1}$	-	Williams (2005)
Water use efficiency (Iota)	1.0085	-	-	Williams (2005)
Root Resistance	150	$MPa\ s\ g\ mmol^{-1}$	Calibrated using KL	Ewers et al. (2005)
Tower Height	31	m	-	Jarvis et al. (1997)
PAR leaf reflectance	0.11	-	Tuned	Betts et al. (1997), Baldocchi et al. (2000)
PAR leaf transmission	0.16	-	Tuned	Betts et al. (1997), Baldocchi et al. (2000)
NIR leaf reflectance	0.43	-	Tuned	Betts et al. (1997), Baldocchi et al. (2000)
NIR leaf transmission	0.26	-	Tuned	Betts et al. (1997), Baldocchi et al. (2000)
Below ground distributions				
Organic Fraction	0.0 / 0.5	-	-	Anderson et al (2000), Saxton et al. (1986)
Mineral Fraction	0.0 / 0.5	-	-	Anderson et al (2000), Saxton et al. (1986)
Water/Ice Fraction	0.02 / 0.75	-	-	Cuenca et al. (1997), Cuenca et al. (2000)
Soil Temperature	(-0.2 / 29.4)	°C	-	Jarvis et al. (1997), Jarvis et al. (2000)
Fine root distribution	0.0 / 0.3	m	-	Steele et al. (1997)
Fine Root Biomass	591	$g\ m^{-2}$	-	Steele et al. (1997)
Sand fraction	0.65 / 0.90	-	-	Anderson et al (2000)
Clay fraction	0.10 / 0.15	-	-	Anderson et al (2000)
Silt fraction	0.00 / 0.26	-	-	Anderson et al (2000)
Atmospheric parameters				
Air Temperature (above canopy)	-10.8 / 29.4	°C	-	Jarvis et al. (1997), Jarvis et al. (2000)
VPD (above canopy)	0.0 / 3.11	kPa	-	Jarvis et al. (1997), Jarvis et al. (2000)
PAR (above canopy)	0 / 2277	$\mu mol\ m\text{-}2\ s^{-1}$	-	Jarvis et al. (1997), Jarvis et al. (2000)
Wind Speed (above canopy)	0.0 / 9.0	$m\ s^{-1}$	-	Jarvis et al. (1997), Jarvis et al. (2000)
Precipitation	0 / 33	$mm\ d^{-1}$	-	Jarvis et al. (1997), Jarvis et al. (2000)
Roughness length (Zo)	1	m	-	Holtslag et al. (1983)
Albedo	0.093	-	-	Betts et al. (1997), Baldocchi et al. (2000)
Fractional cloud cover	0 / 0.7	-	-	Jarvis et al. (1997), Jarvis et al. (2000)
Horzontal Wind Speed (u & v)	0.0 / 5.8 (DoY 167)	$m\ s^{-1}$	-	Barr et al. (2000), Barr et al. (2000), Barr et al. (1997)
	0.0 / 8.8 (DoY 250)	$m\ s^{-1}$	-	Barr et al. (2000), Barr et al. (2000), Barr et al. (1997)
Potential temperature (0 - 3000m)	282.1 / 294.1 (DoY 167)	K	-	Barr et al. (2000), Barr et al. (2000), Barr et al. (1997)
	286.7 / 302.1 (DoY 250)	K	-	Barr et al. (2000), Barr et al. (2000), Barr et al. (1997)
Mixing Ratio (0 - 3000m)	1.0 / 5.4 (DoY 167)	$g\ kg^{-1}$	-	Barr et al. (2000), Barr et al. (2000), Barr et al. (1997)
	4.7 / 6.9 (DoY 250)	$g\ kg^{-1}$	-	Barr et al. (2000), Barr et al. (2000), Barr et al. (1997)
Soil carbon parameters				
t1 - Litter decomposition rate constant	0.0000044	$gC\ m^{-2}\ d^{-1}$	Fitted within range	Williams et al. (2005)
t2 - Autotrophic Repsiration (Frac GPP)	0.5	-	Fitted within range	Williams et al. (2005)
t3 - Frac NPP allocated to Foliage	0.08	-	total above+belowNPP	Jarvis et al. (1997), Gower et al (1997)
t4 - Frac NPP allocated to fine roots	0.47	-	total above+belowNPP	Jarvis et al. (1997), Gower et al (1997)
t5 - Turnover rate Foliage	0.0005	$gC\ m^{-2}\ d^{-1}$	Fitted within range	Williams et al. (2005)
t6 - Turnover rate woody matter	0.0001	$gC\ m^{-2}\ d^{-1}$	Fitted within range	Williams et al. (2005)
t7 - Turnover rate fine roots	0.00007	$gC\ m^{-2}\ d^{-1}$	1.5/365	Steele et al. (1997)
t8 - Mineralization rate fresh litter	0.0015	$gC\ m^{-2}\ d^{-1}$	Fitted within range	Williams et al. (2005)
t9 - Mineralization rate Soil org matter + woody debris	0.000023	$gC\ m^{-2}\ d^{-1}$	Fitted within range	Williams et al. (2005)
Cf - folige	556	$gC\ m^{-2}$	fresh+old+understory	Gower et al. (1997)
Cw - Wood (stems + coarse roots)	5985	$gC\ m^{-2}$	stem / trunk + live coarse rootmass	Steele et al. (1997), Gower et al. (1997)
Cr - fine roots	591	$gC\ m^{-2}$	-	Steele et al. (1997)
Clit - fresh foliar and fine root litter	363.6	$gC\ m^{-2}$	dead fine roots+liter	Gower et al. (1997), Nakane et al. (1997)
Csom - soil Org Matter + woody debris	20616	$gC\ m^{-2}$	-	Gower et al. (1997), Savage et al. (1997)
Tresponse	0.79	-	-	Williams et al. (2005)

Table 1: NSA-OBS site model parameters are taken directly from the literature unless otherwise stated.

available at the start of this period, but it took until DoY 191 before the whole profile was unfrozen. A 31 m tall tower carried the instrumentation [*Goulden, et al.*, 1997; *Newcomer, et al.*, 2000; *Wofsy, et al.*, 2000]. Black spruce was the dominant vegetation for several kilometres around the site, which was largely level. However, small changes in the topography resulted in significant changes in the vegetation. Higher ground was dominated by 10 m tall black spruce, with an under-story of sparse shrubs and continuous feather moss. Lower areas were vegetated by sparse black spruce up to 6 m in height, with a continuous layer of *Sphagnum* moss. Average LAI at the site was 5.6 [*Chen, et al.*, 1997]. Large gaps within meteorological data were filled using data from the northern study area old jack pine (NSA-OJP) site [*Fitzjarrald and Moore*, 2000; *Newcomer, et al.*, 2000]. The NSA-OJP site was located ~10 km away from the NSA-OBS site. Due to the close proximity of the sites, agreement between meteorological time series data was high and unbiased. The above canopy air temperatures at the two sites had a R^2 correlation of 0.997, PAR had a R^2 correlation of 0.91 and wind speed had the lowest R^2 correlation of 0.56.

For both the NSA-OBS and the SSA-OBS sites, the leaf reflectance and transmission of near infrared (NIR) and PAR were tuned using soil reflectance data, above canopy measurements of albedo and the radiative transfer scheme in SPA [*Baldocchi, et al.*, 2000; *Betts and Ball*, 1997].

Flux errors

Eddy covariance measurements provide powerful long-term monitoring of whole ecosystem fluxes. However the technique is not devoid of errors and uncertainties, these can crudely be described as either random or systematic (though actual errors maybe a combination of both). We use the approach used by *Goulden, et al.* (1996), and separate errors on flux estimates into four categories: uniform systematic, selective systematic, sampling uncertainty, and instrumentation uncertainty. Sampling uncertainties are important when aggregating long time series data with data dropout. In this study, we do not aggregate fluxes and, as we are looking at short periods of time, therefore we can discount this category of error. Uniform errors, from instrument mis-calibration, are typically between 5-10% [*Goulden, et al.*, 1996]. Consequently, we assumed a systematic error of +/- 10% on our flux measurements. Note that, during nocturnal periods, selective errors can be substantial; Night time selective errors can result from katabatic flows and/or sporadic mixing in the surface layer. Both selective uncertainties and

instrumentation uncertainty can contribute to random errors in the fluxes. Random errors were estimated using the method outlined by *Hollinger*, 2005, *see also Appendix A*. The method allows random error estimates to be generated from a single tower by utilising pairs of half-hourly data points separated by 24 hours. Using data with sufficiently similar meteorological conditions, differences between pairs of data points are used to build up an error distribution. Conditions were deemed to be similar when the difference between the pairs was less than 75 μmol m^{-2} s^{-1} PAR, 3 K air temperature and 1 m s^{-1} wind speed [*Hollinger and Richardson*, 2005]. When this is done for the whole time series, a Laplace distribution is built up. The mean absolute deviation for the Laplace distribution can be calculated; which is analogous to the standard deviation of a Gaussian distribution. To differentiate between daytime and night time errors, we binned the paired data points according to PAR. To obtain a sufficient number of paired points in each bin, the binning was limited to daytime (PAR > 25 μmol m^{-2} s^{-1}) and night time bins (PAR ≤ 25 μmol m^{-2} s^{-1}). This analysis was performed for the two eddy covariance sites, for both latent energy (LE) and net ecosystem exchange (NEE). The NSA-OBS error analysis was performed over the whole 1994 -1996 time series, and applied to the 120 day study period.

Soils data

Soil moisture, composition and temperature data sets were used to initialise the model at both the study sites. Half-hourly soil temperature measurements were recorded for the SSA-OBS site [*Jarvis, et al.*, 1997; *Jarvis and Moncrieff*, 2000; *Newcomer, et al.*, 2000] and NSA-OBS site [*Goulden, et al.*, 1997; *Newcomer, et al.*, 2000; *Wofsy, et al.*, 2000]. Thermocouples were used to measure the soil temperatures at depths of 0.025, 0.05, 0.1, 0.2 and 0.5 m, with a reference at 1 m. Volumetric water content was measured at both sites using a time domain reflectometer, [*Cuenca*, 2000; *Cuenca, et al.*, 1997; *Newcomer, et al.*, 2000]. Organic and mineral profiles of the soils were generated using the soil properties data set [*Anderson*, 2000; *Newcomer, et al.*, 2000].

Atmospheric data

Atmospheric profile data were from the National Research Council of Canada's Twin Otter aircraft. The Twin Otter aircraft took measurement soundings through the boundary layer, including CO_2 profiles [*Barr, et al.*, 1997; *MacPherson and Desjardins*, 2000; *Newcomer, et al.*, 2000]. Data were collected from ground level to 2-2.5 km. Flight plans

consisted of two or more straight, ascending/descending legs with a common origin. Flights were performed over both the southern study area (SSA) and the northern study area (NSA). Atmospheric profiles are available for 42 days during the 1994 study period. Profiles from the aircraft were used for the verification and parameterisation of the CAB model.

Test days

The CAB model was run for two days which were selected on the basis of best fulfilling the following criteria:

7. Two or more aircraft soundings must be taken; one must be during the morning and another after midday.
8. The aircraft sounding must be taken over black spruce dominated area, near the relevant study site.
9. Days should be within periods of stable synoptic weather conditions, with stable high pressure systems.
10. Eddy flux data should be available for the day.

Aircraft soundings were not specifically intended for use within this study setup, consequently, based on these criteria the only two suitable days were DoY 205 SSA-OBS and DoY 159 NSA-OBS.

Model Structure

Two models were coupled to form the Coupled-Atmosphere-Biosphere model [*Hill, et al.*, 2007], the Soil-Plant-Atmosphere model [*Williams, et al.*, 1996], and the Oregon State University 1-Dimensional Planetary Boundary Layer (OSU1DPBL) model [*Mahrt and Pan*, 1984; *Troen and Mahrt*, 1986]. Based on meteorological drivers and initial parameters, the SPA model predicts gross primary production, the total C fixed by plants in the ecosystem. However the C flux measured by eddy covariance systems is the net ecosystem exchange, the net accumulation of C in the ecosystem. The sum of the two is ecosystem respiration: GPP + NEE. Simulation of respiration was performed by a third model, a simple box model used in the Data Assimilation Linked Ecosystem C model [*Williams, et al.*, 2005].

Biosphere model

SPA, the main component of the biosphere model, has been successfully used in a wide range of studies at various latitudes: i.e. Amazonia [*Fisher, et al.*, 2006], Oregon [*Schwarz,*

et al., 2004; *Williams, et al.*, 1997] and the Artic [*Van Wijk, et al.*, 2003; *Williams, et al.*, 2000; *Williams, et al.*, 2001b]. In order to fulfil the modelling requirements of the CAB model, SPA was adapted to run on a variable time step.

SPA is a detailed, process based vegetation model (10 canopy layers and 20 soil layers) which links stomatal conductance in leaves with the assimilation rate of C. Stomatal conductance is varied within the model to maximise daily C gain within the constraints imposed by the plants' hydraulic limitations. Stomata are adjusted to maximise photosynthesis, whilst minimising the risk of cavitations within the xylem. SPA carries out radiative transfer calculations within the canopy, and can determine the full surface balance. A full description of the model can be found in *Williams, et al.* (2001) and *Williams, et al.* (1996).

Respiration is calculated in a simple C box model. C is stored in five pools; foliage, woody stems/coarse roots, fine roots, fresh leaf/fine root litter and soil organic matter. A fixed proportion of the previous day's GPP is allocated to autotrophic respiration and the remainder is allocated to the vegetation C pools. Autotrophic respiration is disaggregated from a daily flux using a simple sinusoidal function. The vegetation C pools feed into the litter and organic matter pools, according to fixed turnover rates. Heterotrophic respiration fluxes from the litter and soil organic matter pools are controlled by a combination of constant turnover rates and an exponential dependence on soil temperature. When available, turnover rate parameters and C pool sizes are based on literature values, (Table 1). Turnover rates were fitted within a range of values [*Williams, et al.*, 2005], and tuned to maintain C pool sizes over the 120 day study periods. A more in-depth technical description of the model can be found in the user manual [*Williams, et al.*, 2005].

The C flux model was chosen due to its simplicity and stability. The duration and nature of the modelling period performed with the CAB model lends itself to this simple form of box model. The short study period negates one of the potential problems with box modelling; that is, running a simple box model for long periods allows slight imbalances in the fluxes between C pools to result in unrealistic C pool depletion and/or accumulation. In this study, the unknown turnover rates between the C pools are parameterised to maintain a stable pool size, for the duration of the study. As part of the CAB model, the C sub-model is only run for a single day; in this role, we expect the respiration model to perform well. In addition, due to GPP determining the

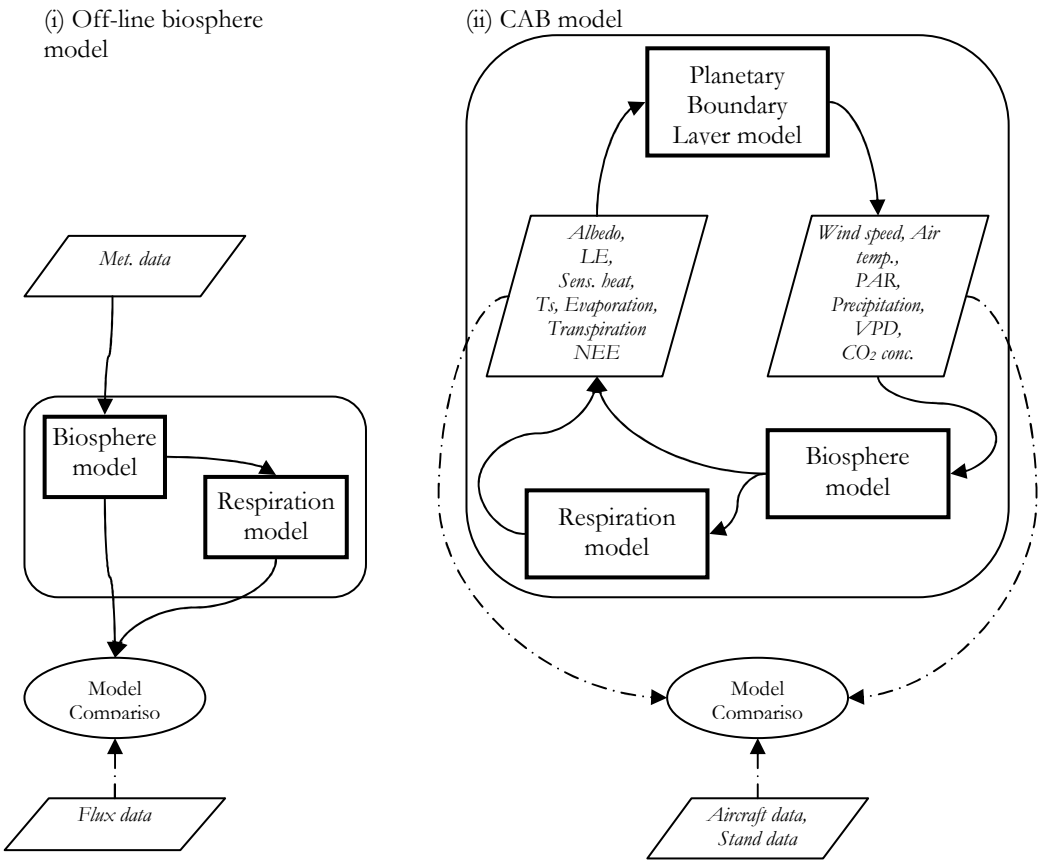

Figure 1: Flow diagram of the CAB model. (i) The biosphere (SPA and DALEC) models are run offline and compared to eddy covariance data. (ii) The verified biosphere model is run as part of the fully coupled CAB model. The CAB model is initialised using the 1st atmospheric profile of the day as a guide. Model outputs are then compared to PBL aircraft data and stand data.

influx of C into the respiration sub-model, the total quantity of C is conserved. The C pool model is expected to have slightly lower temperature dependence than with the standard Q_{10} approach as only the heterotrophic component of respiration has the Q_{10} dependence.

Atmosphere model

OSU1DPBL is the atmospheric component of the CAB model. It is a medium resolution boundary layer model consisting of 68 model layers, from ground level to 10 km. The model is capable of modelling the transition between stable and unstable PBL conditions and has been used in multiple studies [*Guichard, et al.*, 2004; *Holtslag, et al.*, 1990; *Holtslag and Ek*, 1996; *Lee and Mahrt*, 2004; *Murthy, et al.*, 2004]. In this study, the original simple surface scheme [*Louis*, 1979] has been replaced by SPA. This replacement allows realistic modelling of water, energy and C fluxes which can be

parameterised with ecosystem observations and corroborated using eddy flux measurements.

Modelling Scheme

The CAB model was run in two stages: (1) SPA, the biosphere component, and the respiration sub-model, were run for the two black spruce sites (Figure 1i). Soil and vegetation parameters from the literature were used to initialise the model. The model was driven using meteorological data obtained at the eddy covariance towers. The full range of parameters, initialisations and drivers used for the NSA-OBS site can be seen in Table 1, and for the SSA-OBS site they can be found in [*Hill, et al.*, 2007]. (2) Once the stand-alone biosphere component had been verified, the parameterisations were used in the coupled biosphere model nested within the CAB model, (Figure 1ii). The CAB model was initialised at midnight local-time, with precipitation being the only external driver required by the model. The fully coupled CAB model was then run in a prognostic mode. Within the CAB model, the biosphere component provided the energy partitioning and the surface fluxes of water and CO_2. Responding to this forcing, the atmospheric component updates the meteorological conditions in the boundary layer and the above-canopy drivers (i.e. wind-speed, CO_2 concentration, radiation, air temperature and VPD).

Assessing the strength of the diurnal CO_2 cycle

Firstly, we devised an experimental setup to assess the importance to productivity of the diurnal CO_2 concentration cycle. To make this assessment, we ran two instances of the CAB model for each site: (1) The first CAB model run used the parameterisation taken from the SSA-OBS site on DoY 205. (2) In the second run, the predicted above canopy atmospheric CO_2 concentrations were replaced with the diurnal average. For DoY 205, the average CO_2 concentration was 365.9 ppm. The two runs were compared to assess the impact of the diurnal CO_2 concentrations on GPP.

Assessing the strength of feedbacks caused by the presence of vegetation

The second aim was to assess the impact of feedbacks induced by the presence of vegetation. We sought to differentiate between the one-way forcing imposed by changes in the biosphere (i.e. changes to land surface exchanges resulting in a modification of

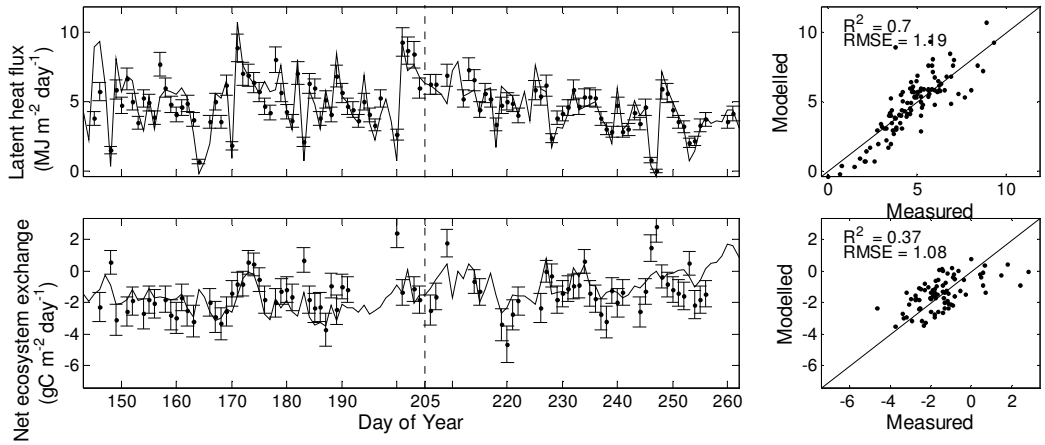

Figure 2: Modelled response of the off-line biosphere model compared to the SSA-OBS eddy flux tower measurements during the 1994 study period; comparisons of daily aggregated LE and NEE are shown. Days with less than 44 half-hourly values are excluded from the measurement plots. The model is shown using a solid line (——) and the measurements are shown using points (·····) with random and uniform systematic errors. A scatter plot showing the modelled and measured data is included: In addition to daily R^2 and RMSE values a 1:1 plotted. A vertical dashed line (- - - -) indicates the test day.

the atmosphere) and the (two-way) feedbacks induced (i.e. the response of the system to the atmospheric modifications). To make this distinction, three instances of the CAB model were used: (1) The first CAB model run used the parameterisations for the SSA-OBS site on DoY 205. We shall refer to this as the nominal run. (2) The second CAB model was run for DoY 205 at the SSA-OBS site with vegetation being removed, leaving only bare soil. We shall refer to this as the bare soil run. (3) Thirdly, the CAB model was again run for the SSA-OBS site on DoY 205, with the surface meteorology from the bare soil run used. By comparing the 1st and 3rd CAB runs, the feedbacks induced by the presence of the black spruce can be isolated from those of simple forcing.

Results

The land surface over the study period

At a daily time-step, LE from the biosphere model compares favourably to data, (Figures 2 and 3). R^2 LE flux values for the southern and northern sites were 0.70 and 0.58 respectively, and the root mean square errors (RMSE) were 1.19 MJ m^{-2} day^{-1} and 1.37 MJ m^{-2} day^{-1}, respectively. Inspection of the scatter plots revealed only small

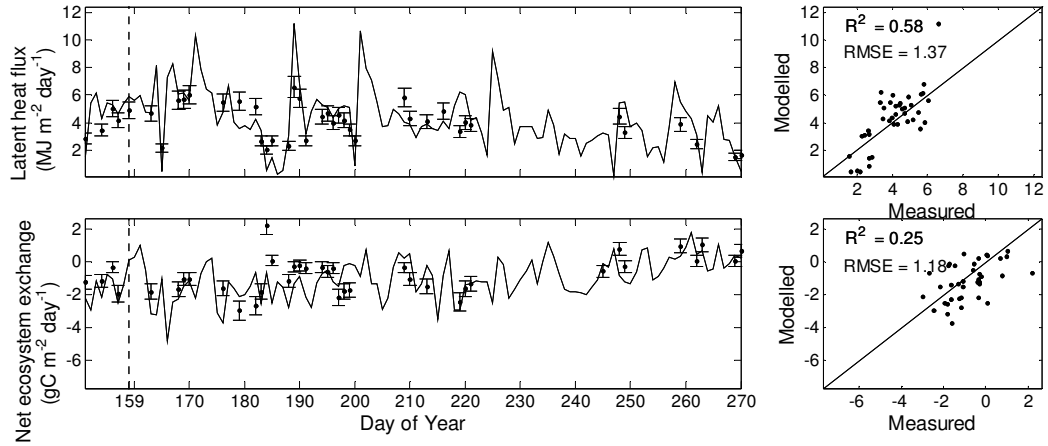

Figure 3: Modelled response of the off-line biosphere model compared to the NSA-OBS eddy flux tower measurements during the 1994 study period; comparisons of daily aggregated LE and NEE are shown. Days with less than 44 half-hourly values are excluded from the measurement plots. The model is shown using a solid line (——) and the measurements are shown using points (·····) with random and uniform systematic errors. A scatter plot showing the modelled and measured data is included: In addition to daily R^2 and RMSE values a 1:1 plotted. A vertical dashed line (- - - -) indicates the test day.

amounts of model-measurement correlation structure, with the SSA-OBS simulation giving an under-prediction at low LEs. Correlation on a half-hourly time step was higher, LE flux R^2 values were 0.72 and 0.59 and the RMSEs were 40 W m^{-2} and 42 W m^{-2}, for the southern and northern sites respectively (not shown).

NEE on a daily time-step showed a lower correlation with measurements than LE. NEE R^2 values of 0.37 and 0.25 and RMSE values of 1.08 gC m^{-2} day^{-1} and 1.18 gC m^{-2} day^{-1} were obtained for the SSA-OBS and the NSA-OBS site respectively. At a half-hourly time-step the southern and northern NEE R^2 values were 0.59 and 0.62 and the RMSE values were 4 μmol m^{-2} s^{-1} and 3.4 μmol m^{-2} s^{-1} respectively. Limited eddy covariance data were available for the NSA-OBS site.

The land surface on the study days

Comparisons between the biosphere model (SPA) and measurements were performed on a half-hourly time-step for DoY 205 (SSA-OBS) and DoY 159 (NSA-OBS) - (Figure 4). LE comparisons for both days showed that the general trends were captured by the model, but the daytime peaks in the measurements were not. The errors on the measurements were small and did not fully cover the model measurement differences.

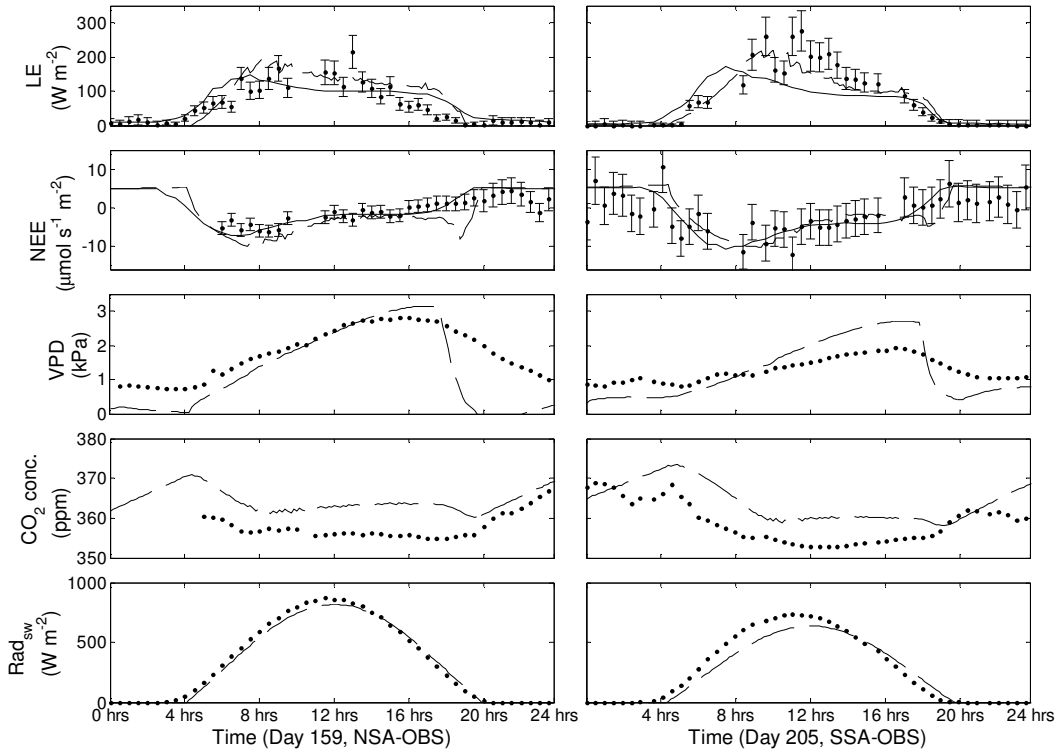

Figure 4: Half-hourly modelled responses of SPA and the CAB model are compared to eddy flux tower measurements for days 205 (SSA-OBS) and 159 (NSA-OBS), 1994. The biosphere model is shown using a solid line (——), CAB is shown with a dashed line (- - -). Measurements are shown with points (·····) and with associated errors (random + uniform systematic).

However the errors exceeded the model-measurement residuals for 53% of the LE and 75% of the NEE data points.

CAB model

CAB model estimates of the NEE and LE fluxes were slightly higher than both the SPA model's simulated fluxes and actual measurements (Figure 4). Predictions of LE and NEE fluxes stayed largely within the error bounds of the measurements. The diurnal cycles of VPD were greater in the CAB model than indicated by observations; modelled VPDs were ~0.5 kPa lower at night and peaked at ~0.5-1 kPa higher during the day. The diurnal trend in CO_2 concentration was captured by the model, but tended to be ~5 ppm higher than the measurements.

Comparing the CAB model output to the aircraft soundings revealed good model-measurement agreement (Figure 5). The modelled profiles compared well to the measurements on both the test days, capturing the important features of the boundary

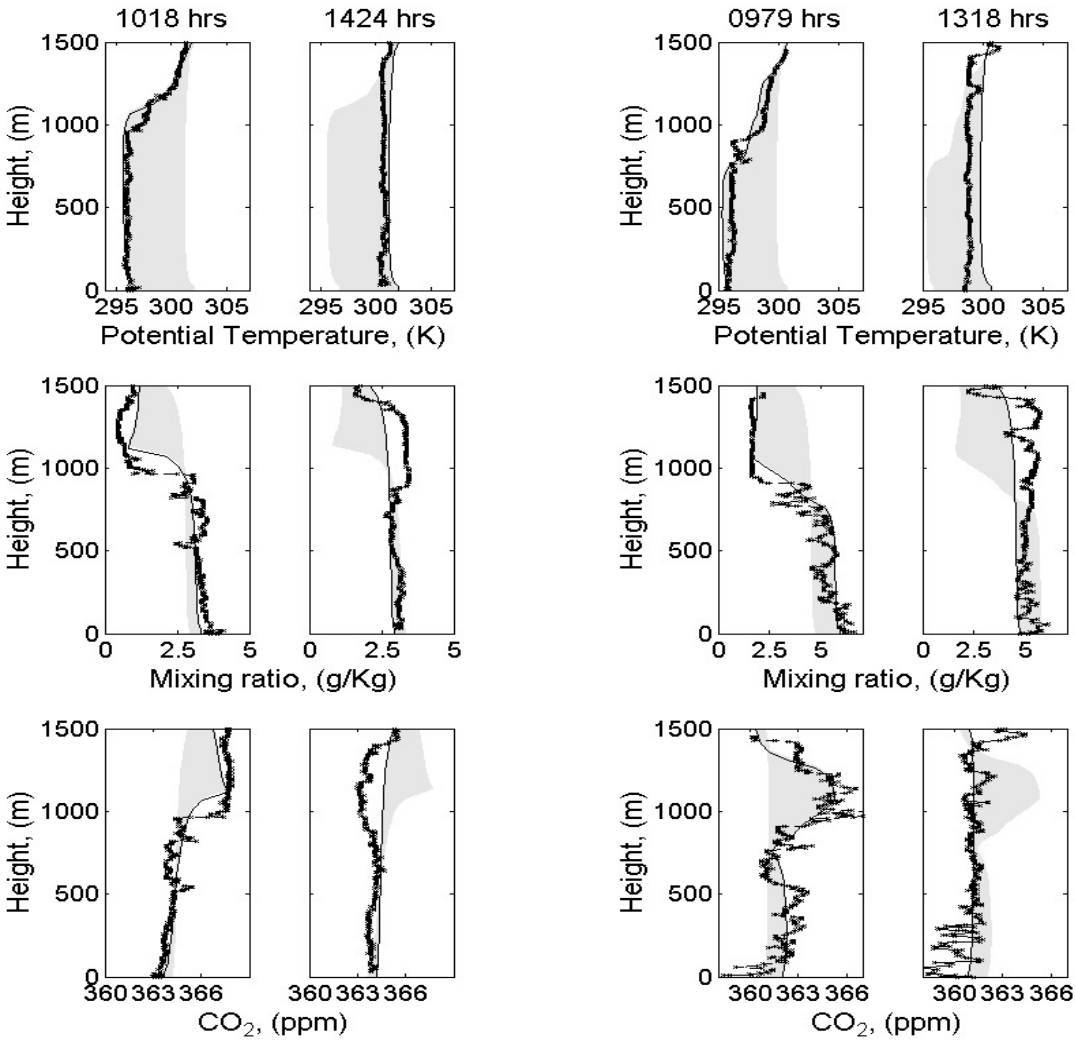

Figure 5: Modelled and measured boundary layer profiles of potential temperature, mixing ratio and CO_2 concentration for DoY 159 (NSA-OBS, left six panels) and for DoY 205 (SSA-OBS, right six panels), 1994. Profiles are from aircraft flights through the boundary layer; local time is shown. Measurements are shown as diagonal crosses and modelled data by solid lines. The grey shaded area shows the full extent covered by the modelled profiles and is shown to provide a visual guide for the diurnal progression of the measured and modelled profiles.

layer. The profiles indicated that the model predicted the correct daytime drawdown of CO_2 from the atmosphere by the land surface.

Assessing the strength of the diurnal CO_2 cycle

The diurnal cycle in CO_2 concentrations resulted in a morning increase in GPP, and a corresponding afternoon decrease (Figure 6). These changes mirrored the form of the diurnal cycle of modelled CO_2 concentrations. The magnitude of these changes is small

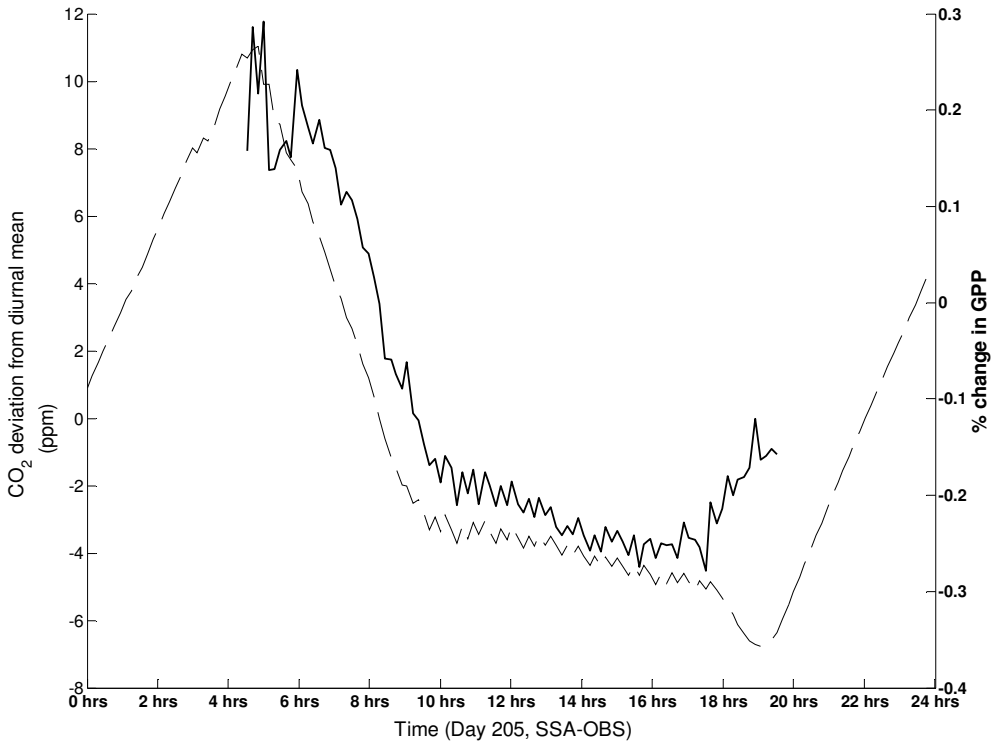

Figure 6: The dashed line (— — —) shows the surface CO_2 concentration deviation from the diurnal mean for DoY 205 (SSA-OBS). The solid line (———) shows the change in GPP resulting from the inclusion of dynamic surface CO_2 concentration changes, compared to using the diurnal average.

(approximately ± 0.3% GPP), and overall there was a marginal drop in the predicted GPP for the day.

Assessing the strength of feedbacks caused by the presence of vegetation

The impact of removing vegetation was an atmosphere that was ~2 K warmer, above canopy windspeeds up to 1 m s^{-1} higher and ~0.6 kPa higher VPDs (Figure7, bottom three panels). The feedback decreased LE fluxes and increased the GPP, (Figure 7, top 2 panels).

Discussion

Capturing the atmosphere-biosphere system

The first stage in the modelling scheme was the verification of the biosphere model, SPA. Virtually all vegetation parameterisations used by SPA were based on literature values. The exceptions were leaf capacitance and ι (the water use efficiency parameter

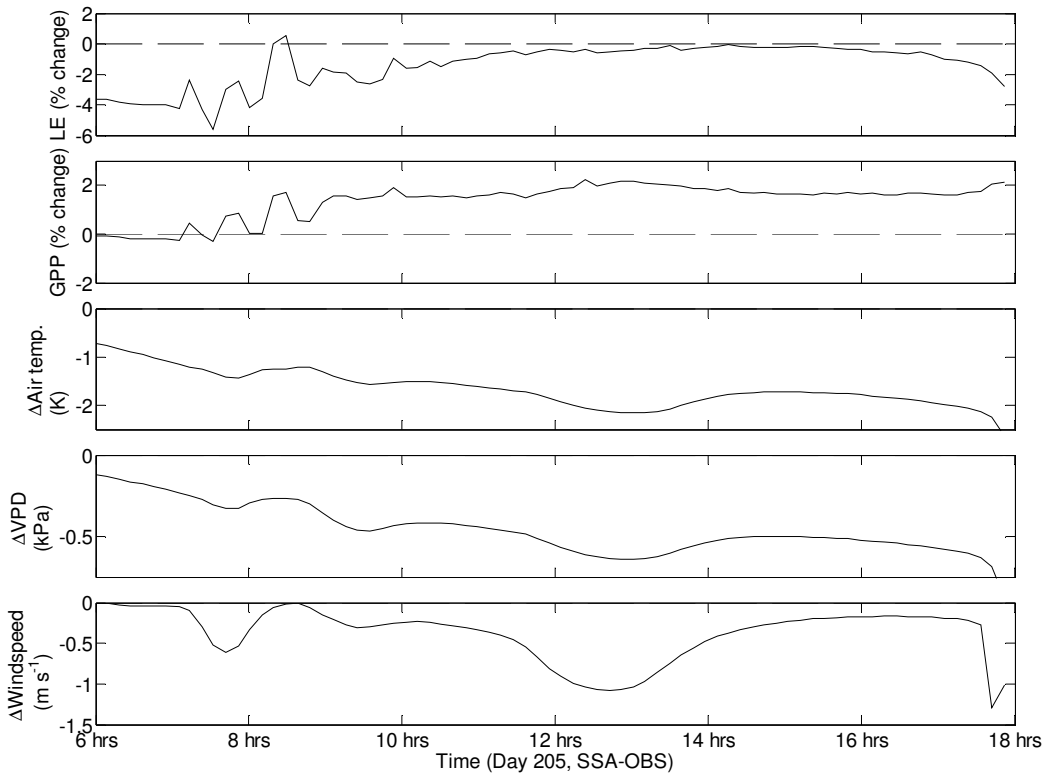

Figure 7: The effect of feedbacks on the coupled atmosphere-biosphere system. The same vegetation (DoY 205, SSA-OBS) is used for two CAB model runs. The impact of atmosphere-biosphere feedbacks (initiated by the vegetation) are shown as % changes in latent heat flux and gross primary production. The bottom three panels show the forcing that the vegetation exerts on the atmosphere, compared to that of bare soil.

[*Williams, et al.*, 1996]), which were fitted within ranges [*Williams*, 2005]. Respiration parameterisations were less accurately defined. Values for the C pool sizes came from literature, but most of the turnover rates were tuned to maintain C pool sizes. We were not attempting to aggregate the respiration fluxes, but rather required accurate fluxes over single days. Thus, by tuning the turnover rates to maintain stable C pools, we could simulate accurate respiration fluxes which were robust in formulation and suitable for use in the CAB model. Though it should be noted that, we are not advocating using this method of tuning in all situations, and also we acknowledge measurements to be preferable. Since most parameterisations came from literature, and the C pool turnover rates were calibrated with pool sizes, there was no need to tune the model against eddy covariance measurements. As a result, once corroborated, greater confidence could be placed in the model's prognostic abilities.

The primary means of corroborating the SPA model were comparisons with eddy covariance measurements at both the NSA-OBS site and SSA-OBS site. The model was broadly supported by the eddy covariance flux data on both the daily and the half-hourly time-scale (Figures 2, 3 and 5). Model-measurement residuals were largely neutral (Figures 2 and 3, scatter plots).

However, for both our sites the agreement between SPA observations were not as high as expected; this was particularly true for NEE. The SPA model had been corroborated at numerous other sites, so the general validity of the SPA model was not in question. Rather, the model-measurement disagreements were attributable to the application of the SPA and DALEC models at the black spruce sites, and/or the observations; we shall discuss both possibilities later. The disagreements will be discussed largely in terms of the NEE, as generally the model agreement with NEE was poorer than with LE. Broadly these disagreements can be attributed to separate modelling and measurement issues. However, we shall also discuss the model's under prediction of low latent energy heat fluxes at the SSA-OBS site, and perhaps the NSA-OBS site too.

Modelling issues

Model errors could arise from the calculation of GPP or respiration. The respiration model (DALEC) was less constrained by measurements than the SPA model, both in terms of parameterisation and verification. Considering the greater freedom in the DALEC model, and the SPA model's good agreement with the LE heat flux, it is probable that more errors were associated with the calculation of respiration, than the estimates of GPP.

Taking our working hypothesis to be that the respiration sub-model did not capture the magnitude of the respiration fluxes correctly we are presented with several possible mechanisms. One possible mechanism for this poor simulation could have been the surface soil layer and the blanket of moss, drying out, and heating up. Potentially this could have resulted in a large, highly variable respiration efflux which was not captured by the models. Additionally, the lack of a dedicated moss model was a likely cause of the slight underestimate in LE at low light-levels, when moss provides a large wet surface area for evaporation [*Betts, et al.*, 2001]. A second mechanism could

have been model errors introduced by the uncertainties in parameterisation of the turnover rates.

There are several other omissions from the SPA model, such as the modelling of katabatic flows, and the explicit representation of spatial heterogeneity of the land cover. It is probable that these also contribute to the poor estimates of the C fluxes.

Measurement issues

Flux measurements made as part of the BOREAS field campaign, were amongst the first to be made over sustained periods of time. At the time, longer study periods were becoming possible, due to advances in instrumentation, and data acquisition techniques [*Baldocchi*, 2003]. However, data storage was still limited, and consequently not all the raw data are still available. The lack of the complete original data sets made the application of up-to-date corrections to the flux data difficult [*Baldocchi*, 2003]. This added an additional level of uncertainty to the flux measurements. Whilst we estimated the random errors and uniform systematic errors associated with the measurements, we could not correct the selective systematic errors that were evident in these early flux measurements. There are several physical causes of systematic errors which can be hard to correct, such as the night time drainage of CO_2 by katabatic flows. Several artefacts (such as measurements of strong daytime CO_2 respiration fluxes) were visible in the daily NEE fluxes (Figure 3), and also the half-hourly data (Figure 4).

We are led to the somewhat unsatisfactory conclusion that the model-measurement disagreements arose from uncertainties with both the models and the observations. We suppose that a sizeable contribution of the model-measurement deviations came from the uncertainties in the respiration sub-model and its parameterisation. Interestingly, the model-measurement agreement was substantially higher on a half-hourly time step than on the daily. This is contrary to the expectation that uncertainties reduce as data is aggregated, and suggests that the model captured the half-hourly variability, but did not quite capture the extremes. That is, the model lost too much variability when daily averages were taken. In the context of the CAB model it was more important to capture the LE heat flux than the NEE, as this was one of the key determining factors in the surface energy partitioning. It was also more important to capture the day time NEE data, which has less variability than the night time observations and directly impacted the atmospheric CO_2 observations. Both daytime

NEE and LE fluxes showed higher model-measurement agreement, than the night time NEE.

Once confidence had been gained in the formulation and parameterisation of the SPA model, we proceeded to use them in the coupled CAB model. The biosphere model was driven by meteorology, as predicted by the CAB model. This allowed comparisons of the above-canopy air measurements (Figure 4), with the CAB model predictions. We saw that the diurnal evolution of the measurements was captured by the model. CAB model flux estimates were close, but not identical, to the SPA simulations, suggesting that the prognostic capabilities of the CAB model were good. The deviations of the CAB model from those of the SPA model brought it closer to the measurements. This deviation was attributed to the mid-day overestimation of VPD by the CAB model.

Inspection of the atmospheric profiles (Figure 5) showed that the elevated VPDs were the result of lower atmospheric layers being too warm. The CAB model simulated the diurnal evolution of the PBL extremely well (Figure 5). However, for the SSA-OBS site on DoY 205, the model over estimated the temperature of the afternoon mixed layer. At this point, model-measurement differences were large (~1 K) and were unlikely to be attributable to the biosphere model. The cause of this model-measurement deviation is unclear.

Assessing the strength of the diurnal CO_2 cycle

Compared to a daily mean value, the diurnal cycle in CO_2 concentration had elevations of 11 ppm in the morning and, depletions of 7 ppm in the evening (Figure 6). By midmorning the CO_2 concentrations were lower than the daily mean. The diurnal cycle was imposed by the combination of NEE and the rectifier effect [*Denning, et al.*, 1995]. Respiration dominated the NEE signal during the night time periods, increasing modelled CO_2 concentrations. The rectifier effect amplified the night time increase in CO_2 concentrations; as the low nocturnal PBL trapped the respired CO_2 near the surface, accentuating the rise in CO_2 concentrations. Over the course of the day, the response of GPP had a very similar form to that of the diurnal CO_2 concentration cycle. This occurred because the GPP depends on the rate of photosynthesis, and the rate of photosynthesis partially depends on the rate of CO_2 diffusion out of leaves. This rate is dependant on both the internal and external CO_2 concentrations (Fick's 1st law). The % change in the GPP associated with the diurnal cycle of CO_2 concentrations was small

(+/- 0.3%, Figure 6). Furthermore, the effect was almost entirely smoothed out when averaged over a day, and can safely be ignored for the purposes of driving soil-vegetation-atmosphere-transport (SVAT) models.

Assessing the strength of feedbacks caused by the presence of vegetation

Our results showed that vegetation significantly modified the immediate atmosphere. Removal of the vegetation (leaving bare soil) resulted in a much warmer atmosphere, with higher wind speeds and VPDs than in the nominal case (bottom 3 panels, Figure 7). The increase was due to the changes in energy partitioning at the land surface. The loss of the canopy rules out transpiration, leaving only minimal surface area (the ground) for evaporation. This drastically reduced the latent heat flux. To conserve energy, the energy partitioning into both the sensible heat flux, and the ground heat flux was increased, warming both the ground and the PBL.

The modified atmosphere was used to drive the nominal vegetation, and the difference between this run and the nominal run showed the impact of the feedbacks induced by the vegetation on the land surface response (top 2 panels, Figure 7). Inclusion of the feedbacks decreased the latent energy flux by up to 5% and increased the GPP by up to 2%. The nominal run was the cooler, with less atmospheric demand for water. This allows the black spruce to increase the stomatal conductance without risking damage to its hydraulic system. Consequently, in the uncoupled run, higher atmospheric demand for water meant that the stomata must be closed to reduce transpiration and allow the vegetation to maintain safe leaf water potentials, avoiding cavitations in the xylem. However, despite the decreases in stomatal conductance (in the uncoupled run) we saw an increase in the LE, which was attributable to the higher VPD (Figure 7). The lower stomatal conductance also reduced productivity (Figure 7). So feedbacks induced by the black spruce cooled the atmosphere and reduced atmospheric demand for water, allowing greater productivity and water use efficiency.

Conclusions

With the predicted increases in CO_2, expected changes to the current climate pose a serious threat to the stability of Earth system. Anthropogenic emissions of CO_2 are driving up the concentrations of CO_2, and forcing the climate to change. We need to quantify how these changes will impact ecosystems and their interactions with the

atmosphere. Steps have been taken towards this goal using top-down and bottom-up methodologies; we now need to bridge the gap between these two approaches. We have demonstrated and verified a CAB model, which provides a partial-bridge between top-down and bottom-up methodologies, linking processes at the land surface to processes and measurements in the boundary layer. In this study, we corroborated the mode at two sites with stand-based eddy covariance data and atmospheric water, CO_2 and temperature boundary layer profiles. The verified CAB model allowed the interactions between the biosphere and the PBL to be identified and studied.

We showed a method of quantifying the biosphere's modification of the overlying atmosphere in response to changes in climate. We can expect these modifications to be important in a changing climate and to have impacts on both the vegetation and the climate. We have shown that the diurnal CO_2 concentration cycle (driven by the rectifier effect and NEE) to have negligible impact on the response of SVAT models. However, the modification of the atmosphere by the vegetation is potentially large and needs to be accounted for in prognostic models and perturbation studies.

Given the pedigree of the SPA model, we expect this model to be generally applicable at a wide range of latitudes, and not limited to boreal regions. Additionally we expect the CAB model to have further applications: (1) Bayesian inversions of the CAB model will allow investigation of the interplay between the model, its parameters and predictions (this would highlight critical ecological parameters, measurement accuracy requirements and uncertainty propagation through the CAB model). (2) Data assimilation of synoptic weather conditions and ecological measurements [*Williams, et al.*, 2005] would permit the CAB model to be run for extended periods of time. This would allow long term feedback investigations with the CAB model, or the assimilation of atmospheric measurements into long term flux studies, to help constrain flux estimates of NEE. (3) Inclusion in a combined field experiment/modelling approach to FACE studies.

References

Anderson, D. W. (2000), "General Soil Survey for Primary Sites in SSA (OA, OBS, OJP, YJP, Fen)." In Collected Data of The Boreal Ecosystem-Atmosphere Study., edited by J. Newcomer, et al.

Baldocchi, D., et al. (2001), FLUXNET: A new tool to study the temporal and spatial variability of ecosystem-scale carbon dioxide, water vapor, and energy flux densities, *Bulletin of the American Meteorological Society*, *82*, 2415-2434.

Baldocchi, D., et al. (2000), Climate and vegetation controls on boreal zone energy exchange, *Global Change Biology*, *6*, 69-83.

Baldocchi, D. D. (2003), Assessing the eddy covariance technique for evaluating carbon dioxide exchange rates of ecosystems: past, present and future, *Global Change Biology*, *9*, 479-492.

Barr, A., and C. Hrynkiw (2000), BOREAS AFM-5 Level-1 Upper Air Network Data, Volume 8, NASA.

Barr, A. a. A. B. (2000), "Upper-Air Network (AFM-05) Boundary Layer Research For BOREAS (AFM-08)." In Collected Data of The Boreal Ecosystem-Atmosphere Study., edited by J. Newcomer, et al.

Barr, A. G., et al. (1997), Comparison of regional surface fluxes from boundary-layer budgets and aircraft measurements above boreal forest, *Journal of Geophysical Research-Atmospheres*, *102*, 29213-29218.

Betts, A. K., and J. H. Ball (1997), Albedo over the boreal forest, *Journal of Geophysical Research-Atmospheres*, *102*, 28901-28909.

Betts, A. K., et al. (2001), Near-surface climate in the boreal forest, *Journal of Geophysical Research-Atmospheres*, *106*, 33529-33541.

Bonan, G. B., and H. H. Shugart (1989), Environmental-Factors and Ecological Processes in Boreal Forests, *Annual Review of Ecology and Systematics*, *20*, 1-28.

Chen, J. M., et al. (1997), Leaf area index of boreal forests: Theory, techniques, and measurements, *Journal of Geophysical Research-Atmospheres*, *102*, 29429-29443.

Cuenca, R. H. (2000), "Coupled Atmosphere-Forest Canopy-Soil Profile Monitoring and Simulation." In Collected Data of The Boreal Ecosystem-Atmosphere Study., edited by J. Newcomer, et al.

Cuenca, R. H., et al. (1997), Soil water balance in a boreal forest, *Journal of Geophysical Research-Atmospheres*, *102*, 29355-29365.

Denning, A. S., et al. (1995), Latitudinal Gradient of Atmospheric Co2 Due to Seasonal Exchange with Land Biota, *Nature*, *376*, 240-243.

Ewers, B. E., et al. (2005), Effects of stand age and tree species on canopy transpiration and average stomatal conductance of boreal forests, *Plant Cell and Environment*, *28*, 660-678.

Fisher, R. A., et al. (2006), Evidence from Amazonian forests is consistent with isohydric control of leaf water potential, *Plant Cell and Environment*, *29*, 151-165.

Fitzjarrald, D. R., and K. E. Moore (2000), "Surface Exchange Observations in the Canadian Boreal Forest Region." In Collected Data of The Boreal Ecosystem-Atmosphere Study., edited by J. Newcomer, et al.

Goulden, M. L., et al. (1997), Physiological responses of a black spruce forest to weather, *Journal of Geophysical Research-Atmospheres*, *102*, 28987-28996.

Goulden, M. L., et al. (1996), Measurements of carbon sequestration by long-term eddy covariance: Methods and a critical evaluation of accuracy, *Global Change Biology*, *2*, 169-182.

Gower, S. T., et al. (1997), Carbon distribution and aboveground net primary production in aspen, jack pine, and black spruce stands in Saskatchewan and Manitoba, Canada, *Journal of Geophysical Research-Atmospheres*, *102*, 29029-29041.

Guichard, F., et al. (2004), Modelling the diurnal cycle of deep precipitating convection over land with cloud-resolving models and single-column models, *Quarterly Journal of the Royal Meteorological Society*, *130*, 3139-3172.

Hill, T. C., et al. (2007), Interactions between a boreal forest stand and the planetary boundary layer, *In preparation.*

Hollinger, D. Y., and A. D. Richardson (2005), Uncertainty in eddy covariance measurements and its application to physiological models, *Tree Physiology*, *25*, 873-885.

Holtslag, A. A. M., et al. (1990), A High-Resolution Air-Mass Transformation Model for Short-Range Weather Forecasting, *Monthly Weather Review*, *118*, 1561-1575.

Holtslag, A. A. M., and M. Ek (1996), Simulation of surface fluxes and boundary layer development over the pine forest in HAPEX-MOBILHY, *Journal of Applied Meteorology*, *35*, 202-213.

Holtslag, A. A. M., and A. P. Vanulden (1983), A Simple Scheme for Daytime Estimates of the Surface Fluxes from Routine Weather Data, *Journal of Climate and Applied Meteorology*, *22*, 517-529.

Houghton, R. A. (2003), Why are estimates of the terrestrial carbon balance so different?, *Global Change Biology*, *9*, 500-509.

Jarvis, P. G., et al. (1997), Seasonal variation of carbon dioxide, water vapor, and energy exchanges of a boreal black spruce forest, *Journal of Geophysical Research-Atmospheres*, *102*, 28953-28966.

Jarvis, P. G., and J. B. Moncrieff (2000), "The CO2 Exchanges of Boreal Black Spruce Forest." In Collected Data of The Boreal Ecosystem-Atmosphere Study., edited by J. Newcomer, et al.

Kljun, N., et al. (2004), A simple parameterisation for flux footprint predictions, *Boundary-Layer Meteorology*, *112*, 503-523.

Lawrence, D. M., and J. M. Slingo (2004), An annual cycle of vegetation in a GCM. Part I: implementation and impact on evaporation, *Climate Dynamics*, *22*, 87-105.

Lee, Y. H., and L. Mahrt (2004), Comparison of heat and moisture fluxes from a modified soil-plant-atmosphere model with observations from BOREAS, *Journal of Geophysical Research-Atmospheres*, *109*, -.

Louis, J. F. (1979), Parametric Model of Vertical Eddy Fluxes in the Atmosphere, *Boundary-Layer Meteorology*, *17*, 187-202.

MacPherson, J. I., and R. L. Desjardins (2000), "Atmospheric Boundary Layer Analyses from Canadian Twin Otter Aircraft." In Collected Data of The Boreal Ecosystem-Atmosphere Study., edited by J. Newcomer, et al.

Mahrt, L., and H. Pan (1984), A 2-Layer Model of Soil Hydrology, *Boundary-Layer Meteorology*, *29*, 1-20.

Miller, J. R., et al. (1997), Seasonal change in understory reflectance of boreal forests and influence on canopy vegetation indices, *Journal of Geophysical Research-Atmospheres*, *102*, 29475-29482.

Murthy, B. S., et al. (2004), Interactions of the land-surface with the atmospheric boundary layer: case studies from LASPEX, *Current Science*, *86*, 1128-1134.

Nakane, K., et al. (1997), Soil carbon cycling at a black spruce (Picea mariana) forest stand in Saskatchewan, Canada, *Journal of Geophysical Research-Atmospheres*, *102*, 28785-28793.

Newcomer, J., et al. (2000), Collected Data of The Boreal Ecosystem-Atmosphere Study. NASA., edited.

Rayment, M. B., et al. (2002), Photosynthesis and respiration of black spruce at three organizational scales: shoot, branch and canopy, *Tree Physiology*, *22*, 219-229.

Running, S. W., et al. (1999), A global terrestrial monitoring network integrating tower fluxes, flask sampling, ecosystem modeling and EOS satellite data, *Remote Sensing of Environment*, *70*, 108-127.

Savage, K., et al. (1997), Methane and carbon dioxide exchanges between the atmosphere and northern boreal forest soils, *Journal of Geophysical Research-Atmospheres*, *102*, 29279-29288.

Saxton, K. E., et al. (1986), Estimating Generalized Soil-Water Characteristics from Texture, *Soil Science Society of America Journal*, *50*, 1031-1036.

Schmid, H. P. (1994), Source Areas for Scalars and Scalar Fluxes, *Boundary-Layer Meteorology*, *67*, 293-318.

Schwarz, P. A., et al. (2004), Climatic versus biotic constraints on carbon and water fluxes in seasonally drought-affected ponderosa pine ecosystems, *Global Biogeochemical Cycles*, *18*, -.

Sellers, P. J., et al. (1997), BOREAS in 1997: Experiment overview, scientific results, and future directions, *Journal of Geophysical Research-Atmospheres*, *102*, 28731-28769.

Shuttleworth, W. J. (1991), Insight from Large-Scale Observational Studies of Land Atmosphere Interactions, *Surveys in Geophysics*, *12*, 3-30.

Troen, I., and L. Mahrt (1986), A Simple-Model of the Atmospheric Boundary-Layer - Sensitivity to Surface Evaporation, *Boundary-Layer Meteorology*, *37*, 129-148.

Van Wijk, M. T., et al. (2003), Interannual variability of plant phenology in tussock tundra: modelling interactions of plant productivity, plant phenology, snowmelt and soil thaw, *Global Change Biology*, *9*, 743-758.

Williams, M. (2005), The Soil-Plant-Atmosphere model: Manual, version 1.2, April 2005, edited, p. 32, University of Edinburgh.

Williams, M., et al. (2000), The controls on net ecosystem productivity along an Arctic transect: a model comparison with flux measurements, *Global Change Biology*, *6*, 116-126.

Williams, M., et al. (2001a), Use of a simulation model and ecosystem flux data to examine carbon-water interactions in ponderosa pine, *Tree Physiology*, *21*, 287-298.

Williams, M., et al. (1997), Predicting gross primary productivity in terrestrial ecosystems, *Ecological Applications*, *7*, 882-894.

Williams, M., et al. (1996), Modelling the soil-plant-atmosphere continuum in a Quercus-Acer stand at Harvard forest: The regulation of stomatal conductance by light, nitrogen and soil/plant hydraulic properties, *Plant Cell and Environment*, *19*, 911-927.

Williams, M., et al. (2001b), Primary production of an arctic watershed: An uncertainty analysis, *Ecological Applications*, *11*, 1800-1816.

Williams, M., et al. (2005), An improved analysis of forest carbon dynamics using data assimilation, *Global Change Biology*, *11*, 89-105.

Wofsy, S. C., et al. (2000), "Eddy Correlation Flux Measurements of CO2 for BOREAS." In Collected Data of The Boreal Ecosystem-Atmosphere Study., edited by J. Newcomer, et al.

Paper 3: A simple inverse modelling approach applied to a coupled terrestrial ecosystem / planetary boundary layer model.

T.C. Hill[1,2] and M. Williams[1,2]

[1]School of GeoSciences and NERC Centre for Terrestrial Carbon Dynamics, Crew Building, University of Edinburgh, EH9 3JN, UK

[2]NERC Centre for Terrestrial Carbon Dynamics, UK

(Intended for submission to Global Change Biology)

Abstract

Quantifying the carbon (C), water and energy dynamics of the land surface is critical for improving predictions of climate change. Observations have been broadly classified into either top-down (spatially averaged) and bottom-up (site/species specific) approaches. The spatial heterogeneity of C, water and energy fluxes causes difficulties when attempting to relate the different measurement approaches to one another. Site/species specific approaches are difficult to up scale due to the limited number of biomes sampled. Thus it remains a difficult task to relate the two (top-down/bottom-up) approaches, but the planetary boundary layer (PBL) provides a potential stepping stone. The PBL is in direct contact with the land-surface, and dynamics with in this atmospheric region are driven by ecosystem processes. Models of the PBL and biosphere provides a link between the top-down atmospheric and bottom-up ecosystem measurements by simulating processes independent of scale. The same models can be used to invert PBL observations to provide information about land surface parameters.

In this study we use a simple Monte Carlo inversion scheme and a coupled atmosphere-biosphere model to investigate the interactions of the atmospheric (spatially averaged) and biosphere (site specific) systems. The inversion scheme is initially demonstrated with a conceptual ecosystem model; conclusions from which are used to design informative inversions of select group of parameters for the fully coupled model. We then show that inversions of atmospheric and/or eddy covariance observations have the potential to give good estimates of ecosystem parameters such as leaf area index and the respiration rate. However, the observations contain less information about foliar nitrogen, plant hydraulic conductance and albedo, and no information on the surface roughness. Inverting both atmospheric and eddy covariance data improves the performance of the inversions by reducing the average uncertainty on the *posterori* distributions by 84% (compared to eddy covariance data only) and 74% (compared to atmospheric profile data only). We then proceed to investigate the impact on the inversions of observation uncertainty, and biases in our prior knowledge. We conclude that the magnitude of uncertainty has little impact on the inversions when compared to biases.

Introduction

The complexity of terrestrial ecosystems has resulted in conflicting predictions about vegetation response to climate change [*Friedlingstein, et al.*, 2006]. These conflicts range from differing reports about the potential for die-back of Amazonian rainforests over the next 50 years [*Betts, et al.*, 2004; *Cox, et al.*, 2000; *Fisher, et al.*, 2006], to the complications added when considering the radiative forcing of boreal forests [*Betts*, 2000]. Consequently, it remains an important task to quantify and understand the exchanges of C, energy and water on local, regional and global scales [*Running, et al.*, 1999; *Schimel*, 1995]. Approaches for improving understanding of these fluxes can generally be divided into bottom-up (e.g. eddy covariance [*Baldocchi*, 2003; *Moncrieff, et al.*, 1997]) or top-down (e.g. global inversions [*Gurney, et al.*, 2002; *Gurney, et al.*, 2003]).

Eddy covariance datasets provide the most in-depth quantification of a particular ecosystem's mass and energy exchanges. However fluxes of water, energy and CO_2 from the land surface are temporally and spatially heterogeneous, and eddy covariance systems are only able to capture the response at individual sites. This leaves the spatial heterogeneity of the land surface largely uncharacterised. To combat this problem, networks of eddy covariance towers (e.g. FLUXNET, CarboEurope) have been established [*Aubinet, et al.*, 2000; *Baldocchi, et al.*, 2001; *Dolman, et al.*, 2006]. However there is still some difficulty relating the limited range of biomes covered by these networks, to regional and global fluxes. An alternative approach uses global atmospheric observations, which provide both good spatial and temporal coverage. Unfortunately, atmospheric observations can prove difficult to relate to surface processes [*Heinsch, et al.*, 2006], and it is desirable to find an intermediate scale to bridge the gap.

Measurements and modelling in the planetary boundary layer have the potential to provide this bridge between top-down and bottom-up approaches [*Shuttleworth*, 1991]. The PBL is in direct contact with the land surface and responds rapidly to changes in the surface energy partitioning and fluxes of water and CO_2. The PBL integrates over a footprint which can extend from ~1-100 km^2, depending on the height in the PBL and the atmospheric conditions [*Kljun, et al.*, 2004]. This footprint allows measurements within the PBL to be used to investigate surface exchanges of water, energy and C on scales larger than individual plots and forest-stands. Atmospheric measurements within the PBL can be made using multiple instrument platforms, such as tall towers, aircraft

and radiosondes. Each of these platforms has their own advantages, but common to all the measurement platforms is that they can make use of the integrating power of the PBL. On their own, these observations cannot be used to determine land surface parameters (such as leaf area index (LAI)). Thus a model is required to make any inferences about the land surface parameters from PBL data. This concept is not new and work has already been done using atmospheric models to link atmospheric measurements to surface processes, e.g. *Denning, et al.*, (2003).

In this paper, we take a new approach, using synthetic data to show the extent to which eddy covariance data, PBL measurements and a coupled model can be used to make inferences about land surface parameters (i.e. the *data resolution*). Here we use the term data resolution to describe the ability of an (inverted) model to determine initial model parameterisations from a set of observations. We use a coupled atmosphere-biosphere (CAB) model in a Monte Carlo inversion scheme, to perform the investigation. The CAB model is well suited to this role as it is quick to run, and has previously been used to relate stand-based biogeophysical observations, and eddy covariance data, to both atmospheric profiles from radiosondes and aircraft [*Hill, et al.*, 2007a; *Hill, et al.*, 2007b]. The CAB model was run within the framework of a relatively simple inversion scheme. The scheme makes use of both Monte Carlo (stochastic processes) and Bayesian (revision of previously held knowledge) techniques.

We first demonstrate the inversion scheme using a simple conceptual terrestrial ecosystem model, which we use for two purposes; (1) to illustrate some of the pitfalls of the simple inversion method, (2) to generate guidelines for the inversion of the CAB model. This demonstration leads to the formulation of a novel Bayesian inversion scheme which looks at a limited range of parameters and facilitates the easy implementation of the inversion, reduces the computational cost and allows a wider range of investigations to be performed.

Objectives

Based on the guide lines from the conceptual model, the inversion scheme is applied to the CAB model to answer a series of questions that are important to both scaling and land-atmosphere interactions between the biosphere and the PBL: (1) What biosphere parameter likelihoods can be inferred from eddy-covariance data and aircraft PBL measurements? (2) How well do measurements of CO_2 concentrations and/or fluxes help constrain the system? (3) How does the resolving power of the observations

deteriorate with uncertainty? (4) How do biases in our prior knowledge affect our ability to determine the true parameter values?

Motivation for the Monte Carlo inversion approach

At the level of the stand, eddy covariance systems, and terrestrial ecosystem models (TEM) have markedly improved understanding of ecosystem processes [*Baldocchi*, 2003]. The combined approach is robust and has been applied to numerous biomes, at a wide range of latitudes [*Williams, et al.*, 2001a; *Williams, et al.*, 2001b]. However there are a number of uncertainties associated with the models and the data, e.g. the models struggle to capture spatial heterogeneity, and the data can suffer from poor performance under stable night-time conditions [*Goulden, et al.*, 1996]. Despite these drawbacks the combined approach remains a powerful tool for studying whole ecosystem responses to climate change.

The sensitivity analysis is a traditional tool for modellers working with TEMs, allowing studies to be extended beyond the limits of actual measurements. Sensitivity analyses reveal the response of a model to changes in parameters, providing modellers with a tool to study the behaviour and characteristic responses of their models. Critical (controlling) and missing processes can also be identified by studying the sensitivity of each model, e.g. *Williams, et al.*, (1998). To perform these analyses, the model is repeatedly run in a 'forward' mode, where each run uses a different combination of model parameters.

The sensitivity analysis can provide information about model responses, but an alternative is required if you wish to resolve information about the system, and its parameters, based on model predictions and observations. The ideal solution would be an adjoint, which is effectively a version of the model that runs in reverse [*Kaminski, et al.*, 1999]. Theoretically an adjoint could be initialised with observations, and run to determine the model parameterisations, e.g. *Kaminski, et al.*, (2002). The adjoint could also be used to infer the data resolution that is achievable from any given set of observations. This process is analogous to running the traditional sensitivity analysis in reverse.

Unfortunately for most models, adjoints are hard to produce and a more generally applicable solution is desirable. A conceptually simple way of negating the need for an adjoint, would be to run the normal (forward) model for all possible

parameter combinations, and then perform a maximum likelihood analysis to determine the parameter likelihoods. For most actual models the large number of parameter combinations would lead to this being numerically time consuming (even to the extent of practically impossible). As a result, more elegant solutions have been devised which attempt to guide the exploration of 'parameter space' in an optimal manner [*Gelman*, 1995]. (Where parameter space can be thought of as an *n*-dimensional hypercube that is formed when each of the *n* parameters is used to represent a single dimension)

Optimal exploration of parameter space sufficiently samples the variable distribution in as few model runs as possible. In an attempt to achieve this optimal solution, the path taken is guided to preferentially sample regions of interest by a combination of model comparisons with observations, and *a priori* (previous held) knowledge about parameters. This use of *a priori* knowledge leads to these techniques being known under the umbrella term of bayesian modelling. Such bayesian inversion schemes can be used to 'invert' models, and achieve similar goals to those of an adjoint.

Despite requiring substantially less setup-time than an adjoint, these inversion schemes require an initial investment of time to implement, which can sometimes act as a barrier to ecosystem modellers. Additionally, inversion schemes often include many parameters, leading to misleading (e.g. unrealistic solutions) and/or unfocussed analysis. To sufficiently sample high dimensional parameter spaces, the model needs to be either extremely simple, tightly constrained (with smooth responses), or run with large computational resources. Often, none of these conditions are met, as TEMs tend to be moderately complex models developed for desktop computers. As a result, inversion studies are often not performed and a valuable avenue of investigation is left unexplored. This has motivated us to devise a simplified bayesian inversion scheme that is useful, practical to implement, and can act as a primer for more rigorous approaches.

Terrestrial ecosystem models are particularly suitable for inverse modelling due to the wealth of observations available (from, in particular, eddy-covariance towers). Eddy-covariance towers provide long-term continuous measurements of latent energy (LE) fluxes and the net ecosystem exchange (NEE) of small regions (up to ~2 km). In this paper, we demonstrate the inversion scheme in the context of a TEM, which has been coupled to a PBL model.

Description of the simple Monte Carlo approach

The Monte Carlo inversion method we describe (and demonstrate) is just one form of analysis which is based on Baye's theorem, circa 1763. Bayes' theory allows *a priori* knowledge about a system to be revised using new observations. The basic assumption is that, although neither our *a priori* knowledge, nor our model/observations are wholly correct, there is some optimum combination which gets as close to the 'truth' as possible. In the context of the inverse modelling scheme set out in this paper, this means we update our *a priori* knowledge of the system (e.g. leaf area, foliar nitrogen content) using observations of eddy covariance data (latent energy and NEE) and aircraft PBL profiles (temperature, mixing ratio and CO_2 concentration). This allows us to use the model to determine the *posterori* distribution, the optimal combination of *a priori* knowledge and observations. Inversions can be used to determine key ecological parameters, the importance of their uncertainties and quantify how this information propagates through the model.

The Monte Carlo inverse method is described here in practical terms and has been described elsewhere in more general terms [*Knorr and Kattge*, 2005; *Mosegaard and Tarantola*, 1995]. There are of course many other similar methods: (1) Bayesian methods very similar to the methods outlined in this paper have been applied to parameter estimation in ecosystem model [*Franks and Beven*, 1997; *Van Oijen, et al.*, 2005]. (2) Data assimilation techniques have been applied to obtain the best estimates of ecosystem C exchanges, e.g. the ensemble Kalman filter [*Williams, et al.*, 2005]. But neither the estimation of parameters, nor the constraint of ecosystem fluxes is the goal of this paper; rather we wish to determine the limits to which information can be inferred from observations.

The approach uses a guided walk through parameter space to efficiently sample the whole distribution. Newly proposed parameter 'steps' on the walk are randomly generated to allow the walk to progress. Each proposed parameter step can be rejected on the basis of certain criteria, if rejected, an alternative parameter step is proposed. These new steps are randomly generated until one of the proposed steps is accepted, and the random walk progresses.

For efficiency, we use a two stage accept/reject (A/R) criterion. Firstly, we A/R on the based on *a priori*, and secondly we A/R based on comparisons of the model output with data. This allows the time consuming processes of running the model to be

avoided if rejection occurs on the basis of *a priori* knowledge. We break down the process into nine steps (Outlined below and pictorially in Figure 2):

Step 1: Using our previously held knowledge about the parameters (from theory or measurement) we define the *a priori*' values ($\underline{P}_{i,0}$) and *a priori* uncertainties for each of the *i* model parameters. In the context of a TEM, it normally makes sense to convert these to log-normalised parameters (P_i). This has the benefit of keeping parameters positive. The new parameter value ($\underline{P}_i$) is now:

$$\underline{P}_i = \underline{P}_{i,0}.\exp(P_i - 1)$$

Step 2: Perform an initial model run to obtain the current model predictions (m^j) for the *j*-th model step. Parameters for the model can be seeded randomly, or taken to be the *a priori* values. If the model is initialised from a random location then care should be taken to ensure that this starting point is not non-physical.

Step 3: Propose a new model parameter step (P_i^{j+1}) by stepping from the current model parameter (P_i^j) at the current step *j*. Each parameter is stepped (perturbed) simultaneously on a Latin-hypercube (an n-dimensional square grid), with a $1/3^{rd}$ chance of increasing in value, a $1/3^{rd}$ chance of decreasing in value and a $1/3^{rd}$ chance of staying at the current value (P_i^j) (from tests we have performed, using a Latin-hyper cube is more efficient than selecting a parameter step randomly from a Gaussian distribution).

Step size is determined by the spacing of the points in the Latin-hypercube. A smaller step size results in more acceptances, but requires more accepted steps to sufficiently explore parameter space. Too large, or too small a step size will result in an inefficient parameter space exploration. For efficient parameter space exploration, the step size was set to achieve an acceptance probability of between 0.2 and 0.8.

Step 4: Accept/reject on the basis of the log-normalised *a priori* ($\underline{P}_{i,0}$; normally 1), the current accepted parameters (P_i^j) and the proposed parameter step (P_i^{j+1}). The A/R routine always accepts the proposed step if it is closer to the *a priori*, and conditionally accepts it if it further away. This conditional acceptance allows the walk to escape local minima, by (potentially) accepting steps that are heading away from the *a priori*. For these steps, the acceptance rate is defined such that the probability of acceptance drops as the proposed steps makes larger steps away from the *a priori*. Assuming independently identical Gaussian uncertainty distributions, we can express the A/R as:

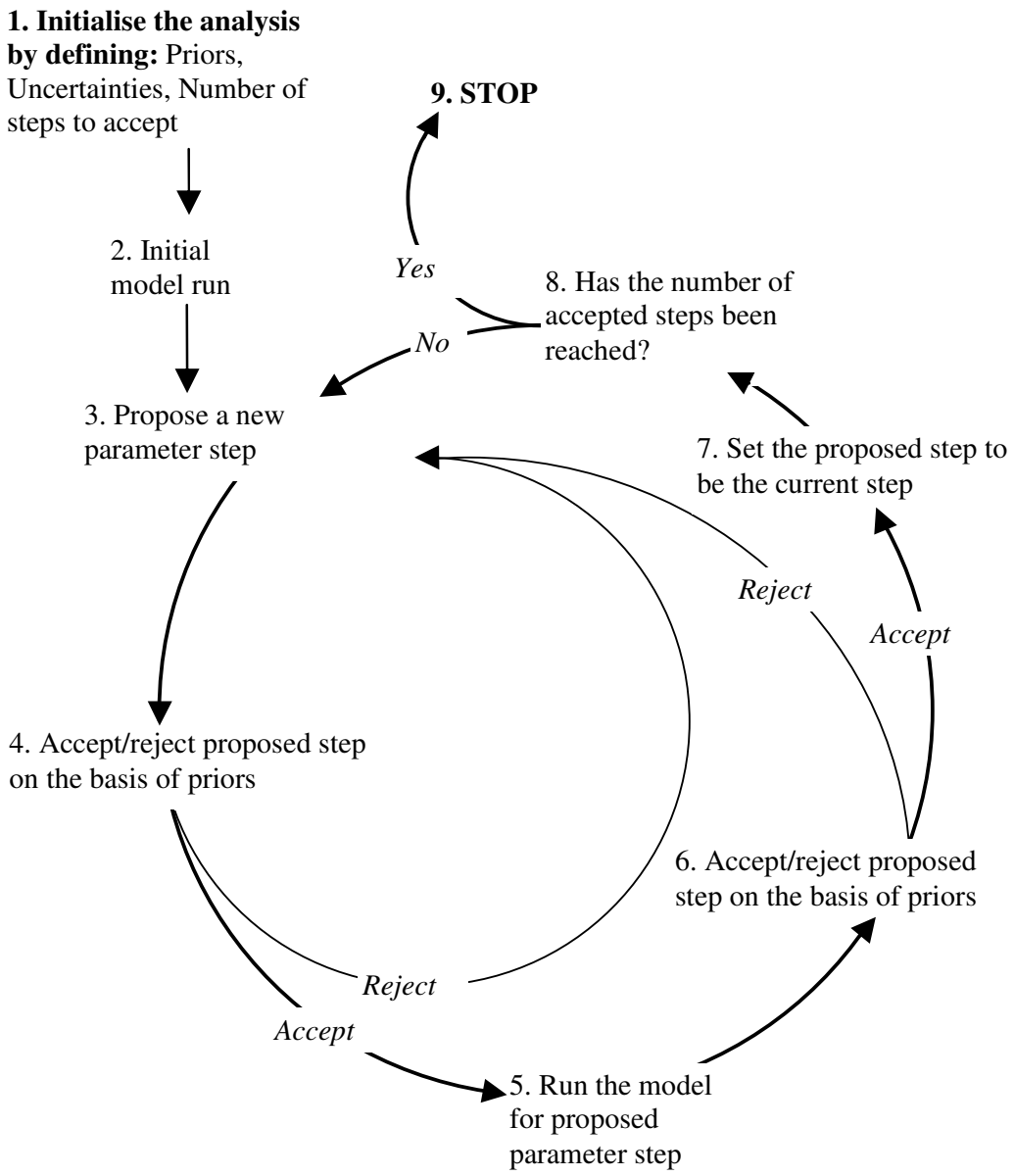

Figure 1: Flow diagram of the Monte Carlo inversion. The analysis continues until the required number of parameter steps are accepted. Steps are described in the text.

$$P_{accept} = \begin{cases} 1 & \text{, if } S\left(P_i^{j+1}\right) \le S\left(P_i^{j}\right) \\ \exp\left(\dfrac{S\left(P_i^{j}\right) - S\left(P_i^{j+1}\right)}{p^2}\right) & \text{, if } S\left(P_i^{j+1}\right) > S\left(P_i^{j}\right) \end{cases}$$

Where

$$S(P) = \frac{1}{2}\sum (P - P_0)^2$$

and p^2 is the variance of the *a priori*. If rejected return, to Step 3 and propose a new parameter step.

Step 5: Run the model to calculate the new model prediction (m^{j+1}) for this proposed parameter step.

Step 6: Corroborate the current model predictions (m^j) and the potential step's predictions (m^{j+1}) with observations; A/R using an appropriate likelihood estimator. Assuming the observations have errors which are independently identical Gaussian uncertainty distributions, our likelihood estimator ($L(m)$) can be expressed as [*Mosegaard and Tarantola*, 1995]:

$$L(m) = \exp\left(-\frac{S(m)}{s^2}\right)$$

Where $S(m)$ depends on model predictions (m) and the observations (obs) and s^2 is the variance on the measurements, including the errors associated with inaccuracies in the modelled processes.

$$S(m) = \frac{1}{2}\sum(m - obs)^2$$

This results in the A/R criteria:

$$P_{accept} = \begin{cases} 1 & \text{, if } S(m^{j+1}) \le S(m^j) \\ \exp\left(\dfrac{S(m^j) - S(m^{j+1})}{s^2}\right) & \text{, if } S(m^{j+1}) > S((m^j) \end{cases}$$

If rejected, return to Step 3 and propose a new potential parameter step. In a similar manner to the A/R criteria in Step 4, this conditional A/R criteria allows the walk to escape local minima.

Step 7: On acceptance, update the current parameters to be that of the proposed step ($P_i^j = P_i^{j+1}$), and likewise do the same for the model predictions ($m^j = m^{j+1}$).

Step 8: Check to see if the total number of accepted runs has reached the required number: if it has, stop the analysis (Step 9) if not, then return to Step 3. It is important to assess the number of runs needed to sufficiently sample parameter space. Too few runs will lead to spurious results resulting from partial sampling of the parameter space. We assess the number of runs needed by using the Gelman criteria [*Gelman*, 1995]. This criterion describes a reduction factor which is a function of the intra-run and between-

run variances of an ensemble of Monte Carlo model runs. The result is expressed as a reduction factor which tends to 1 for infinite length runs, when the variance captured by each model inversion became identical, as they were sampling the same parameter space. We require the factor to be consistently less than 1.05 for all parameters.

Step 9: Stop the analysis. The *posterori* distribution is generated from the walk through parameter space. To avoid correlations at the starting point of the run, a 'burn-in' period is removed from the final analysis. The burn-in period is determined by requiring all parameters to have reached a Gelman reduction factor of less than 1.2.

The example of a simple conceptual model

Motivation for the conceptual model

Monte Carlo inversions are stochastic processes used to improve understanding of a model's initial parameters. If (as is very likely) these model parameters are strongly correlated with one another, then the assumptions used in the likelihood estimator are incorrect. To account for the correlation, the error covariance matrix is calculated. This matrix describes the covariance of model parameters in parameter space.

To simplify the analysis, a common approach is to assume that the parameters are independent. The assumption of independence allows all the off-diagonal elements of the error covariance matrix to be zero. However, this assumption is unlikely to be true for most TEMs, which can have a large number of parameters.

We propose that by reducing the scope of the analysis to a few key parameters, and by constraining the model with multiple observations, the independence assumption can still be used. This approach has the additional benefit of reducing the computational resources required, which in turn allows a suite of inversions to be used. A simple conceptual model, described below, was used to demonstrate the Monte Carlo inversion scheme for a TEM with few model parameters.

The conceptual model

The conceptual model represents the key features of a typical TEM, i.e. energy partitioning and C flux. The conceptual model used a set of 3 simple equations with 3 model parameters. Model outputs were the latent energy flux (λE), the gross primary production (C_{GPP}) and the net ecosystem exchange (C_{NEE}). The three model

parameters were; the leaf area index (L), foliar nitrogen per leaf area (N) and the respiration rate (R):

$$\lambda E = d \cdot L$$
$$C_{GPP} = d \cdot L \cdot N$$
$$C_{NEE} = R - C_{GPP}$$

where d was the diurnal signal (range 0-1) represented by a half-wave rectified sinusoid. L, N and R were given normalised values of 1.

Inverting the conceptual model

We used the conceptual model as part of a twin experiment. We ran the model using specified parameter values to generate synthetic observations. We then used the Monte Carlo inversion scheme to invert these (synthetic) observations and find the *posterori* distributions. The *posterori* distribution represents the updated estimates of the parameters and their uncertainty. The advantage of the twin approach is that we know the exact parameters that gave rise to the (synthetic) observations.

We performed this inversion for two cases (both with an *a priori* uncertainty standard deviation of 0.25); (1) with our *a priori* correctly defined to be 1, and (2) with incorrectly defined *a priori* of 2. The first case was our control, where we expected the inversion would find the correct parameters (left panels, Figure 2). The second case simulated the (likely) possibility of incomplete/incorrect *a priori* knowledge (right panels, Figure 2).

For each case we ran four analyses which varied in the degree to which they constrained the system; (1) C_{NEE} observations and flat (non-informative) *a priori*, (2) C_{NEE} observations and true *a priori*, (3) C_{NEE}, C_{GPP}, λE observations and flat, non-informative, (i.e. no *a priori* knowledge, except perhaps high/low bounds) *a priori*, and (4) C_{NEE}, C_{GPP}, λE observations and true *a priori*. As expected, running the analysis with C_{NEE} observations and flat *a priori* constrained the parameters the least, and the best constrained run used all available information: the *a priori* and C_{NEE}, C_{GPP}, λE observations.

Results and discussion for the conceptual model

From the equations it could easily be predicted that the conceptual model would not constrain any of the parameters using just C_{NEP} observations. Too many degrees of

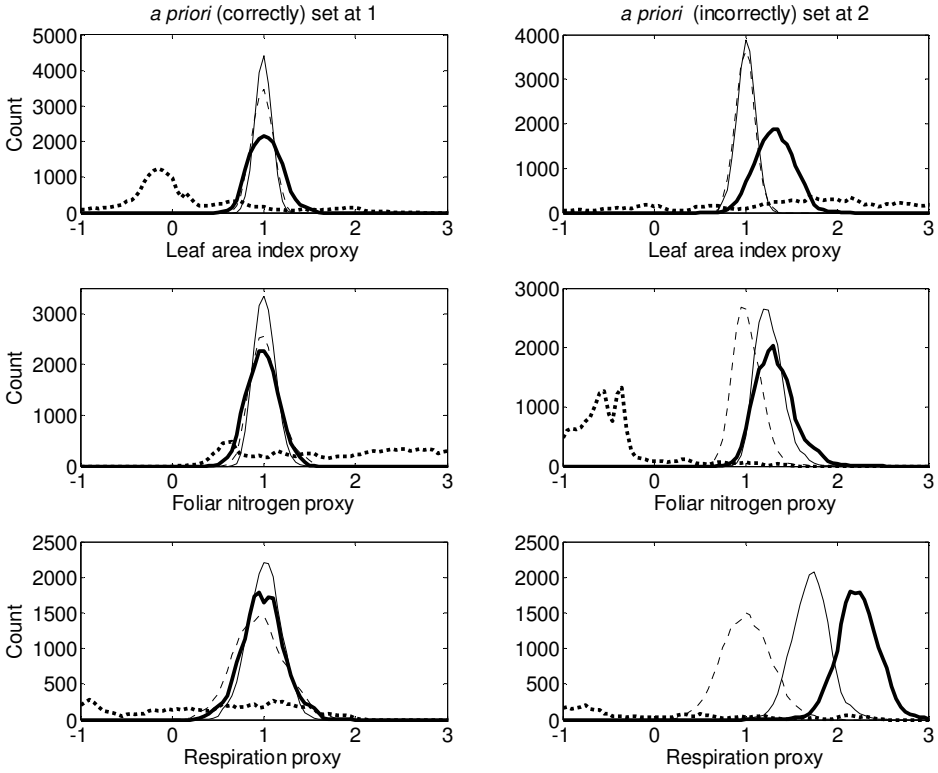

Figure 2: *Posterori* distributions for the simple conceptual model, which is based on a set of three equations and three parameters. The analysis was run for two cases; correctly defined *a priori* which match the observations and incorrectly defined *a priori*. For each of these cases four runs were performed with varying degrees of constraint on the system. Where (——) GPP + LE + NEE + *A priori*, (- - -) GPP + LE + NEE, (——) NEE + *A priori* and, (·····) NEE.

freedom exist in the equations for NEE, and without constraining the other equations, there were no constraints on any of the model parameters. This is almost what we saw in the inversion of the conceptual model (left panels, Figure 2); where both L and R were unconstrained. N appeared to be partially constrained with a strong peak around -0.3. However, this peak was a spurious result caused by the structure of the inversion and the model. Due to being unconstrained, the other parameters (L and N) had reached extreme values. Since parameter steps were chosen as neighbouring points on a Latin-hypercube, steps made from already extreme parameter values had very little impact on the model predictions (as the percentage change in the parameter was small). This effect left N as the only parameter to have an impact on model predictions. Consequently the peak was formed. When exactly the same inversion model was rerun, the spurious nature of this peak became obvious, as its location was random (right panels, Figure 2).

Inverting both the C_{NEE} observations and *a priori* returned reasonable posterori, however we know that just the C_{NEE} observations did not provide any additional information (left panels, Figure 2). Thus, the *posterori* were really just the unmodified *a priori*.

Inverting C_{NEE}, C_{GPP}, λE and flat (non-informative) *a priori* constrained the system, returning the expected *posterori* (left panels, Figure 2). When non-flat *a priori* were also used the system was further constrained, as expected. This final setup is particularly suitable for inversions, as the observations were able to inform and update the *a priori*.

In the case where we had incorrect *a priori* information (right panels, Figure 2), we see that the *posterori* distributions were much closer to the 'truth' for the well constrained system. When just C_{NEE} and *a priori* were used in the inversion, the *posterori* estimates of R were shifted by more than the bias in the *a priori*. The biased *a priori* tended to 'push' the L, N and R parameters higher than they actually were. The observations work to reduce this pushing effect. R, as the least constrained parameter, exhibited the greatest bias. This effect is much reduced for the inversion using C_{NEP}, C_{GPP}, λE and the *a priori*, due the improved observational constraints.

Looking at Figure 2, one might be tempted to conclude that constraining the system using observations and flat *a priori* would provide the best solution. However, when using 'real' TEMs and measurements a large amount of uncertainty will be associated with the model and the observations and so the inclusion of *a priori* is desirable.

Conclusions from the conceptual model

We can draw several conclusions (some obvious) from the conceptual model: (1) sufficient constraining observations need to be used in the inversion analysis. If too few are used, then the model returns the *a priori* unmodified, this can be a misleading result as it returns only what you expect to see. (2) Using flat (non-informative) *a priori* can be a useful tool for analysing the constraints placed on the system by the observations. They allow us to infer the limits of what the model and observations can and cannot tell us about the parameters. However, this does not imply that we should always use flat *a priori*, as this would ignore a valuable source of information. (3) Badly defined *a priori* can result in the *posterori* distributions of some parameters being biased by more than the *a*

priori. This is obvious if the *posterori* distributions are not within the bounds of either the *a priori* or *posterori* distributions generated with flat *a priori*.

The Coupled-Atmosphere-Biosphere inversion setup

The coupled atmosphere-biosphere model [*Hill, et al.*, 2007a; *Hill, et al.*, 2007b] used in the inversion was a combination of three separate models; the soil-plant-atmosphere (SPA) model [*Williams*, 2005; *Williams, et al.*, 2001a; *Williams, et al.*, 1996], a respiration box model [*Williams, et al.*, 2005] and the Oregon State University one-dimensional planetary boundary layer (OSU1DPBL) model [*Mahrt and Pan*, 1984; *Troen and Mahrt*, 1986]. The CAB model relates leaf-level processes and measurements to stand-based observations (eddy covariance data) and the PBL (radiosonde and aircraft profiles). It is initialised by a set of parameters describing the state of the vegetation, soil and the atmosphere. Our analysis used parameterisations based on a black spruce boreal forest [*Hill, et al.*, 2007a; *Jarvis, et al.*, 1997; *Jarvis and Moncrieff*, 2000; *Newcomer, et al.*, 2000].

The setup of the experiment was based on the conclusions of the conceptual model, and to reduce parameter covariance, only looked at the model response to 6 parameters; leaf area index, foliar nitrogen per leaf area, plant hydraulic conductance, roughness length, albedo and a respiration scaling factor. A respiration scaling factor was used, because in the box model there was no overall rate controlling the respiration that was suitable for scaling.

Twin (synthetic) data were used in this analysis. The interpretation of twin data is inherently simpler as the model has the inherent ability to reproduce the twin data using realistic parameters. However, the use of twin data does not preclude the possibility of an informative analysis. On the contrary, if we acknowledge the fact that the model has the ability to reproduce the twin data, then we can use this to find the limits of the analysis, and to explore potential effect of biases (which can be specified). The twin data were generated by running the CAB model for the black spruce parameters. The output from this CAB model run was used as the twin data, and various uncertainties and biases added (Table 1).

Uncertainties (not just measurement error) for eddy covariance measurements and aircraft profiles are hard to estimate. This was particularly true for real datasets as the errors that we considered included real processes that are captured by eddy covariance systems (e.g. katabatic flows) or aircraft profiles of the PBL (e.g. advection)

but were not explicitly captured in the model. Both the systematic and random errors associated with eddy covariance data have been extensively studied [*Goulden, et al.*, 1996; *Hollinger and Richardson*, 2005]. *Loescher, et al.,* (2006) conclude that the treatments of errors are inherently site specific, and so reasonable assumptions for the errors in our twin experiment have to be made. In the twin experiment, as we did not have these uncertainties, 'standard' observation uncertainties were assumed to be Gaussian with standard deviations of 20% for LE, 20% for daytime NEE and 50% for night time NEE, as used in other experiments [*Knorr and Kattge*, 2005]. Day and night were distinguished using the PAR as a threshold. Uncertainties on the profile measurements were expressed as standard deviations of 0.5 K for air temperature, 0.25 g kg^{-1} for water mixing ratio, and 0.75 ppm for CO_2 concentration. In the case of real datasets, repeat profiles through the PBL would allow these uncertainties to be found more accurately.

The CAB model was run for a single day and LE and NEE fluxes were compared for each half-hour period. The PBL profile measurements were compared between 200 m and 800 m (the mixed layer for this day) at 1300 hrs local time. PBL comparisons are performed once daily because it is unlikely that real profile data would be available on a half-hourly basis.

Individual experiment setup

A series of experiments were devised to demonstrate the possibilities of the inversion and to answer the questions set out in the introduction. We followed the general Monte Carlo inversion method described above and set up 4 experiments:

Gelman criteria setup: The analysis was run to determine the burn-in period and number of accepted steps required by the inversions. To determine the correct burn-in period and the number of runs to perform, we calculated the Gelman reduction factor using an ensemble of 12 independently identical runs. Each run was performed using 100,000 accepted steps, with log-normal *a priori* of 1 and *a priori* uncertainties of 0.25 (Table 1). Synthetic eddy covariance and aircraft profiles were generated from a single CAB model run using the log-normal *a priori* parameter values. Standard uncertainty, as described above, was added to the synthetic eddy covariance fluxes and aircraft data.

Flat a priori setup: The analysis was run with flat *a priori* and twin data without uncertainty. The permissible range of log-normal parameter values were bounded

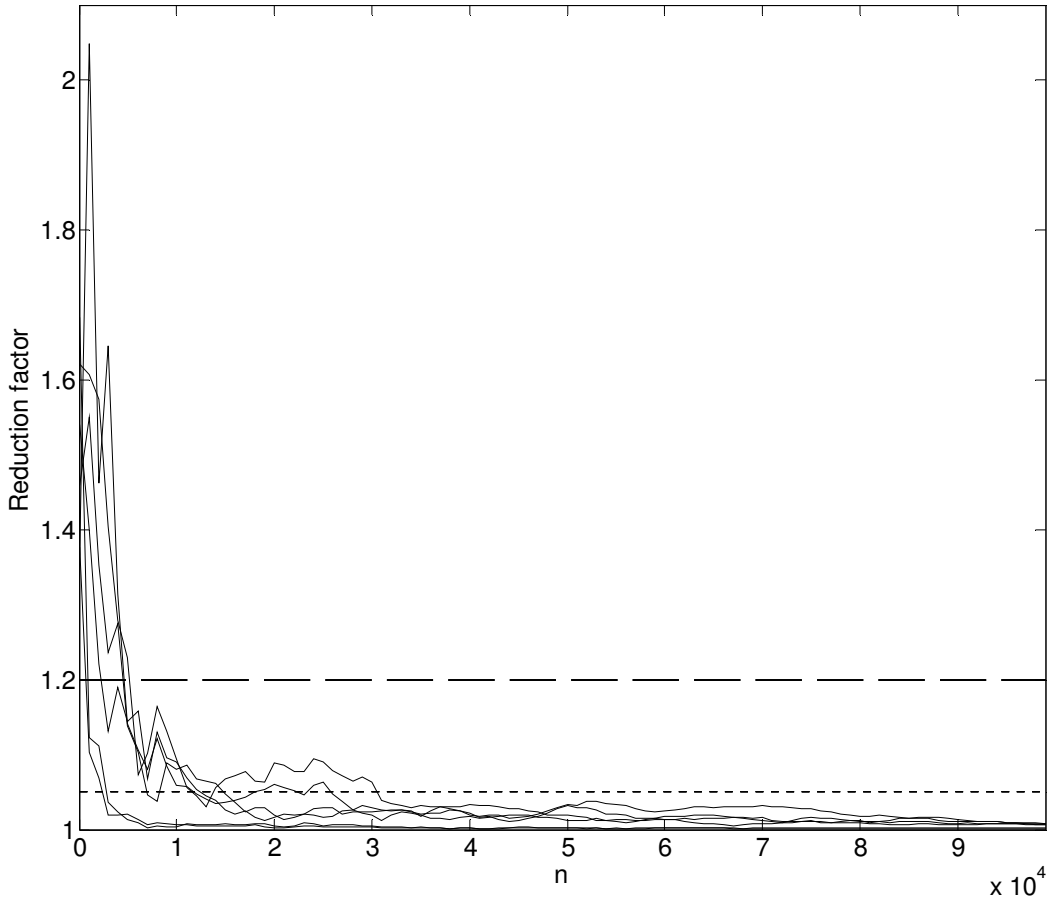

Figure 3: The Gelman reduction factor for n parameter steps of the CAB model inversion. 6 lines are shown representing the reduction factor for each of the CAB model's six parameters. 12 individual analyses were compared to calculate the reduction factor. The burn-in period is set so that a reduction factor of 1.2 (— — —) is achieved by all parameters. Based on these runs, and a threshold of 1.05 (- - - -), we chose n =50000 for log-normal *a priori* uncertainties of 0.25

between -2 and 4. This gave the inversion a loosely bound range of permissible model parameter values (from $1/20^{th}$ to 20 times the *a priori* model parameter value).

The number of accepted steps was increased to 300,000, with a burn-in of 10,000 steps (Table 1). The increase to 300,000 accommodated the flat *a priori*, and thus the lowered constraints on inversion, and the longer walk required in order to sufficiently sample the parameter space.

The experiment consisted of three different setups, which used different combinations of observations to constrain the inversion; (1) using eddy-covariance observations, (2) using PBL measurements, and (3) using both eddy covariance and PBL measurements.

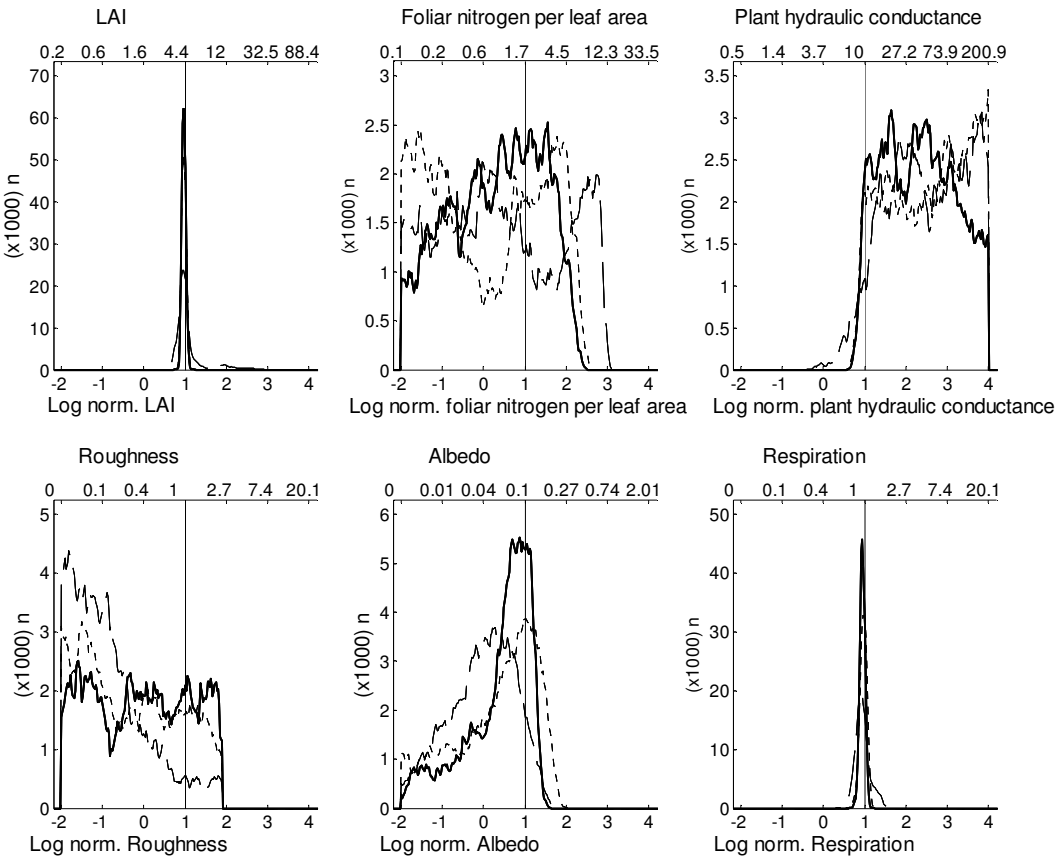

Figure 4: The constraints placed on the *posterori* distributions of 6 parameters by the model and the observations. Flat *a priori* are used for this analysis and the CAB model was constrained by flux data and aircraft observations. Log-normal parameter values are shown on the bottom of each panel, with the actual value on top. Where (——) aircraft soundings + flux data, (- - - -) flux data only and (— — —) aircraft soundings.

Uncertainties setup: The analysis was designed to determine the impact of observational uncertainty on the *posterori* distributions, and was run in two stages. The first stage used twin data with added uncertainty. Three levels of uncertainty were added (Table 1): (1) the standard, 100%, (2) 50%, and (3) 200% uncertainty. The second stage used the standard uncertainty with added bias. In the biased runs the twin data with standard uncertainty were biased by ± 50% of the observations standard deviations (Table 1).

False a priori setup: The analysis was run to discover the likely impacts of poorly chosen *a priori*. The *a priori* were set either high, or low, by 1 standard deviation. Eddy-covariance and aircraft twin data with standard levels of uncertainty were used (Table 1).

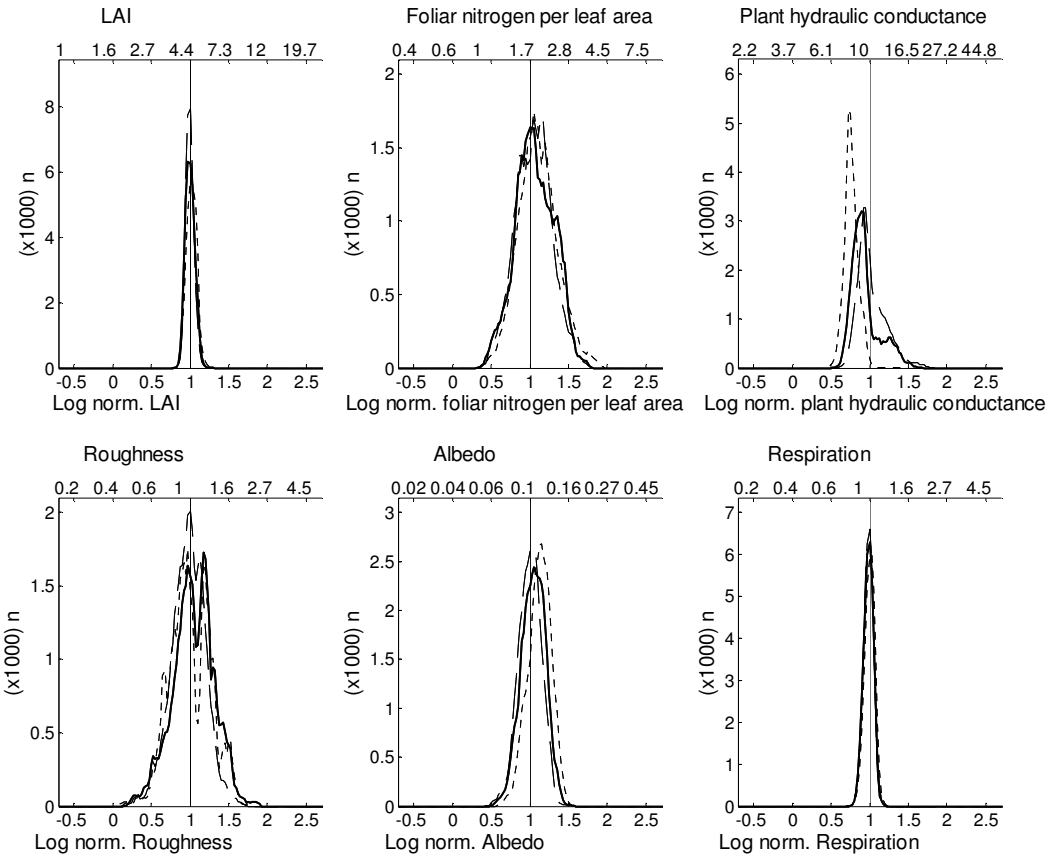

Figure 5: Shows the effect on the *posterori* distributions of increasing (unbiased) observation uncertainty. Log-normal parameter values are shown on the bottom of each panel, with the actual value on top. Where (——) standard uncertainty, (- - - -) 200% standard uncertainty and (— — —) 50% standard uncertainty.

Experiment results

Gelman criteria results: The Gelman reduction factor showed the first 5000 accepted steps significantly under-sampled parameter space (Figure 3). For more than 5,000 accepted steps all six parameters' reduction factors remained under the moderate threshold of a reduction factor of 1.2. After ~35,000 accepted steps, all six reduction factors remained under the more stringent threshold of 1.05. Thus, 50,000 accepted steps with a burn-in period of 10,000 steps will provide a good, robust sampling of parameter space.

Flat a priori results: The inversion had very variable constraints on the different model parameters (Figure 4, Table 2). LAI and respiration were well constrained. Albedo and the plant hydraulic conductance both had strong constraints on one side of the distribution, and little constraint on the other side. Foliar nitrogen was moderately

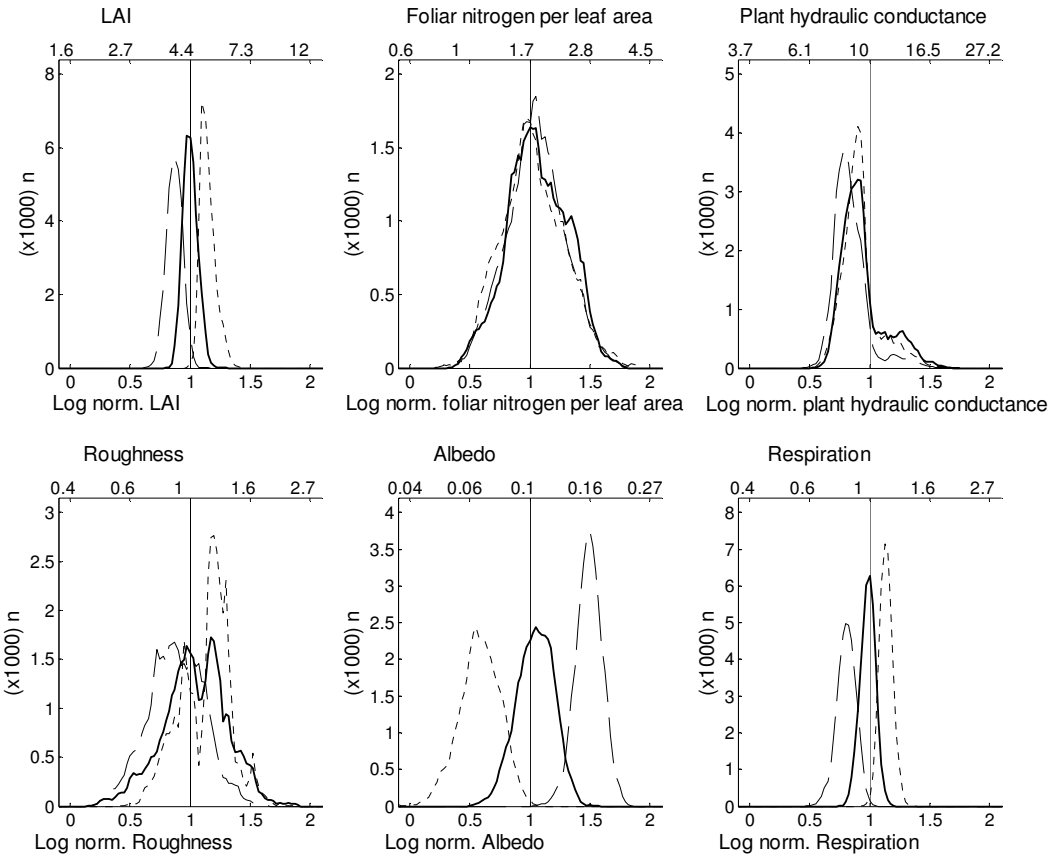

Figure 6: Shows the effect on the *posterori* distributions of biased observation uncertainty. Log-normal parameter values are shown on the bottom of each panel, with the actual value on top. Where (——) standard uncertainty (unbiased), (- - - -) standard uncertainty + 0.5 standard deviation bias and (— — —) standard uncertainty - 0.5 standard deviation bias.

constrained, and roughness was unconstrained. In general, the aircraft constrained the measurements the least, whilst eddy covariance measurements provided a better constraint for the parameters. Using both the eddy-covariance flux measurements and the aircraft profile observations constrained the parameters the most. The combined approach yielded standard deviations that were on average 84% of the eddy covariance only inversion and, 74% of the aircraft only inversion.

Uncertainty results: For the three levels of uncertainty, the six parameters showed consistent means, standard deviations and skews (Figure 5, Table 2). Hydraulic conductance was the only parameter to show large amounts of skew, or mean more than 1 standard deviation from the log-normal actual value of 1.

Biasing the twin data has a much greater impact on the *posterori* distributions than the level of uncertainty added (Figure 6, Table 2). Foliar nitrogen and the plant hydraulic conductance were the only parameters not to be affected much. Most of the

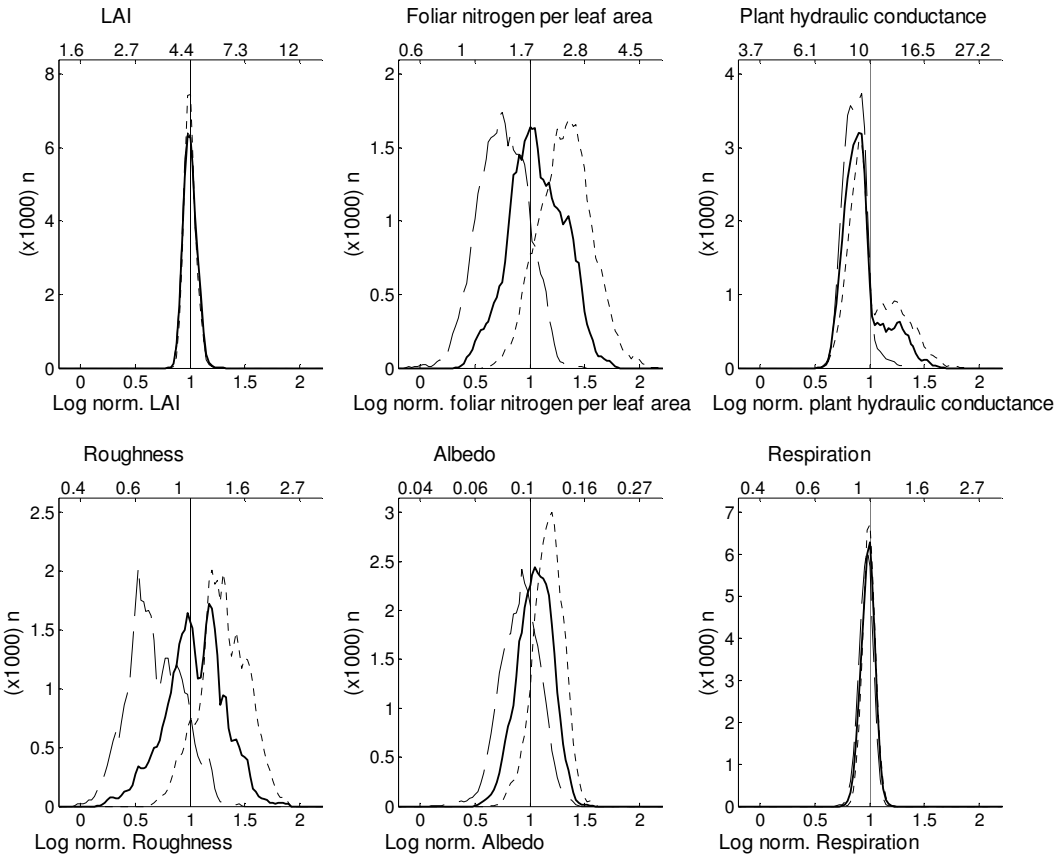

Figure 7: Shows the modification to the *posterori* distributions that can be expected from biased *a priori*. Log-normal parameter values are shown on the bottom of each panel, with the actual value on top. Where (——) (nominal) *a priori*, (- - - -) *a priori* + 1 standard deviation and (— — —) *a priori* - 1 standard deviation.

biases induced in the *posterori* distributions followed the direction of the biases in the twin data; that is a positive bias in the twin data resulted in a positive bias in the *posterori*. This feature was true for all parameters except the albedo, which had its direction of bias reversed.

False a priori results: Using poorly determined *a priori* has little impact on LAI, plant hydraulic conductance or the respiration scaling factor (Figure 7). Impacts on foliar nitrogen, roughness and albedo were large enough to cause the *posterori* to have means further than 1 standard deviation of the log-normal value (Table 2).

Discussion

What biosphere parameter likelihoods can be inferred from eddy-covariance data and aircraft PBL measurements?

Exp. Name	Steps	Runs	Burn-in steps	*a priori*	*a priori* uncert.	Obs. Std.Dev. (%)	Obs. Offset Std. Dev. (%)
Gelman							
All	100000	12	10000	1	0.25	0	0
Flat pri							
Flux	300000	1	10000	Flat	N/A	0	0
Aircraft	300000	1	10000	Flat	N/A	0	0
Both	300000	1	10000	Flat	N/A	0	0
Uncert. 1 (Magnitude)							
50%	50000	1	10000	1	0.25	100	0
Nominal (100%)	50000	1	10000	1	0.25	100	0
200%	50000	1	10000	1	0.25	100	0
Uncert. 2 (Bias)							
Nominal (0%)	50000	1	10000	1	0.25	100	0
-50%	50000	1	10000	1	0.25	100	-50
50%	50000	1	10000	1	0.25	100	50
False Pri.							
Nominal	50000	1	10000	1	0.25	100	0
+1 Std. Dev.	50000	1	10000	1.25	0.25	100	0
-1 Std. Dev.	50000	1	10000	0.75	0.25	100	0

Table 1: Individual model run initialisations.

In the flat a priori experiment, in which *a priori* are specified to be flat and non informative, we explored the theoretical limits of what inverting the observations can tell us about our parameters, i.e. the data resolution. The flat *a priori* experiment showed the LAI and the respiration scaling factor to be well constrained using both aircraft profiles and eddy-covariance measurements (Figure 4, Table 2). These strong constraints on LAI were expected; LAI has a strong impact on all the observations and so can be well constrained by using all 5 observations. Although the impact of the respiration scaling factor only directly affected the NEE flux measurements and the CO_2 PBL profile, as the only parameter to uniformly impact NEE, it was well constrained by the nocturnal respiration. This means that, theoretically at least, we might be able to determine the LAI and respiration using an inversion. However, it should be noted that these experiments do not show that we can determine the LAI and respiration to this accuracy, but rather that these are the theoretical limits.

Both the albedo and the plant hydraulic conductance showed a thresholding effect suggesting that the parameter only has an impact above (or below) a certain critical threshold (Figure 4, Table 2). In the case of albedo, this constraint provides information on the upper limit of albedo, but cannot inform us about the lower limit. Only an upper limit on albedos was evident, because the change in the proportion of incident radiation that was reflected had little impact on the system. This occurs because

Exp. Name	Leaf area index			Foliar nitrogen			Plant hyd. Cond.			Roughness			Albedo			Respiration		
	M.	SD.	Sk.	M.	SD.	Sk.	M.	SD.	Sk.	M.	SD.	Sk.	M.	SD.	Sk.	M.	SD.	Sk.
Gelman																		
All	n/a	n/a	n/a	n/a	n/a	n/a	n/a	n/a	n/a	n/a	n/a	n/a	n/a	n/a	n/a	n/a	n/a	n/a
Flat pri																		
Flux	0.97	0.06	0.16	0.13	1.38	0.01	2.54	0.94	-0.16	-0.32	1.14	0.25	0.30	0.98	-0.67	0.97	0.09	-0.25
Aircraft	1.07	0.35	2.57	0.45	1.45	0.10	2.49	0.95	-0.19	-0.85	0.91	1.03	-0.04	0.80	-0.36	0.95	0.18	0.57
Both	0.97	0.05	0.20	0.28	1.11	-0.22	2.33	0.86	0.11	-0.07	1.15	0.00	0.35	0.80	-1.09	0.94	0.06	-0.10
Uncert. 1 (Magnitude)																		
50%	1.00	0.05	0.36	1.05	0.23	0.02	1.02	0.19	0.98	0.98	0.22	-0.22	1.00	0.15	-0.18	0.98	0.06	-0.25
Nom. (100%)	1.00	0.06	0.26	1.06	0.25	-0.02	0.94	0.18	1.12	1.04	0.27	-0.18	1.05	0.16	-0.22	0.98	0.06	-0.14
200%	1.02	0.07	0.15	1.10	0.25	0.21	0.76	0.09	0.48	1.00	0.27	-0.05	1.12	0.15	-0.30	1.00	0.07	-0.19
Uncert. 2 (Bias)																		
Nom. (0%)	1.00	0.06	0.26	1.06	0.25	-0.02	0.94	0.18	1.12	1.04	0.27	-0.18	1.05	0.16	-0.22	0.98	0.06	-0.14
-50%	0.87	0.07	-0.06	1.05	0.25	0.03	0.84	0.15	1.61	0.88	0.23	-0.08	1.49	0.11	-0.18	0.81	0.08	-0.30
50%	1.15	0.06	0.77	1.03	0.26	0.16	0.92	0.16	1.22	1.13	0.21	-0.24	0.58	0.17	-0.28	1.14	0.06	0.14
False Pri.																		
Nominal	1.00	0.06	0.26	1.06	0.25	-0.02	0.94	0.18	1.12	1.04	0.27	-0.18	1.05	0.16	-0.22	0.98	0.06	-0.14
+1 Std. Dev.	1.00	0.05	0.44	1.32	0.24	0.09	1.02	0.22	0.84	1.30	0.22	-0.07	1.17	0.14	-0.24	0.99	0.06	0.01
-1 Std. Dev.	1.00	0.06	0.23	0.75	0.22	-0.10	0.87	0.10	0.53	0.68	0.24	0.17	0.91	0.18	-0.25	0.97	0.06	-0.23

Table 2: Log-normal means (M), standard deviations (SD) and skews (Sk) for the CAB model experiments. Shading denotes parameter-experiment combinations which have means within 1 standard deviation of the log-normalised *a priori* (i.e. 1).

the energy partitioning of the vegetation was the controlling factor. For plant hydraulic conductance we similarly obtained a lower limit. In addition to suggesting that below this threshold the hydraulic conductance was the limiting factor determining the transpiration rate, but above the threshold, other processes imposed the limit.

How well do measurements of CO_2 concentrations and/or fluxes help constrain the system?

As foliar nitrogen only directly impacts the NEE and atmospheric CO_2, we consequently expect it to be slightly less constrained than LAI. However, the large uncertainty in foliar nitrogen indicates that it is not well constrained by the NEE and the atmospheric CO_2. This is because the inversion is largely constrained by processes tied to transpiration, and thus energy partitioning at the land surface (Figure 4, Table 2). As foliar nitrogen has little impact on the dynamics of the PBL, it is equally difficult to constrain with aircraft measurements.

Roughness also appears to be unconstrained in our inversions (Figure 4, Table 2), and likely is not a controlling parameter in the system. Surface wind speeds on this particular day were relatively low (<2.5 m s^{-1}), and the dynamics are driven by the turbulent mixing from sensible heating. Thus, the energy partitioning at the land surface performed by the vegetation largely determines the dynamics of the system, and not the mechanical roughness of the land-surface.

How does the resolving power of observations deteriorate with uncertainty?

As the uncertainty on observations increases it could be expected that the observation resolution should also decrease. However we do not see this, instead a fourfold increase in measurement uncertainty resulted in nearly identical means, standard deviations and skews (Table 2). This means that the (unbiased) uncertainty of the measurements is not critical to the inversion process.

In turn, biases in the observations had a strong impact on the *posterori* distributions (Figure 6, Table 2). These impacts were evident despite the fact that the bias applied was less than the increase in standard deviation used in the unbiased uncertainty experiments. Looking at the mean values and standard uncertainties (Table 2) we can see that the model has strongly impacted the inversion's ability to identify the correct parameters.

How do biases in our a priori knowledge affect our ability to determine the true parameter values?

In the false a priori experiment, the offset in the *posterori* distribution resulting from the biased *a priori* was only noticeable for certain parameters (Figure 7, Table 2). The unbiased parameters were the ones that were best constrained in the flat a priori experiment (Figure 4, Table 2), i.e. LAI, plant hydraulic conductance and the respiration scaling factor. The *posterori* distribution for these parameters remained virtually unaltered. For the less constrained parameters (albedo, foliar nitrogen and roughness) the mean values were offset by up to 1.5 standard deviations (Table 2). This means that for some parameters the *posterori* distribution had been offset further than the *a priori* offset. With the bias in the *a priori,* the inversion was under a 'tension' between the corroboration with the observations and the *a priori*. This tension resulted in the *posterori* distribution of the parameters experiencing an exaggerated bias, much like in the example of the conceptual model (Figure 2).

Conclusions

We have demonstrated a simple inversion method and also the use of this method with a simple conceptual model. The conceptual model was used to show the benefit of a high ratio of constraints to parameters. The conceptual model was also used to demonstrate the possibilities of using flat, non-informative *a priori*, which can be used to determine limiting processes. The same inversion scheme was then applied to the more complicated CAB model.

In the CAB model inversion we use these principles to show that there is potential for resolving robust unbiased estimates of LAI, the lower threshold plant hydraulic conductance and the respiration scaling factor. However the other parameters in the study were less well constrained and vulnerable to biases in both the *a priori* estimates and the observations. The study also shows that there is potential to invert just atmospheric measurements to find surface parameters, but that the approach is likely to yield poorer estimates, with greater uncertainty than inversions of eddy covariance or the combination of the two. However it is possible good estimates of the LAI and the respiration flux could be obtained, as well as thresholds for the hydraulic conductance of the vegetation. However application of any of these techniques to real data would require a thorough treatment of the associated errors.

References

Aubinet, M., et al. (2000), Estimates of the annual net carbon and water exchange of forests: The EUROFLUX methodology, *Advances in Ecological Research, Vol 30*, *30*, 113-175.

Baldocchi, D., et al. (2001), FLUXNET: A new tool to study the temporal and spatial variability of ecosystem-scale carbon dioxide, water vapor, and energy flux densities, *Bulletin of the American Meteorological Society*, *82*, 2415-2434.

Baldocchi, D. D. (2003), Assessing the eddy covariance technique for evaluating carbon dioxide exchange rates of ecosystems: past, present and future, *Global Change Biology*, *9*, 479-492.

Bayes, T. (1763), An Essay Towards Solving a Problem in the Doctrine of Chances, *Philosophical Transactions*, *53*, 370-418.

Betts, R. A. (2000), Offset of the potential carbon sink from boreal forestation by decreases in surface albedo, *Nature*, *408*, 187-190.

Betts, R. A., et al. (2004), The role of ecosystem-atmosphere interactions in simulated Amazonian precipitation decrease and forest dieback under global climate warming, *Theoretical and Applied Climatology*, *78*, 157-175.

Cox, P. M., et al. (2000), Acceleration of global warming due to carbon-cycle feedbacks in a coupled climate model, *Nature*, *408*, 184-187.

Denning, A. S., et al. (2003), Simulated variations in atmospheric CO2 over a Wisconsin forest using a coupled ecosystem-atmosphere model, *Global Change Biology*, *9*, 1241-1250.

Dolman, A. J., et al. (2006), The CarboEurope regional experiment strategy, *Bulletin of the American Meteorological Society*, *87*, 1367-+.

Fisher, R. A., et al. (2006), Evidence from Amazonian forests is consistent with isohydric control of leaf water potential, *Plant Cell and Environment*, *29*, 151-165.

Franks, S. W., and K. J. Beven (1997), Bayesian estimation of uncertainty in land surface-atmosphere flux predictions, *Journal of Geophysical Research-Atmospheres*, *102*, 23991-23999.

Friedlingstein, P., et al. (2006), Climate-carbon cycle feedback analysis: Results from the (CMIP)-M-4 model intercomparison, *Journal of Climate*, *19*, 3337-3353.

Gelman, A. (1995), *Bayesian data analysis*, xix, 526p. pp., Chapman & Hall, London.

Goulden, M. L., et al. (1996), Measurements of carbon sequestration by long-term eddy covariance: Methods and a critical evaluation of accuracy, *Global Change Biology*, *2*, 169-182.

Gurney, K. R., et al. (2002), Towards robust regional estimates of CO2 sources and sinks using atmospheric transport models, *Nature*, *415*, 626-630.

Gurney, K. R., et al. (2003), TransCom 3 CO2 inversion intercomparison: 1. Annual mean control results and sensitivity to transport and prior flux information, *Tellus Series B-Chemical and Physical Meteorology*, *55*, 555-579.

Heinsch, F. A., et al. (2006), Evaluation of remote sensing based terrestrial productivity from MODIS using regional tower eddy flux network observations, *Ieee Transactions on Geoscience and Remote Sensing*, *44*, 1908-1925.

Hill, T. C., et al. (2007a), Interactions between a boreal forest stand and the planetary boundary layer, *In preparation.*

Hill, T. C., et al. (2007b), Testing the carbon, water and energy flux predictions of a coupled atmosphere-biosphere model above a boreal forest., *In preparation*.

Hollinger, D. Y., and A. D. Richardson (2005), Uncertainty in eddy covariance measurements and its application to physiological models, *Tree Physiology*, *25*, 873-885.

Jarvis, P. G., et al. (1997), Seasonal variation of carbon dioxide, water vapor, and energy exchanges of a boreal black spruce forest, *Journal of Geophysical Research-Atmospheres*, *102*, 28953-28966.

Jarvis, P. G., and J. B. Moncrieff (2000), "The CO2 Exchanges of Boreal Black Spruce Forest." In Collected Data of The Boreal Ecosystem-Atmosphere Study., edited by J. Newcomer, et al.

Kaminski, T., et al. (1999), A coarse grid three-dimensional global inverse model of the atmospheric transport - 1. Adjoint model and Jacobian matrix, *Journal of Geophysical Research-Atmospheres*, *104*, 18535-18553.

Kaminski, T., et al. (2002), Assimilating atmospheric data into a terrestrial biosphere model: A case study of the seasonal cycle, *Global Biogeochemical Cycles*, *16*, -.

Kljun, N., et al. (2004), A simple parameterisation for flux footprint predictions, *Boundary-Layer Meteorology*, *112*, 503-523.

Knorr, W., and J. Kattge (2005), Inversion of terrestrial ecosystem model parameter values against eddy covariance measurements by Monte Carlo sampling, *Global Change Biology*, *11*, 1333-1351.

Loescher, H. W., et al. (2006), Uncertainties in, and interpretation of, carbon flux estimates using the eddy covariance technique, *Journal of Geophysical Research-Atmospheres*, *111*, -.

Mahrt, L., and H. Pan (1984), A 2-Layer Model of Soil Hydrology, *Boundary-Layer Meteorology*, *29*, 1-20.

Moncrieff, J. B., et al. (1997), A system to measure surface fluxes of momentum, sensible heat, water vapour and carbon dioxide, *Journal of Hydrology*, *189*, 589-611.

Mosegaard, K., and A. Tarantola (1995), Monte-Carlo Sampling of Solutions to Inverse Problems, *Journal of Geophysical Research-Solid Earth*, *100*, 12431-12447.

Newcomer, J., et al. (2000), Collected Data of The Boreal Ecosystem-Atmosphere Study. NASA., edited.

Running, S. W., et al. (1999), A global terrestrial monitoring network integrating tower fluxes, flask sampling, ecosystem modeling and EOS satellite data, *Remote Sensing of Environment*, *70*, 108-127.

Schimel, D. S. (1995), Terrestrial Ecosystems and the Carbon-Cycle, *Global Change Biology*, *1*, 77-91.

Shuttleworth, W. J. (1991), Insight from Large-Scale Observational Studies of Land Atmosphere Interactions, *Surveys in Geophysics*, *12*, 3-30.

Troen, I., and L. Mahrt (1986), A Simple-Model of the Atmospheric Boundary-Layer - Sensitivity to Surface Evaporation, *Boundary-Layer Meteorology*, *37*, 129-148.

Van Oijen, M., et al. (2005), Bayesian calibration of process-based forest models: bridging the gap between models and data, *Tree Physiology*, *25*, 915-927.

Williams, M. (2005), The Soil-Plant-Atmosphere model: Manual, version 1.2, April 2005, edited, p. 32, University of Edinburgh.

Williams, M., et al. (2001a), Use of a simulation model and ecosystem flux data to examine carbon-water interactions in ponderosa pine, *Tree Physiology*, *21*, 287-298.

Williams, M., et al. (1998), Seasonal variation in net carbon exchange and evapotranspiration in a Brazilian rain forest: a modelling analysis, *Plant Cell and Environment*, *21*, 953-968.

Williams, M., et al. (1996), Modelling the soil-plant-atmosphere continuum in a Quercus-Acer stand at Harvard forest: The regulation of stomatal conductance by light, nitrogen and soil/plant hydraulic properties, *Plant Cell and Environment*, *19*, 911-927.

Williams, M., et al. (2001b), Primary production of an arctic watershed: An uncertainty analysis, *Ecological Applications*, *11*, 1800-1816.

Williams, M., et al. (2005), An improved analysis of forest carbon dynamics using data assimilation, *Global Change Biology*, *11*, 89-105.

The Coupled Atmosphere-Biosphere model discussion

Climate change is expected to have a severe impact on the planet [*Houghton*, 2001]. Large amounts of uncertainty persist in our comprehension of the changes to the climate and their drivers. But the overwhelming consensus is that atmospheric carbon dioxide is one of the major causes of warming in the Earth system. The carbon dioxide levels in the atmosphere have been rising since industrial times [*Keeling*, 1960; *Keeling, et al.*, 1976], and this increase is largely due to anthropogenic activities. In their 4th assessment report, the Intergovernmental Panel on Climate Change (IPCC) stated that *"Most of the observed increase in globally averaged temperatures since the mid-20th century is very likely due to the observed increase in anthropogenic greenhouse gas concentrations"*, this represented a strengthening of similar assertions in the 3rd assessment report [*Houghton*, 2001; *Richard Alley, et al.*, 2007].

In order to assess the impact of a changing climate and to develop strategies to limit or mitigate the negative impacts, we must quantify the carbon cycle on local, regional and global scales [*Running, et al.*, 1999; *Ryan*, 2000; *Sellers, et al.*, 1997; *Shuttleworth*, 1991]. Due to the complexity of the carbon cycle, this task requires a combined modelling/measurement approach across multiple temporal and spatial scales (i.e. leaf-level processes to global feedbacks). Both models and measurements exist which operate on these scales, however inter-comparisons between (in particular) measurements at these scales are difficult, and require the use of intermediate models. Despite these difficulties, quantifying interactions between the land surface carbon cycling and the changing climate remains vital, as this component of the climate system contributes ~1.5 °C of uncertainty to global temperature predictions over the 21st century [*Meir, et al.*, 2006]. A crucial part of this quantification is the scaling up of leaf level processes to be globally applicable.

Scaling between the level of individual leaves and that of whole stands is performed using Soil-Vegetation-Atmosphere-Transport (SVAT) models and Terrestrial-Ecosystem Models (TEM). In order to investigate the processes linking this (stand-level) scale to larger regional scales, the Soil-Plant-Atmosphere (SPA) model [*Williams, et al.*, 1996] was coupled to the Oregon State University 1D Planetary Boundary Layer (OSU1DPBL) model [*Troen and Mahrt*, 1986] and a respiration box model [*Williams, et al.*, 2005]. The PBL is influenced by the land surface fluxes of mass,

water and energy on scales larger than individual stands. Thus models of this atmospheric region provide a spatial integrator for the spatial heterogeneity of land surface fluxes and processes.

Testing the Coupled Atmosphere-Biosphere model

The Coupled Atmosphere-Biosphere (CAB) model is the key modelling tool in this thesis. The model is verified in two stages: Firstly the biosphere parameterisations are verified using the offline biosphere component of the model. Secondly the fully coupled CAB model is run in a prognostic mode, predicting the dynamics of the biosphere and atmosphere, and the interactions between them.

At the land-surface

The offline biosphere model was comprised of the Soil Plant Atmosphere (SPA) model [*Williams, et al.*, 1996] and a carbon pool respiration model [*Williams, et al.*, 2005]. The offline biosphere model was tested against above ground observations (latent energy (LE) and net ecosystem exchange (NEE) eddy covariance flux measurements), and below ground measurements (soil temperature and moisture observations). The offline biosphere model was shown to be broadly supported by the daily aggregated fluxes over a whole growing season. Diurnal responses, resolved at the half-hourly timescale, were also captured. In general, agreement was higher between the modelled and measured LE than the NEE. This is attributable to the additional biosphere processes, measurement uncertainty and model components that were involved in the NEE comparisons. Modelled NEE agreed better with the half-hourly observations than the daily aggregates of NEE, indicating that inter-day variations were under estimated by the model. In general, the model measurement residuals were attributed to a combination of modelling issues (in particular the respiration box model) and measurement uncertainties.

Corroboration of the offline biosphere model was largely a test of the SPA model. The SPA model was shown to be able to competently simulate biosphere responses, this is in agreement with previous studies which applied the SPA model at a wide range of latitudes [*Engel, et al.*, 2002; *Fisher, et al.*, 2006; *Schwarz, et al.*, 2004; *Van Wijk, et al.*, 2003; *Williams, et al.*, 2000; *Williams, et al.*, 2001; *Williams, et al.*, 1997; *Williams, et al.*, 1996]. Consequently, we can expect the offline-biosphere model to be also applicable at a wide range of sites and latitudes.

The CAB model was in part verified by the offline-biosphere model, which used the exact same processes and parameters. Additional verification of the CAB model used comparisons with half-hourly land surface LE and NEE fluxes, and above canopy measurements of vapour pressure deficit and CO_2 concentration. The agreement between the CAB model and these land surface observations was good, with the model capturing the diurnal cycle, though some offsets occurred.

In the planetary boundary layer

CAB model predictions were corroborated with radiosonde and aircraft profiles of air temperature and mixing ratio and aircraft profiles of CO_2 concentration. The model managed to capture the evolution of the PBL. Suggesting that the model is correctly capturing the interaction of land surface processes and atmospheric dynamics within the PBL

Applying the CAB model

The CAB model, once corroborated at two old black spruce sites in the Boreal Ecosystem-Atmosphere Study (BOREAS), was used to investigate and partition feedbacks between the PBL and the biosphere:

(1) Can we identify feedbacks between the planetary boundary layer (PBL) and the biosphere, and what are their impacts on vegetation and PBL responses? The effect of altering a forest canopy was investigated by comparing the response of a changing canopy, to that of a nominal (fixed) canopy. Changes to the forest stand can be thought of as having two separate effects: (1) Physical changes to the biosphere can impact the ecosystem processes (e.g. stomatal dynamics). These changes directly impact fluxes of mass and energy, and therefore they also affect the PBL and surface meteorology. (2) The second effect is the feedback response of the biosphere to the changes in atmospheric conditions (due to effect 1). We demonstrated that the impact of these feedbacks was a moderation of (effect 1) the impacts on surface fluxes of LE, the above canopy air temperature and the water mixing ratio, by 22%, 37% and 27% respectively.

(2) What is the relative importance to the coupled system of changes to in the hydraulic, mechanical, and radiative properties of the biosphere? The CAB model was then used to decompose the feedbacks into radiative, hydrological and mechanical components. It was shown that both the radiative and the hydrological impacts were comparable in magnitude, and were both substantially larger than the mechanical impact.

(3) What is the importance of the diurnal CO_2 concentration cycle at the land surface? The impact of the diurnal cycle in CO_2 concentration was shown to have an insignificant effect on the productivity and energy balance of the vegetation.

(4) What is the overall impact of feedbacks between the atmosphere and ecosystem? The effects of the modifications made to the atmosphere by the vegetation (i.e. humidification and reduced air temperatures) were studied. The modification of the atmosphere by the vegetation (as compared to bare soil) caused a 5% drop in LE and 2% increase in gross primary production for the same vegetation cover. This occurred because the presence of vegetation permitted greater evapotranspiration. Thus cooling and humidifying the atmosphere, resulting in more favourable conditions for the plants.

(5) What biosphere parameter likelihoods can be inferred from eddy-covariance data and aircraft PBL measurements? The inversions showed that there was a good chance that both eddy covariance data and atmospheric profiles can be inverted (using the CAB model) to provide estimates of LAI, a lower threshold to plant hydraulic conductance and an estimation of the respiration rate.

(6) How well do measurements of CO_2 concentrations and/or fluxes help constrain the system? CO_2 flux measurements and PBL profiles provide one of the only direct constraints to foliar nitrogen. However since the CO_2 flux measurements and PBL profiles are dependant on many other factors (e.g. the leaf area) then their constraining power is low. Another reason for the CO_2 flux measurements' and PBL profiles' low constraining ability is the fact that CO_2, unlike temperature and humidity, does not directly impact the dynamics of the system.

(7) How does the resolving power of observations deteriorate with uncertainty? The effect of uncertainty on these inversions was also studied; unbiased uncertainty had little effect on the inversion results; a fourfold increase in measurement uncertainty resulted in nearly identical means and standard deviations. However biases in the observations had strong impacts on the system.

(8) How do biases in our prior knowledge affect our ability to determine the true parameter values? Biases in the prior knowledge also had strong impacts on the less constrained biosphere parameters. With some parameters being offset a greater amount than the prior bias. This occurred due to 'tension' between model components which resulted in the weakly constrained parameters experiencing an enhanced bias.

Model limitations

There are several limitations to the CAB model, ranging from issues that are common to all single column PBL models, to CAB specific issues:

(1) High data requirements. The CAB model has high data requirements, both in terms of the temporal resolution and the breadth of datasets required. This was one of the considerations for using BOREAS study sites, where vast contiguous datasets for the biosphere and atmosphere existed.

The high data requirements are an intrinsic part of studying the coupled-biosphere-atmosphere system. However it does not necessarily follow that it is always a weakness. The third (Bayesian) paper showed that the CAB model can be used to related observations on differing scales to constrain parameters. This means that the CAB model can be used to transfer knowledge from one component of the modelled system to another.

(2) *Synoptic weather conditions*. Synoptic weather conditions are not simulated in the CAB model; the scope of single column models means that the synoptic weather conditions have to be prescribed. Currently there is no mechanism within CAB to deal with PBL changes that synoptic conditions cause, and the CAB model can only be run out-with unstable periods of synoptic weather conditions.

To deal with synoptic weather conditions the atmospheric profile state vectors within the CAB model could be 'nudged' to allow the frontal resets associated with synoptic weather patterns. This process would essentially be performed using data assimilation, with the data being provided by new atmospheric profiles, back forecasts or predictions from a regional atmospheric model. This would allow the atmospheric dynamics to be reset, whilst maintaining continuity in the biosphere state vectors, such as soil water and temperature.

(3) Cloud formation. During the development of the CAB model the cloud formation routine was bypassed due to disagreements between the model's prediction of boundary layer clouds and the observations. Unfortunately this eliminated the possibility of studying a potentially strong feedback.

In certain circumstances it would be appropriate for the cloud formation routine to be reinstated. This would be particularly suitable when the absolute response of the system is not so critical (i.e. in sensitivity studies), however verifying the nominal response of the system could be problematic. A better solution would be the inclusion

of an updated cloud formation routine, possibly incorporating the role of isoprene in cloud seeding.

(4) *The footprint of the CAB model.* The footprint of the PBL is large, and in certain regions (e.g. the UK) this footprint can be larger than the continuous patches of land cover. This presents a problem for direct comparisons of the land surface with atmospheric profiles, as biosphere processes reflected in the PBL come from the combined response of many different biomes. However this can also be seen as a benefit, as there is potential to relate the response of the each of the biomes to the integrated response of the PBL, and in this way cross spatial scales. Several possible methods of achieving this are possible, and will be discussed later in this chapter.

Alternatives approaches

There are several alternative approaches to those used in this thesis which are worth discussing:

(1) Bulk modelling of the PBL. The PBL is a complex region of the atmosphere, but a simple bulk model approximation could provide a simple solution to studying the feedbacks between the PBL and the biosphere.

A simple bulk model would treat the PBL as a closed system, which was well mixed throughout the boundary layer. The depth of the PBL can be estimated with empirical relationships, or retrieved from back forecasts. The method could be capable of capturing some of the effects of feedbacks, but would miss the subtleties of some processes such as the rectifier effect. The model would also be difficult to validate against atmospheric data.

Intrinsically such a simple atmospheric formulation would incur very low computational costs. However since the computational cost of running the atmospheric and biosphere components of the CAB model are comparable, there would be limited speed gains to be made by replacing OSU1DPBL with a bulk model. Instead the atmospheric bulk modelling approach maybe better suited to coupling with the Aggregated Canopy Model (ACM) [*Williams, et al.*, 1997]. This would allow large ensembles runs to be used in investigations.

(2) Large Eddy Simulation (LES) models. LES models explicitly resolve large scale turbulent motion, whilst maintaining parameterisations for the sub-grid (~ 50 m) turbulence. This approach has the advantage that sub-grid turbulence is more consistent throughout the

PBL and thus easier to parameterise. LES models have the potential to provide highly accurate simulations of PBL dynamics and coupled to a SVAT model they would provide a powerful tool for studying the dynamics and coupling of the atmosphere-biosphere system [*Denning, et al.*, 2003]. Either 2-D or 3-D LES models would be ideally suited to studying spatial heterogeneity, and would provide excellent corroborative potential with aircraft flux measurements. However the major drawback to LES models is the number of the calculations and the computation expense incurred. This seriously limits the application of LES modelling to atmosphere-biosphere interactions.

(3) Lagrangian dispersion models. In a Lagrangian dispersion model particle paths are modelled [*Flesch, et al.*, 1995; *Rotach, et al.*, 1996; *Wilson and Sawford*, 1996]. The particles are subject to the random velocity field, which is described statistically. Many particles are modelled in order to determine the dispersion due to the turbulent transport. These models can be run forwards (to determine the dispersion of a gas) or backwards (to work out the source of an emission). This would allow them unique applications when coupled to a SVAT model or TEM. The difficulty in running a Lagrangian model comes from the need to determine the statistical description of the velocity field. Additionally there is no intrinsic mechanism to update these descriptions in response to biosphere processes, and so feedbacks between the biosphere and atmosphere cannot be studied using a Lagrangian approach.

Future applications

The scope and extent of a PhD is necessarily quite focused, and while much can be achieved within the time constraints of PhD, there are many additional approaches left to explore:

(1) Multiple biomes within the CAB model. The CAB model is currently restricted to a single species or group of species that can be represented by the 10 canopy layers of the SPA model. This approach works well for the homogeneous stands studied so far. However, the approach is inappropriate for regions with spatial heterogeneity in the land-cover on scale much less than the foot print of the PBL. A simple solution to this problem is the inclusion of more than one biome in the CAB model. The meteorology predicted within CAB would be used to drive an instance of the SPA model for each plant functional type (or species) within the PBL footprint. The fluxes of energy and matter from these groups would be aggregated according to their fractional land-cover, and the resulting

fluxes used to drive the PBL model. Using this approach there is some potential to invert atmospheric measurements to estimate fractional land-cover.

(2) Application of the Bayesian approach to real data. The third paper described a Bayesian inversion method, which was demonstrated using twin (synthetic) data, it would be beneficial to perform a validation of these techniques with real data.

(3) Integration of the CAB model within a semi-lagrangian transport model. The CAB model could be advected over the land surface following the tracks of particles (calculated by a Lagrangian dispersion model). Using the approach outlined in (1), changes in land-cover due to the spatial heterogeneity could be accounted for. This modelling scheme would provide a powerful tool for interpreting the observations made from tall towers; allowing the history of the gas concentrations measured by the tall tower to be determined.

(4) Assimilation of atmospheric data into the CAB model. Data assimilation provides a powerful means of bringing together the sum of knowledge about known processes (i.e. models) and the state of the system (i.e. observations). In the context of the CAB model this would allow the uncertainties in the processes (i.e. the resetting of the PBL due to synoptic weather conditions), to be updated by fresh observations. This would allow the CAB model to be run for extended periods of time to provide long term carbon balance estimates.

(5) Using Bayesian inversions to guide the design of field campaigns. With the offline SPA model and an extended eddy covariance dataset, the Bayesian framework could be used to design measuring campaigns. The SPA model could be inverted to determine the data resolution of the full eddy covariance dataset. Subsections of the eddy covariance dataset could then be inverted to find out the minimum/optimum dataset required to characterise the response of the system (e.g. three long periods, one before green-up, one during green-up and one after senescence).

References

Denning, A. S., et al. (2003), Simulated variations in atmospheric CO2 over a Wisconsin forest using a coupled ecosystem-atmosphere model, *Global Change Biology*, *9*, 1241-1250.

Engel, V. C., et al. (2002), Forest canopy hydraulic properties and catchment water balance: observations and modeling, *Ecological Modelling*, *154*, 263-288.

Fisher, R. A., et al. (2006), Evidence from Amazonian forests is consistent with isohydric control of leaf water potential, *Plant Cell and Environment*, *29*, 151-165.

Flesch, T. K., et al. (1995), Backward-Time Lagrangian Stochastic Dispersion Models and Their Application to Estimate Gaseous Emissions, *Journal of Applied Meteorology*, *34*, 1320-1332.

Houghton, J. T. (2001), *Climate change 2001 : the scientific basis*, x, 881 p. pp., Cambridge University Press, Cambridge.

Keeling, C. D. (1960), The Concentration and Isotopic Abundances of Carbon Dioxide in the Atmosphere, *Tellus*, *12*, 200-203.

Keeling, C. D., et al. (1976), Atmospheric Carbon-Dioxide Variations at Mauna-Loa Observatory, Hawaii, *Tellus*, *28*, 538-551.

Meir, P., et al. (2006), The influence of terrestrial ecosystems on climate, *Trends in Ecology & Evolution*, *21*, 254-260.

Richard Alley, et al. (2007), *Climate Change 2007: The Physical Science Basis, Summary for Policymakers*, 18 pp.

Rotach, M. W., et al. (1996), A two-dimensional Lagrangian stochastic dispersion model for daytime conditions, *Quarterly Journal of the Royal Meteorological Society*, *122*, 367-389.

Running, S. W., et al. (1999), A global terrestrial monitoring network integrating tower fluxes, flask sampling, ecosystem modeling and EOS satellite data, *Remote Sensing of Environment*, *70*, 108-127.

Ryan, M. G. (2000), Introduction to BOREAS special issue, *Tree Physiology*, *20*, 709-711.

Schwarz, P. A., et al. (2004), Climatic versus biotic constraints on carbon and water fluxes in seasonally drought-affected ponderosa pine ecosystems, *Global Biogeochemical Cycles*, *18*, -.

Sellers, P. J., et al. (1997), BOREAS in 1997: Experiment overview, scientific results, and future directions, *Journal of Geophysical Research-Atmospheres*, *102*, 28731-28769.

Shuttleworth, W. J. (1991), Insight from Large-Scale Observational Studies of Land Atmosphere Interactions, *Surveys in Geophysics*, *12*, 3-30.

Troen, I., and L. Mahrt (1986), A Simple-Model of the Atmospheric Boundary-Layer - Sensitivity to Surface Evaporation, *Boundary-Layer Meteorology*, *37*, 129-148.

Van Wijk, M. T., et al. (2003), Interannual variability of plant phenology in tussock tundra: modelling interactions of plant productivity, plant phenology, snowmelt and soil thaw, *Global Change Biology*, *9*, 743-758.

Williams, M., et al. (2000), The controls on net ecosystem productivity along an Arctic transect: a model comparison with flux measurements, *Global Change Biology*, *6*, 116-126.

Williams, M., et al. (2001), Use of a simulation model and ecosystem flux data to examine carbon-water interactions in ponderosa pine, *Tree Physiology*, *21*, 287-298.

Williams, M., et al. (1997), Predicting gross primary productivity in terrestrial ecosystems, *Ecological Applications*, *7*, 882-894.

Williams, M., et al. (1996), Modelling the soil-plant-atmosphere continuum in a Quercus-Acer stand at Harvard forest: The regulation of stomatal conductance by light, nitrogen and soil/plant hydraulic properties, *Plant Cell and Environment*, *19*, 911-927.

Williams, M., et al. (2005), An improved analysis of forest carbon dynamics using data assimilation, *Global Change Biology*, *11*, 89-105.

Wilson, J. D., and B. L. Sawford (1996), Review of Lagrangian stochastic models for trajectories in the turbulent atmosphere, *Boundary-Layer Meteorology*, *78*, 191-210.

Appendix A: Treatment of random errors

Eddy covariance flux data contains a lot of noise. In this thesis flux data noise has been attributed to random, systematic and sampling errors [*Goulden, et al.*, 1996].

Sampling errors are important when long-term average fluxes are being calculated form periods of months or years, and occur due to periods of missing data. If long term flux averages are not required, then this source of uncertainty can be largely discounted. Though, attention has to be paid to daily aggregated fluxes, which show a similar source of uncertainty. To minimise this uncertainty when calculating daily aggregates, daily means are disregarded if they contain more than 10% missing half-hourly data points.

Systematic errors are attributed to either instrumentation errors (e.g. mis-calibration) or selective systematic errors (e.g. nocturnal katabatic flows).

Random errors on the half-hourly flux estimates were calculated using the

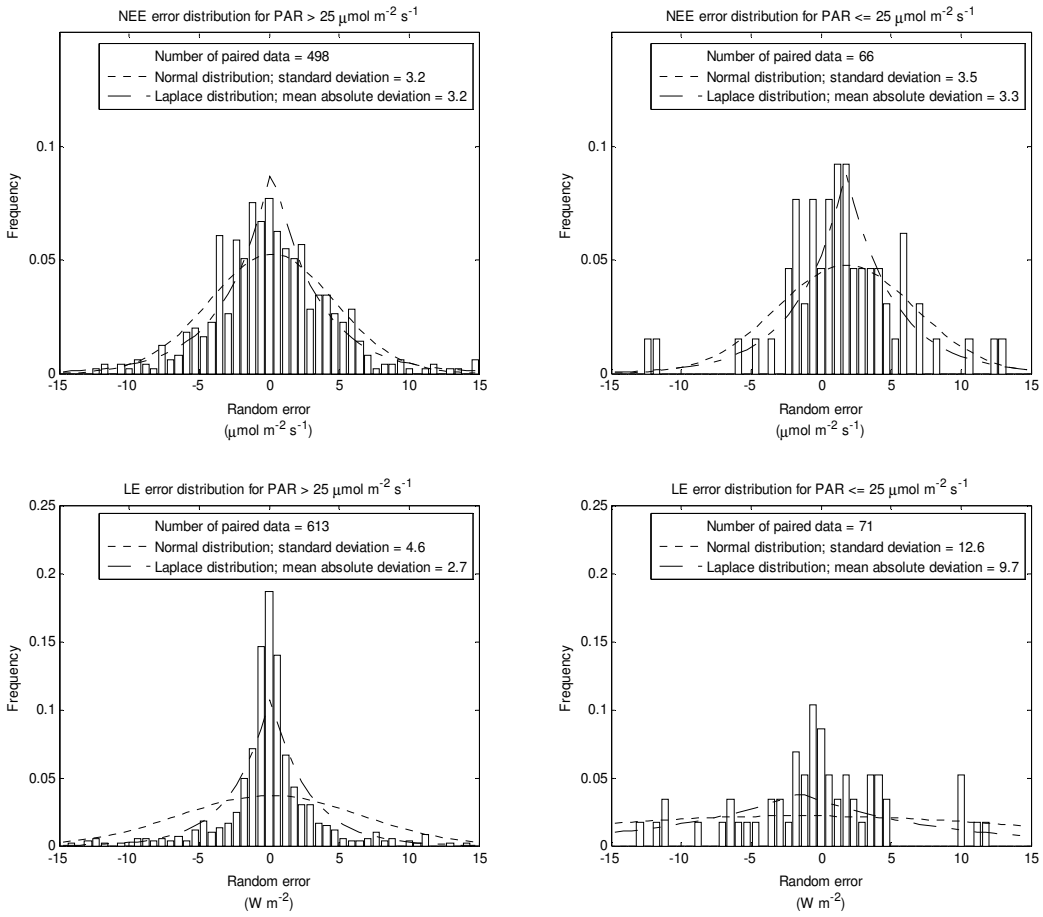

Figure 1: The SSA-OBS error analysis was performed over the 120 day study period. The mean absolute deviations for the Laplace distribution fits and the standard deviations for the normal distribution fits are shown.

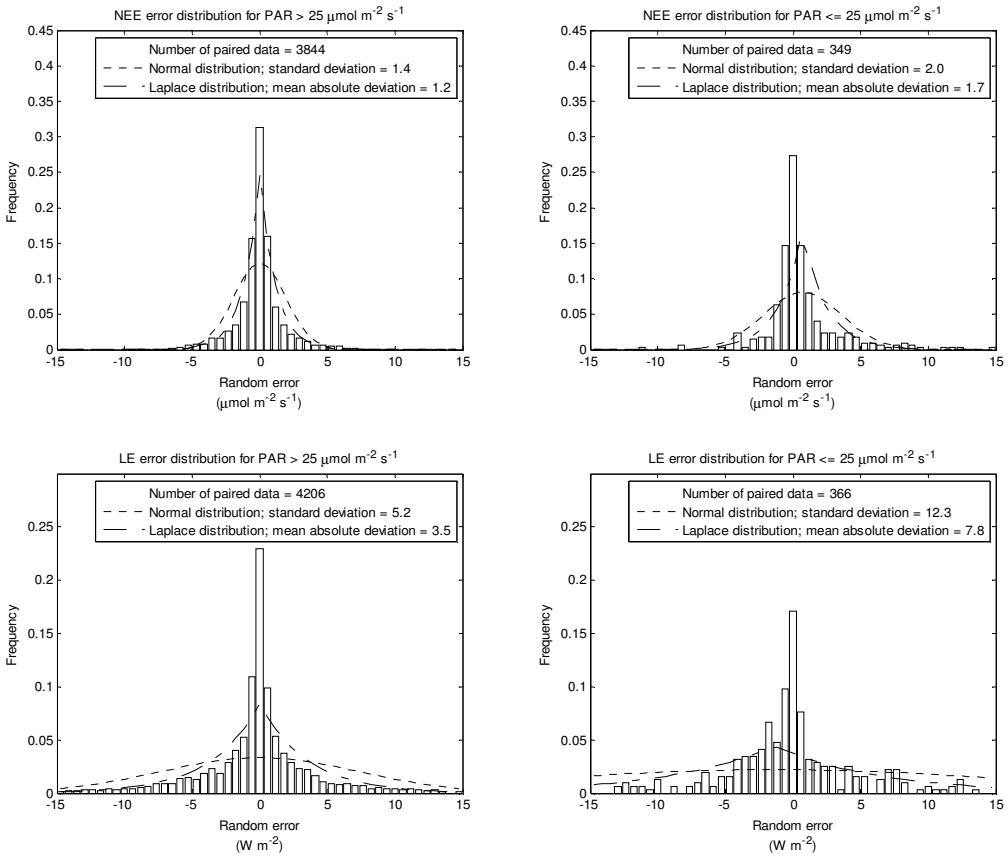

Figure 2: The NSA-OBS error analysis was performed over the whole 1994 -1996 time series, and applied to the 120 day study period. The mean absolute deviations for the Laplace distribution fits and the standard deviations for the normal distribution fits are shown.

method outlined by *Hollinger*, 2005 [*Hollinger and Richardson*, 2005]. This approach for estimating random errors, originated from the comparison of fluxes from a pair of flux towers (less than one km apart) which were simultaneously sampling similar vegetation. Using data from these two towers it was shown that random errors could be generated by comparing pairs of half-hourly data. The difference in these flux pairs is used to build up a distribution the random errors. When paired points are found for the whole time series, it becomes evident that a Laplace (and not a normal) distribution is built up.

Hollinger then showed that the same calculation could be synthesized for a single tower. This synthesis is performed by looking for data points (within a single towers flux data) that are separated by 24 hours, with the condition that the meteorology that the paired data points experience is similar. In order to find pairs of data point under similar conditions the meterological difference between the pairs had to be less than 75 μmol m^{-2} s^{-1} of photosynthetically active radiation (PAR), 3 K air temperature and 1 m s^{-1} wind speed.

The criteria set down by Hollinger are not the only ones that can be applied; in order to differentiate between daytime, and night time errors, the paired half-hourly data points were separated according to levels of PAR. To obtain a sufficient number of paired points in each bin, the binning was limited to only a daytime bin (PAR > 25 μmol m^{-2} s^{-1}) and a night time bin (PAR ≤ 25 μmol m^{-2} s^{-1}). This analysis of random errors was performed for latent energy (LE) and net ecosystem exchange (NEE) at both the southern study area old black spruce (SSA-OBS) site (Figure 1) and the northern study area old black spruce (NSA-OBS) site (Figure 2). Curves for the distributions were calculated using a maximum likelihood fitting routine and, mean absolute deviations calculated.

References

Goulden, M. L., et al. (1996), Measurements of carbon sequestration by long-term eddy covariance: Methods and a critical evaluation of accuracy, *Global Change Biology*, *2*, 169-182.

Hollinger, D. Y., and A. D. Richardson (2005), Uncertainty in eddy covariance measurements and its application to physiological models, *Tree Physiology*, *25*, 873-885.

Appendix B: The Coupled-Atmosphere-Biosphere model manual

Version History:

Version 002.001 – Timothy Hill 28/02/07

Timothy Hill

School of GeoSciences

University of Edinburgh

Crew Building

West Mains Road

Edinburgh

EH9 3JN,

UK

Glossary

$(w'\theta')_s$	-	Surface heat flux
A	-	Rate of diffusion limited photosysthesis
A	-	A function for calculating soil thermal conductivity
A_f	-	Foliage allocation rate
A_r	-	Fine root allocation rate
A_w	-	Wood allocation rate
B	-	A function for calculating soil thermal conductivity
C	-	A coefficient of proportionality
c	-	A empirically fitted constant
C	-	A function for calculating soil thermal conductivity
C_a	-	Ambient CO_2 concentration
CAB	-	(the) Coupled Atmosphere-Biosphere (model)
c_h	-	Heat exchange coefficient
CLC	-	Fractional cloud cover
C_m	-	Mesophyll CO_2 concentration
c_p	-	Sepecific heat capacity
C_{SWC}	-	Canopy's saturation water content
c_w	-	Vapour concentration of water
C_{WC}	-	Canopy's water content
D	-	Litter decomposition rate
D	-	A function for calculating soil thermal conductivity
DALEC	-	(the) Data Assimilation Linked ECosystem (model)
E	-	Rate of evaporation
e	-	Vapour pressure
E	-	A function for calculating soil thermal conductivity
e_a	-	Vapour pressure of the bulk atmosphere
E_c	-	Canopy evaporation
E_{dir}	-	Direct evaporation from soil
E_p	-	Potential evaporation
e_s	-	Saturation vapour pressure
E_t	-	Transpiration

E_{tot}	-	Total evaporation
g	-	Transpiration rate constant
$G\downarrow$	-	Ground heat flux
g_h		Conductance of the leaf's boundary layer
GPP	-	Gross Primary Production
g_t	-	Conductance of the leaf and boundary layer to CO_2
g_w	-	Total conductance of the leaf and its boundary layer
h	-	Boundary layer height
$H\uparrow$	-	Sensible heat flux
ι	-	Water use efficiency threshold parameter
IR	-	Infra-red
k	-	von Kármán constant (=0.4)
K_h	-	Diffusivity of heat
K_m	-	Momentum diffusivity
L	-	Monin Obukhov length
LAI	-	Leaf Area Index
$LE\uparrow$	-	Latent heat flux
L_f	-	Leaf litter production rat
L_i	-	LAI of each model layer
L_r	-	Fine root production rate
LW	-	Longwave
L_w	-	Wood production rate
M_A	-	Molecular weight of air
M_w	-	Molecular weight of water
NEE	-	Net ecosystem exchange
OSU1DPBL	-	(the) Oregon State University one-dimensional planetary boundary layer (model)
P	-	Pressure
PAR	-	Photosythetically Active Radiation
PBL	-	Planetary Boundary Layer
PC	-	Plant coefficient
$P_{passing}$	-	Non-intercepted proportion of radiation
Pr	-	Prandtl number

q	-	Mixing ratio of water
R	-	Respiration
R_a	-	Autotrophic repsiration
R_d	-	Respiration rate
R_h	-	Heterotrophic respiration
RH	-	Relative humidity
R_n	-	Net radiation
s	-	Slope of the vapour curve
$S\downarrow$	-	Down-welling shortwave radiation
$S_{CS\downarrow}$	-	Clear sky radiation
SPA	-	(the) Soil Plant Atmosphere (model)
T	-	Fraction of radiation transmitted through complete cloud cover
T	-	Temperature dependence
$T_{@200m}$	-	Temperature at a reference height of 200m
t1	-	Litter decomposition rate constant
t2	-	Autotrophic repsiration
t3	-	Fraction of net primary production allocated to foliage
t4	-	Fraction of net primary production allocated to fine roots
t5	-	Turnover rate of foliage
t6	-	Turnover rate of woody matter
t7	-	Turnover rate of fine roots
t8	-	Mineralization rate of fresh litter
t9	-	Mineralization rate of soil organic matter and woody debris
T_a	-	Temperature of the bulk atmosphere
TC	-	Thermal conductivity
TEM	-	Terrestrial Ecosystem Model
T_o	-	Temperature of the first model layer
T_s	-	Temperature at the leaf's surface
u_*	-	Friction velocity
V_c	-	Rate of carboxylation
V_h	-	Horizontal component of wind peed
VPD	-	Vapour Pressure Deficit

W_c	-	Rate of Rubisco carboxylation
W_j	-	Rate of RuBP carboxylation
w_s	-	Boundary layer velocity scale
w_s	-	Vertical velocity
z	-	Height
α	-	Surface albedo
β	-	Solar elevation
γ	-	Counter gradient term, or the psychrometer constant
Γ^*	-	CO_2 compensation point
δA	-	Increase in the rate of photosynthesis
Δc_w	-	Concentration difference between leaf surface and bulk atmosphere
δe	-	Vapour pressure deficit
δg_s	-	Increment in stomatal conductance
ε	-	Emissivity of the reference height
θ	-	Potential temperature
Θ	-	Soil moisture content
θ_o	-	Potential temperature of the first model layer
Θ_{ref}	-	Reference soil moisture content (for max transpiration)
θ_s	-	Surface temperature
Θ_{wilt}	-	Soil moisture wilting point
λ	-	Latent heat of evaporation
ρ_0	-	Density of air
ρ_a	-	Density of dry air
σ	-	Stephan-boltzman constant
σ_f	-	Canopy shading factor
Φ_C	-	Volume fraction of clay
Φ_M	-	Volume fraction of mineral
Φ_Q	-	Volume fraction of quartz
Φ_s	-	Volume fraction of the soil
Ψ_l	-	Leaf water potential
Ψ_{lmin}	-	Minimum leaf water potential

Φ_h - Nondimensional temperature

Φ_m - Nondimensional shear

1 Introduction

The **C**oupled **A**tmosphere-**B**iosphere (CAB) model is motivated by the need to capture interactions between ecological processes at the land-surface and lower atmospheric dynamics. These interactions take place in the lowest layer of the atmosphere, the Planetary Boundary Layer (PBL). This layer is in direct contact with the land-surface and the land-cover has strong impacts within this region, dictating the energy partitioning and the water exchange at the land-surface. A joint understanding of both the PBL and terrestrial ecosystem allows the study of these interactions, and also provides a means of scaling up measurements from the leaf and stand level to tall tower, radiosonde and aircraft observations. If feedbacks between atmosphere and biosphere are to be captured a processed based terrestrial ecosystem model coupled to an adequately high resolution PBL model is required. This manual describes the structure of the CAB model, which was designed to simulate the coupled system.

The CAB model is comprised of two main components; (1) a PBL model and (2) a terrestrial ecosystem model (TEM), with a respiration sub-model. Development of the Oregon State University one-dimensional planetary boundary layer (OSU1DPBL) model [*Mahrt and Pan*, 1984; *Troen and Mahrt*, 1986] continued till 1995, and at the time of writing the Soil Plant Atmosphere (SPA) model [*Williams, et al.*, 1996] was still undergoing development. The respiration sub-model was based on the DALEC model [*Williams, et al.*, 2005].

This manual has been written to describe; 1) the fundamentals of the two models, such that someone unfamiliar with the subject can grasp the basic principles involved, 2) the coupling between the models, 3) the modifications made to the individual models to make them suitable for coupling and 4) to provide users with a reference manual allowing easy implementation of the CAB model. We aim to provide the reader with a working knowledge of the model (and its components) without having to refer to excessive additional material.

2 Coupling

Fundamentally the coupled model needs to jointly simulate two components and their interactions: 1) the region of the atmosphere known as the PBL, and 2) the biosphere. The atmospheric component of the model deals with the turbulent mixing within the PBL, whilst the OSU1DPBL model deals with the atmospheric component. The biosphere component of the model needs to deal with the exchanges of mass and energy at the land-surface. In reality these exchanges are dealt with by 2 models, which are themselves coupled to form the biosphere component. The SPA model deals with the bulk of the processes occurring in the biosphere, including the photosynthesis and evapotranspiration. However SPA does not simulate respiration, rather SPA models the gross primary production (GPP) of carbon by the system. To equate GPP to the net carbon flux, we need to be able to simulate the carbon that is respired by the plants (autotrophically) and by organisms (heterotrophically). Both these respiration fluxes are simulated in the third model a simple carbon pool box model. We discuss all three models, and any modifications made to them, in later chapters.

2.1 Coupling overview

The CAB model is formed from the coupling of the three models (OSU1DPBL, SPA and the respiration model, DALEC; Figure 1b).

The main component of the biosphere model (SPA; Chapter 3.2) simulates all biosphere processes except for the respiration. To calculate the respiration the SPA model's estimate of GPP (from the previous day) is passed to the respiration box model (Chapter 3.3). The respiration model (DALEC) disaggregates this flux into a respiration flux and carbon pools of leaves, fine roots and woody matter. The coupling between these two models is used for both offline biosphere model runs and coupled model runs (Chapter 8).

In order to simulate the atmospheric turbulence and stability the OSU1DPBL model requires the land-surface boundary conditions generated by the biosphere model. Fluxes of water, CO_2 and energy are passed from the biosphere model to OSU1DPBL, and in return updated estimates of the surface meteorology drive the biosphere model. The parameters exchanges are summarised in Table 1.

		To		
		SPA	*Resp.*	*OSU1DPBL*
From	*SPA*	n/a	GPP Soil temp. Time	Evaporation Soil heat flux Carbon flux Surface temperature Albedo Latent heat flux 1st model layer concentration of CO2 1st model layer mixing ratio of water 1st model layer air temperature
	Resp.	n/a	n/a	NEP
	OSU1DPBL	Date and time Time-step Horizontal components of windspeed Shortwave radiation Longwave radiation Fractional cloud cover 1st model layer temperature (potential and actual) 1st model layer pressure 1st model layer mixing ratio 1st model layer CO2 concentration 1st model layer height 1st model layer depth	n/a	n/a

Table 2: The three models are closely coupled; the parameters that each component requires for this coupling are shown in this table.

3 Source models

The models used in the CAB models are complex and have already been described in the literature [*Pan and Mahrt*, 1987; *Troen and Mahrt*, 1986; *Williams, et al.*, 1996; *Williams, et al.*, 2005]. To furnish the reader with a working knowledge of the components of the CAB model, and also illuminate the motivations behind any alterations made to the models, we include a concise description of each model component.

3.1 Atmospheric component (OSU1DPBL)

The Oregon State University one-dimensional planetary boundary layer (OSU1DPBL) model was coded in FORTRAN 77 and in its original form combines a PBL model with robust soil and vegetation sub-models. OSU1DPBL uses 68 atmospheric layers to simulate the evolution of the PBL. It is also capable of simulating the transition between stable and unstable boundary layers. OSU1DPBL predicts the potential temperature, mixing ratio and wind-speed within the PBL. In order simplify the model, only the vertical diffusion (from turbulent mixing) and advection are considered when calculating the turbulent mixing within the PBL. In its original form OSU1DPBL uses a simple

land-surface scheme. We outline the key features of this scheme and highlight the parts which were replaced or modified.

3.1.1 Atmospheric dynamics

The OSU1DPBL model was designed to be a compromise between complexity (realism and resolution) and simplicity (functionality). Atmospheric dynamics is determined by turbulent mixing of the potential temperature, the water mixing ratio, and the horizontal wind components, which is modified by a counter gradient term for the potential temperature and a subsidence term.

The momentum diffusivity is modelled as [*Brost and Wyngaard*, 1978]

$$K_m = u_* kz \Phi_m^{-1} \left(1 - \frac{z}{h}\right)^{1.5}$$

Where u_* is the friction velocity, h is the boundary layer height, Φ_m is the nondimensional shear and k is the von Kármán constant; the constant of the logarithmic wind profile within the surface layer, $\left(\frac{\partial V_h}{\partial z} = \frac{u_*}{kz}\right)$. Where V_h represents the horizontal component of wind peed, and z is the height. The von Kármán constant is taken to be 0.40, the nondimensional shear (Φ_m) and temperature (Φ_h) are defined for different stability classes to be [*Businger, et al.*, 1971]

$$\Phi_m = \begin{cases} 6.0 & , very\ stable \\ 1.0 + 5.0\frac{z}{L} & , stable \\ \left(1.0 - 15\frac{z}{L}\right)^{-1/3} & , unstable \end{cases}$$

$$\Phi_h = \begin{cases} 6.0 & , very\ stable \\ 1.0 + 5.0\frac{z}{L} & , stable \\ \left(1.0 - 15\frac{z}{L}\right)^{-1/2} & , unstable \end{cases}$$

A counter gradient term (γ) is required to describe the non-local mixing arising from thermals and eddies. These mixing terms may be much larger in extent than the turbulent mixing [*Deardorf.Jw*, 1972]. In the OSU1DPBL model this term is formulated as [*Deardorf.Jw*, 1966; *Mailhot and Benoit*, 1982; *Priestley and Swinbank*, 1947]

$$\gamma = \begin{cases} 0 & \text{, stable} \\ C\dfrac{(w'\theta')_S}{w_S h} & \text{, unstable} \end{cases}$$

Where C is a coefficient of proportionality, $(w'\theta')_S$ is the surface heat flux, and w_S is the velocity scale of the boundary layer. The diffusivities are determined by three prognostic equations

$$\frac{\partial v_h}{\partial t} = \frac{\partial}{\partial z}\left(K_m\left(\frac{\partial v_h}{\partial z}\right)\right) - w\left(\frac{\partial v_h}{\partial z}\right)$$

$$\frac{\partial \theta}{\partial t} = \frac{\partial}{\partial z}\left(K_h\left(\frac{\partial \theta}{\partial z} - \gamma\right)\right) - w\left(\frac{\partial \theta}{\partial z}\right)$$

$$\frac{\partial q}{\partial t} = \frac{\partial}{\partial z}\left(K_h\left(\frac{\partial q}{\partial z}\right)\right) - w\left(\frac{\partial q}{\partial z}\right)$$

The Prandtl number is the non-dimensional ration between coefficients of diffusivity for momentum and heat (K_h):

$$K_h = K_m \,\mathrm{Pr}$$

Where the Prandtl number is

$$\mathrm{Pr} = \begin{cases} 1.0 & \text{, } stable/neutral \\ \left(\Phi_h\left(\dfrac{z}{L}\right)\Big/\Phi_m\left(\dfrac{z}{L}\right) + Ck\dfrac{z}{L}\right) & \text{, } unstable \end{cases}$$

3.1.2 The surface energy balance

The OSU1DPBL surface scheme used a simple two-layer big leaf model of vegetation, combined with 2 soil layers. The surface energy balance at the land surface was solved to find the surface temperature.

$$\underbrace{(1-\alpha)S_{\downarrow}}_{(1)} + L_{\downarrow} - \underbrace{\sigma\theta_S^4}_{(2)} = G_{\downarrow} + H_{\uparrow} + LE_{\uparrow}$$

Where α is the surface albedo, $S_{\downarrow}$ the down-welling shortwave radiation, $L_{\downarrow}$ the down-welling longwave radiation, σ the Stephan-boltzman constant, θ_S the surface temperature, $G_{\downarrow}$ the ground heat flux, $H_{\uparrow}$ the sensible heat flux and $LE_{\uparrow}$ the latent heat flux. Term (1) is the absorbed shortwave radiation, and term (2) the upwelling terrestrial radiation. The down-welling shortwave radiation ($S_{\downarrow}$) is calculated to be the

clear sky radiation ($S_{CS\downarrow}$), adjusted for solar elevation. CLC is the fractional cloud cover, and t is the fraction of radiation transmitted through complete cover

$$S_{\downarrow} = [1-(1-t)CLC]S_{CS\downarrow}$$

The $L_{\downarrow}$ is calculated from the temperature at a reference height of 200m ($T_{@200m}$), the emissivity of the reference height (ε) and an empirically fitted dependence (c) on the CLC:

$$L_{\downarrow} = \varepsilon\sigma T^4_{@200m} + cCLC$$

The ground heat flux is calculated from the thermal diffusivity and the temperature gradient between the soil and atmosphere. $H_{\uparrow}$ is a function of the difference between the surface temperature (θ_S) and the 1st model layer temperature (θ_0):

$$H_{\uparrow} = \rho_0 c_P c_h(\theta_S - \theta_0)$$

Where ρ_0 is the air density of the 1st model layer, c_P the specific heat capacity and c_h the heat exchange coefficient.

3.1.3 Calculation of LE

The calculation of LE within the original OSU1DPBL model was replaced by the SPA model, but we briefly describe it here for completeness. The latent heat flux ($LE_{\uparrow}$) is calculated from the total evaporation (E_{tot}), the sum of the transpiration (E_t) and direct evaporation from the soil surface (E_{dir}) and from the canopy (E_c).

$$E_{tot} = E_{dir} + E_c + E_t$$

Direct evaporation from the soil (E_{dir}) occurs at the potential evaporation rate (E_P) when the soil moisture is sufficient. When the soil dries out, the rate of evaporation is limited to the up-ward diffusion of water.

Direct evaporation is reduced by shading from the canopy (σ_f). Thus, the evaporation of water from the canopy (E_c) is defined as:

$$E_c = E_P\sigma_f\left(\frac{C_{WC}}{C_{SWC}}\right)^{1/2}$$

Where C_{WC} is the canopy's water content and C_{SWC} is the canopy's saturation water content.

Transpiration (E_t) is partially controlled by a 'plant coefficient' (PC), set by the user. The maximum transpiration rate is reduced by the water evaporated directly off the canopy:

$$E_t = PC \cdot E_P \cdot \sigma_f \cdot g(\Theta)\left[1-\left(\frac{C_{WC}}{C_{SWC}}\right)^{1/2}\right]$$

The transpiration is limited by a rate function ($g(\Theta)$), which determines the vegetations response to soil moisture content (Θ). Above a reference moisture content (Θ_{ref}), transpiration is at its maximum. Below the wilting point (Θ_{wilt}) the transpiration is zero, and between the reference and the wilting point the transpiration rate function depends on the wilting point and the reference:

$$g(\Theta) = \begin{cases} 1 & ,\Theta > \Theta_{ref} \\ \dfrac{\Theta - \Theta_{wilt}}{\Theta_{ref} - \Theta_{wilt}} & ,\Theta_{ref} \geq \Theta > \Theta_{wilt} \\ 0 & ,\Theta_{wilt} \geq \Theta \end{cases}$$

The thermal conductivity and heat capacity of the two soil layers are also functions of water content (Θ). Infiltration is allowed between the two soil layers.

3.1.4 Motivation for changing the surface scheme

The default surface scheme was altered due to: (1) The simplistic nature of some of the formulations, which made them difficult to relate to actual processes. The original formulations were kept simple as the biosphere was not a main focus of the model, and computer power was low. Nowadays the computational resources required to run the model do not place the same constraints on model complexity as they did when the surface scheme was first devised, and we can afford to run a more realistic surface scheme. (2) Some parameters in the original surface scheme were hard to relate to measurements. The surface scheme was designed to produce adequate responses to drive the PBL. However, with improvements in both measurements and models of ecosystems a land-surface exchange model can now be parameterised and corroborated from observations. (3) The OSU1DPBL model was not designed to model carbon dynamics.

3.2 Biosphere component (SPA)

The Soil-Plant-Atmosphere model (SPA) is a processed based ecosystem model which is still undergoing development [*Williams*, 2005; *Williams, et al.*, 1996]. The source code for the SPA model was written in FORTRAN 90/95, which can easily be integrated with the FORTRAN 77 of the OSU1DPBL model. The SPA model was chosen to be coupled to the OSU1DPBL model because it has been validated at a wide range of latitudes for a wide range of biomes. SPA is designed to be highly compatible with eddy covariance flux measurements; operating on the same spatial (leaf and canopy level) and temporal (30 minute time-steps) scales as stand-based eddy covariance flux measurements. The standard configuration the model simulates 10 canopy layers and 20 soil layers. To run the model requires the above canopy meteorological drivers: Radiation, wind-speed, air temperature, vapour pressure deficit (VPD), shortwave radiation, photosynthetically active radiation (PAR) and precipitation. In addition to these drivers, canopy and leaf level parameterisations are required. These parameterisations can be also exclusively obtained from measurement. We will briefly describe the main processes simulated by the SPA model, model components, structure and operation are described later.

3.2.1 Radiative Transfer

The SPA model uses a radiative transfer scheme for the transmittance, reflectance and absorption of long-wave (LW), infra-red (IR) and photosynthetically active (PAR) radiation. The radiative transfer modelling in SPA takes into account the elevation (β) of the radiation source, the leaf area index (LAI) of each layer (L_i), and the distribution (G) of the leaves to calculate the non-intercepted proportion of radiation ($P_{pas\sin g}$).

$$P_{pas\sin g} = \exp\left(\frac{-GL_i}{\sin(\beta)}\right)$$

By default a spherical distribution of leaf angels is assumed. The absorption of PAR by the canopy elements is determined using the Beer-Lambert law. The Beer-Lambert law describes the logarithmic dependence of light transmission through a medium. This depends on the opacity and the thickness of the medium. Shaded and unshaded leaf areas are considered for the radiative transfer of PAR; shaded leaves only see diffuse radiation.

3.2.2 Hydraulics

In the SPA model the hydraulic resistance is assumed to increase with canopy height. The hydraulic resistance of the stem is calculated from stem conductivity and so increases linearly with height. However this effect will be minimal if most of the total plant resistance is not in the stem. The user can remove the effect entirely by specifying a stem conductance.

Cavitations within the xylem can cause serious degradation of plant hydraulic conductance. These cavitations occur at high water tensions. In order to avoid these cavitations the plant, reduces the stomatal conductance to limit the water tensions encountered.

3.2.3 Evapotranspiration

The Penman equation is used to describe the evapotranspiration from the surface of a leaf. This derivation of the Penman equation is similar to that performed in [*Jones*, 1992]. We start off by considering the energy balance of a leaf: Ignoring the heat storage of the leaf the steady state energy balance is

$$H_{\uparrow} = (R_n - G_{\uparrow}) - LE_{\uparrow} = (R_n - G_{\uparrow}) - \lambda E$$

Where λ is the latent heat of evaporation, and E the evaporation rate. The rate of evaporation is governed by the ease of evaporation, and the demand for evaporation. Thus, the evaporation of a moist surface can be written as

$$E = g_w \Delta c_w$$

Where g_w is the total conductance of the leaf and its boundary layer, c_w is the (vapour) concentration of water, and Δc_w the concentration difference between leaf surface and the bulk atmosphere. This concentration difference drives the evaporation, Δc_w can also be related to the density of dry air (ρ_a) and the molecular weight of water (M_w) and air (M_A):

$$\Delta c_w = \rho_a \Delta e \left(\frac{M_w}{M_A P} \right), \text{ and } \left(\frac{M_w}{M_A} \right) = 0.622$$

Where P is the pressure, and e the water vapour pressure. Substituting Δc_w into the equation for evaporation, we get:

$$E = \frac{0.622 g_w \rho_a \Delta e}{P} = \frac{0.622 g_w \rho_a (e_{S(T_S)} - e_a)}{P}$$

As $\Delta e = (e_{S(T_S)} - e_a)$ the difference between the saturation vapour pressure at the leaf's surface temperature, and the vapour pressure of the bulk atmosphere. However the surface temperature is hard to measure and must be treated as an unknown. To avoid using the leaf's surface temperature, we first introduce the saturation vapour pressure at the atmosphere temperature in such a way as to keep the equation valid

$$(e_{S(T_S)} - e_a) = (e_{S(T_a)} - e_a) + e_{S(T_S)} - e_{S(T_a)}$$

We can then substitute in the vapour pressure deficit (δe) such that

$$(e_{S(T_S)} - e_a) = \delta e + e_{S(T_S)} - e_{S(T_a)}$$

We now make use the approximation first used by Penman in 1948. In this approximation, the leaf's surface temperature is assumed to be the same as the wet bulb temperature. This is a sensible approximation if the leaves are either transpiring, or in a saturated atmosphere with a VPD of zero. The slope (s) of the saturation vapour curve at the air temperature can be approximated as

$$s = \frac{e_{S(T_S)} - e_{S(T_a)}}{T_a - T_s}$$

Using this substitution we can eliminate the vapour pressure at the leaf's surface temperature from the evaporation equation. This leaves the new form for the evaporation equation

$$E = \frac{0.622 g_w \rho_a}{P}(\delta e + s(T_s - T_a))$$

Using the sensible heat flux in the form, $H = g_h \rho_a c_p (T_s - T_a)$, we eliminate the $(T_s - T_a)$ terms.

$$E = \frac{0.622 g_w \rho_a}{P}(\delta e + \frac{s(H)}{g_h \rho_a c_p})$$

Where g_h is the conductance of heat, and c_p the specific heat capacity of air. Now making use of the original equation for the surface energy balance we get

$$E = \frac{0.622 g_w \rho_a}{P}(\delta e + \frac{s((R_n - G) - \lambda E)}{g_h \rho_a c_p})$$

We then rearrange to find the Penman-Monteith equation, noting that the psychrometer constant (γ) can be expressed as, $\gamma = \frac{Pc_p}{0.622\lambda}$. Where λ is the latent heat of vaporisation for water.

$$E = \frac{g_h \rho_a c_p \delta e + s(R_n - G)}{\lambda\left(s + \left(\frac{\gamma g_h}{g_w}\right)\right)}$$

Wind speeds throughout the canopy, on which the boundary layer conductance (g_h) depends, are modelled as exponential relationship with height.

3.2.4 Photosynthesis

The rate of photosynthesis is determined by balancing the CO_2 diffusion and Rubisco/RuBP limited carboxylation rate. The rate of diffusion limited photosysthesis (A) is a function of the ambient CO_2 concentration (C_a), the mesphyll CO_2 concentration (C_c) and the total combined conductance of the leaf and boundary layer to CO_2 (g_t)

$$A = g_t(C_a - C_c)$$

Carboxylation (V_c) rates are determined by the minimum (limiting) of the Rubisco (W_c) and the RuBP (W_j) rates.

$$V_c = \min(W_c, W_j)$$

The RuBP limitation is a function of the electron transport rate. Once V_c has been determined, the Rubisco/RuBP limit to the photosynthetic rate can be expressed as a function of Γ^*, the CO_2 compensation point, and the respiration rate (R_d).

$$A = V_c\left(1 - \frac{\Gamma^*}{C_c}\right) - R_d$$

We then solve the diffusion equation and the photosynthetic rate equation to find the C_c that satisfies both.

3.2.5 Stomatal dynamics

The SPA model employs a novel coupling between water use and photosynthesis. Stomatal conductance is varied to optimise the water use efficiency, whilst maximising

carbon uptake. When dangerous leaf water potentials are reached, the stomatal conductance is not allowed to increase any further, thus limiting the hydraulic tension.

In the SPA model this stomatal control is implemented as an iterative process where the stomatal conductance is gradually incremented. Stomatal conductance is incremented while it is still beneficial to do so, that is while two conditions are met: (1) The hydraulic tension in the plant must be maintained below a safe threshold. This threshold is exceeded if the leaf water potential (ψ_l) drops below the minimum acceptable leaf water potential ($\psi_{l\min}$) , $\psi_l \le \psi_{l\min}$. (2) The ratio of the increase in photosynthesises (δA) and the increment in stomatal conductance (δg_S) must not drop below a certain efficiency threshold (ι), $\delta A / \delta g_S \le \iota$.

3.3 Respiration component (DALEC)

The SPA model predicts the gross carbon uptake by the vegetation known as the gross primary production (GPP). It does not partition this uptake into either biomass or respiration. Thus the GPP predicted by the SPA model is not the same flux that is measured by the eddy covariance flux measurements. Instead eddy covariance measures the net ecosystem exchange (NEE), the net exchange of carbon in the ecosystem. The difference between the NEE and the GPP is the ecosystem respiration (R):

NEE = R - GPP

In order to corroborate the SPA model with eddy covariance measurements we must calculate the respiration.

3.3.1 Choice of respiration model

The respiration model used in the CAB model needed to be generally applicable to any site. We chose to perform the respiration calculations using a box model approach, which was initially used as part of the Data Assimilation Linked Ecosystem Carbon (DALEC) model [*Williams, et al.*, 2005]. The box model was chosen due to its simplicity, versatility and potential to include a data assimilation approach to respiration (in the future). An important advantage of the box modelling approach was that it conserves the amount of carbon in the system. This is an important feature in a prognostic model, as carbon cannot be respired if it does not exist.

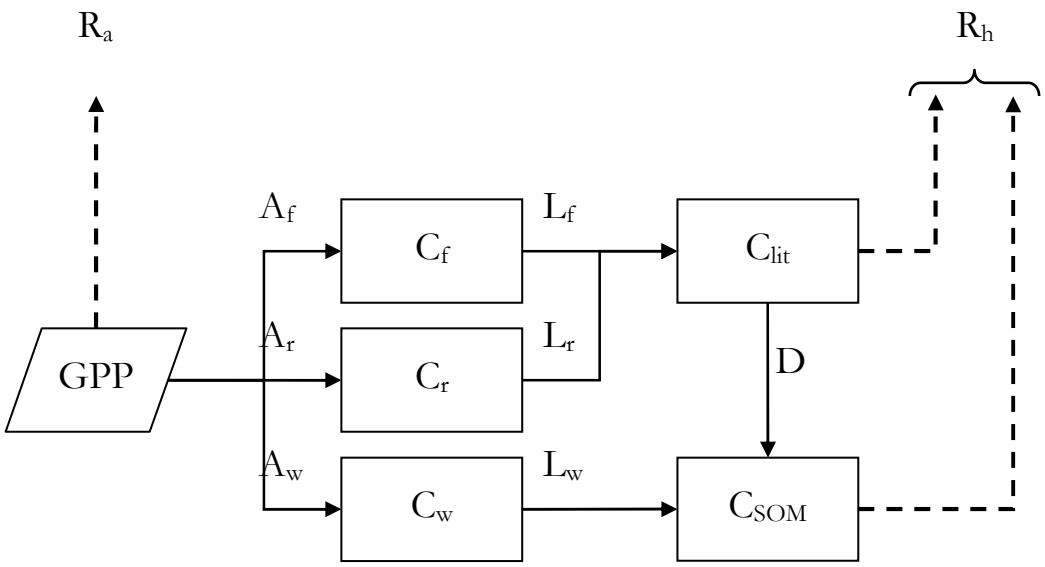

Figure 1: The respiration box model, the model partitions the previous days GPP into autotrophic respiration (Ra) or biomass. The part of GPP assigned to be biomass is split up into either the foliar carbon pool (Cf), the root carbon pool (Cr) or the woody matter pool (Cw). These pools then feed the litter carbon pool (Clit) and the SOM pool (Csom) through the process of decomposition or leaf fall. From these last two pools the heterotrophic respiration term is calculated

A simple carbon pool model of respiration (without any data assimilation) would be unsuitable for long term carbon balance studies. This is because small differences in the carbon pool sizes or the carbon fluxes could (over a long time frame) accumulate into a significant change in the net carbon exchange. This however can be used as an advantage, as we would expect the carbon pool sizes to be (approximately) constant over moderate periods of time. This can therefore be used as a tuning/corroboration aid.

Implementation of the data assimilation scheme [*Williams, et al.*, 2005] would permit the combination of both occasional stock data and flux data to help constrain the pool sizes.

3.3.2 Respiration model structure

The box model accounts for all the carbon fixed by the vegetation. The model simulates the allocation and storage of carbon using 5 carbon pools, and 9 turnover rates that determine the fluxes between the pools (Figure 1). To do this the respiration model takes the previous days GPP and allocates a fraction of it directly into autotrophic respiration (R_a). The remainder is the net primary production (NPP), and this is allocated into the foliage (C_f), wood (C_w) and fine root (C_r) carbon pools. The wood

carbon pool feeds into the soil organic matter (SOM) pool (C_{SOM}). Both the foliage and the fine root pools feed into the litter carbon pool (C_{lit}). The litter pool then partly feeds into the SOM pool, and partly is respired heterotrophically. The other component of the heterotrophic respiration comes from the SOM pool.

The turn over rates between the carbon pools are: t1 (the decomposition rate), t2 (the autotrophically respired fraction of GPP), t3 (the fraction of NPP allocated to foliage), t4 (the fraction of NPP allocated to fine roots), t5 (the turnover rate of foliage), t6 (the turn over rate of wood), t7 (the fine root turnover rate), t8 (the mineralization of litter) and t9 (the mineralization of SOM). The turnover rates determine the fluxes between the carbon pools:

$A_f = (1-t2)\cdot t3\cdot GPP$ (Foliage allocation rate)

$A_w = (1-t2)\cdot(1-t3-t4)\cdot GPP$ (Wood allocation rate)

$A_r = (1-t2)\cdot t4\cdot GPP$ (Fine root allocation rate)

$L_f = t5\cdot C_f$ (Leaf litter production rate)

$L_w = t6\cdot C_w$ (Wood production rate)

$L_r = t7\cdot C_r$ (Fine root production rate)

$D = t1\cdot C_{lit}\cdot T$ (Litter decomposition rate)

$R_a = t2\cdot GPP$ (Autotrophic respiration rate)

$R_h = t8\cdot C_{lit}\cdot T + t9\cdot C_{SOM}\cdot T$ (Heterotrophic respiration rate)

$R = R_a + R_h$ (Total respiration rate)

$T = 0.5\cdot\exp(0.0693 T_{air})$ (Temperature dependence)

Where R is the total respiration, T is the temperature dependence function and T_{air} the air temperature in Celius.

3.3.3 Limitations to the box model

Respiration is poorly understood and so the carbon pools in the box model are likely to slightly misrepresent the actual pool divisions. Additionally, measurements of carbon pool sizes and turnover rates are not always available for all study sites. However there are potential ways around this lack of data. Additionally the box model used here assumes zero leaching of carbon through runoff of dissolved organic carbons.

4 Model alterations

To make the models interface with each other some alterations had to be performed to each of the models. These changes are outlined below, in the CAB model code the changes are highlighted with either *"!CAB_mod: Modification description"*, *"!TS_mod: Modification description"* for modifications related to the variable time step, *"!ORG_mod: Modification description"* for the modifications related to organic soils or *"THERM_mod: Modification description"* for modifications related to the thermal properties of the soil.

The bulk of the SPA and OSU1DPBL models interactions with one another occur through the SPA PBL interface subroutine "SPinterface()" (Chapter 7). This interface routine was added to deal with the repeat calls of the SPA model made by the OSU1DPBL component of the CAB model.

4.1 Changes to OSU1DPBL

4.1.1 Precipitation

The precipitation input routine was altered to accept multiple rain events.

4.1.2 Cloud formation

The original cloud formation routine was found to be producing unrealistic (not supported by the data) clouds. The routine worked by locating the model layer with the greatest relative humidity. The standard deviation of the relative humidity was estimated for this layer, and the fractional cloud cover set to the area under the distribution that exceeded a relative humidity of 1. Clouds were placed at this height.

Instead of this cloud formation routine we specify a fixed fractional cloud cover, which is placed at the model layer with the highest relative humidity.

4.1.3 CO_2

A key feature capability of the CAB model is its ability to model the carbon dynamics within the coupled system. To accommodate this in the PBL model, CO_2 dynamics had to be added. It was added as a tracer gas which did not contribute to the stability or instability of the PBL in anyway. The required surface fluxes of CO_2 were calculated by the SPA and respiration models. PBL profiles of CO_2 ppm now need to be specified in the PBL parameterisation file.

4.1.4 OSU1DPBL surface flux routine

The original OSU1DPBL surface flux routine (SFLX) was replaced by the SPA model (Chapter 7).

4.2 Changes to SPA

4.2.1 Variable time-step

Originally the SPA model was designed to compliment eddy covariance data and so was designed to run with a fixed time-step. The OSU1DPBL model also has a fixed time-step, but for some processes it reduces this step to ½ or ¼ of the standard step. The land-surface calculations are amongst the subroutines that are called with this variable time-step. There were two approaches to solving this problem; 1) fix the time-step for the calls of the land-surface subroutine, or 2) amend the land-surface routine (SPA) to be able to run on a flexible time-step. In order to maintain the consistency within the coupled model the second option was opted for. All amendments to the SPA code are labelled with the annotation with "!TS_mod: *Modification description*".

4.2.2 Daily integrations

The original SPA model summarised the daily fluxes, means and aggregations. However, in the context of the CAB model these averages became largely redundant, and since the introduction of a variable time-step they were more difficult to calculate. Consequently they were removed.

4.2.2 Calculation of diffuse radiation

The SPA model has two approaches to calculating the diffuse radiation; 1) the first subroutine (fracdif) calculates the diffuse radiation from the total potential and actual daily photosynthetically active radiation (PAR). 2) the second subroutine (fracdifhour) uses the current PAR to calculate the diffuse contribution. Due to the variable time-step of the modified SPA model we use the second subroutine.

4.2.3 Meteorological drivers

The CAB model generates its own meteorology and so does not require meteorological drivers. Additionally the meteorology needs to be specified for each call to the land-surface routine (SPA), where as in the original this only occurred at the start of the model run. This assignment of the meteorology is done in the interface file.

4.2.4 Gap filling

The gap filling routine filters for basic errors in the meteorological input file. This subroutine was removed due to being surplus to requirements, as meteorology is generated internally in the CAB model.

4.2.5 Soil organic fraction and water field capacity

The original formulation of the SPA model used a set of equations to calculate the field capacity of soils based on the mineral content [*Saxton, et al.*, 1986]. However this relationship breaks down for organic soils. To deal with this the Saxton equations can be bypassed, and an alternative can be specified based on data. The soil water potential also changes for organic soils (M.R. Nemati, J Caron 2002 SSSA vol66). All these changes are labelled with "!ORG_mod".

4.2.6 Soil thermal conductivity

The original SPA soil thermal conductivity was calculated on the basis of the sand percent, mineral fraction, organic fraction, water fraction and the ice proportion. However for saturated soils with a high organic fractions (and thus high field capacities) this was found not to perform well, giving thermal conductivities that were slightly too high. In order to rectify the effect, an alternative subroutine was implemented. This subroutine calculated the thermal conductivity (TC) from the water fraction (Θ), the volume fraction of the soil (Φ_S), the volume fraction of the quartz (Φ_Q),the volume fraction of mineral (Φ_M) and the volume fraction of clay (Φ_C) [*Campbell*, 1985].

$$A = \frac{0.57 + 1.73\Phi_Q + 0.93\Phi_M}{1 - 0.74\Phi_Q - 0.49\Phi_M} - 2.8\Phi_S(1 - \Phi_S)$$

$$B = 2.8\Phi_S\Theta$$

$$C = 1 + 2.6\Phi_C^{-1/2}$$

$$D = 0.03 + 0.7\Phi_S^2$$

$$E = 4$$

$$TC = A + B\Theta - (A - D)\exp(-(C\Theta)^E)$$

4.2.7 Solving the surface energy balance

The original version of the OSU1DPBL model solved the energy balance to find the effective temperature of the land-surface, but in the coupled model the SPA model takes on this role. The SPA model generates estimates of the ground heat flux and the latent energy heat flux, estimates of down welling long wave and shortwave radiation are provided by the atmospheric component of the model. We are then left with the unknowns of the sensible heat flux ($H_\uparrow$) and the surface potential temperature (θ_S^4).

$$(1-\alpha)S_{\downarrow} + L\downarrow - \sigma\theta_S^4 = G_{\downarrow} + H_{\uparrow} + LE_{\uparrow}$$

To solve this equation we use two approximations, firstly:

$$\sigma\theta_S^4 \approx \sigma T_O^4\left(1 + 4\left(\frac{\theta_S - T_O}{T_O}\right)\right)$$

and secondly that:

$$H_{\uparrow} = \rho c_P c_h[(\theta_S - T_O) - (\theta_O - T_O)]$$

where θ_O is the potential temperature of the first atmospheric model layer, T_O is the temperature of the first atmospheric model layer, ρ is the air density, c_P is the specific heat capacity of dry air and c_h is the surface exchange coefficient for heat. Using these approximations the symbolic mathematics program Maple was used to solve these equations. 4 solutions are possible, of which only one is physically realistic, i.e. within + 230 to 350 K. The 4 solutions can be found in the code.

4.2.8 Calculation of VPD

Since the CAB model generates its own meteorology, the vapour pressure deficit (VPD) has to be calculated. The VPD can be expressed as a function of the saturation vapour pressure (e_S) and the actual vapour pressure (e_a). The e_a be replaced with the relative humidity (RH).

$$VPD = e_S - e_{,a} = e_S(1 - RH)$$

Where RH can be expressed as

$$RH = \frac{e_a}{e_S}$$

Finally the e_S can be expressed as a function of the air temperature in Celcius (°C), and the air pressure (P) [*Buck*, 1981].

$$e_S = \left[1.0007 + 3.46\times10^{-6}P\right]\times 0.61121\exp\left[\frac{17.502T}{240.97+T}\right]$$

Thus the VPD can be expressed as

$$VPD = (1-RH)\times\left[1.0007 + 3.46\times10^{-6}P\right]\times 0.61121\exp\left[\frac{17.502T}{240.97+T}\right]$$

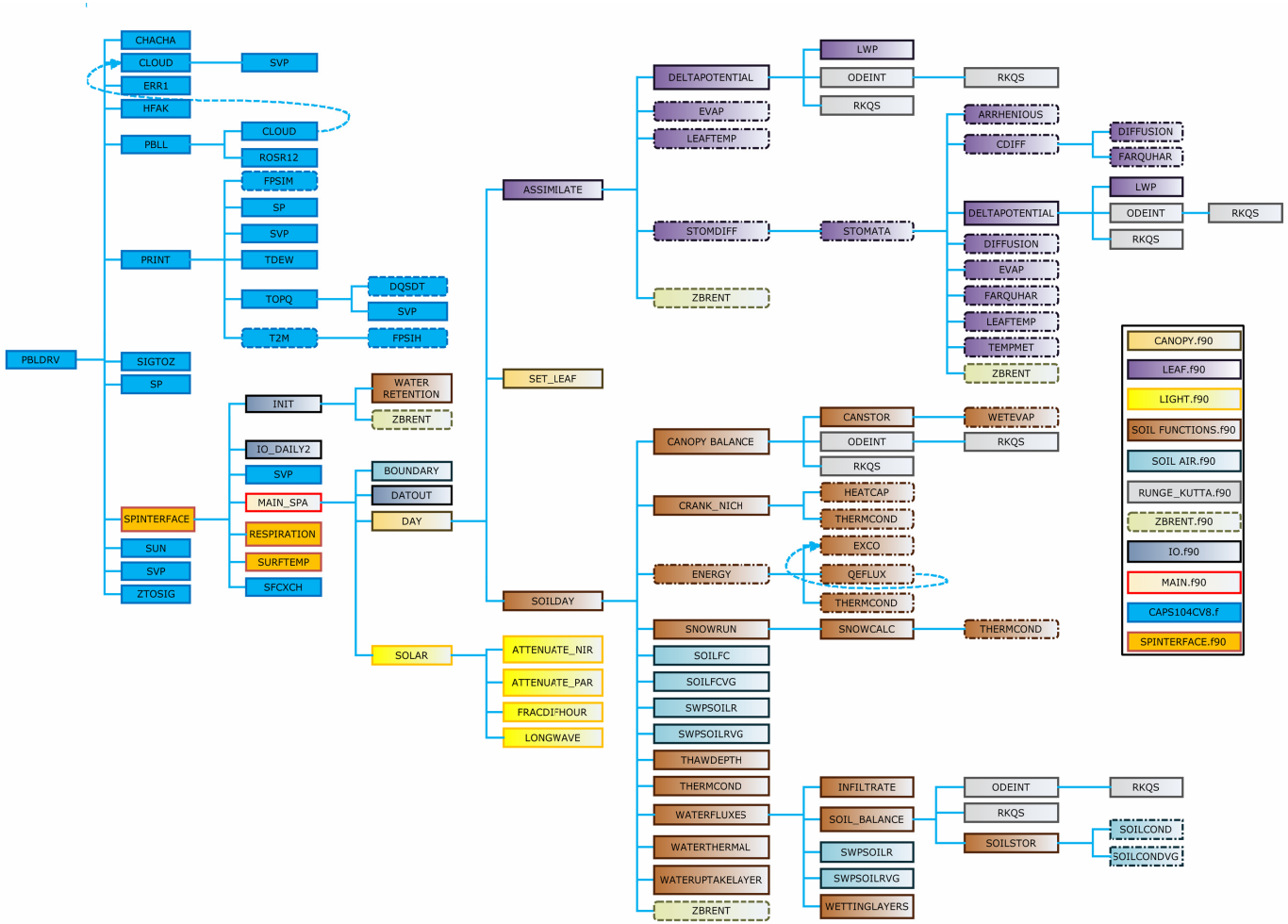

Figure 2: The call tree of the CAB model. Subroutines are shown as solid-edged square-cornered boxes, functions are shown as dashed-edged rounded-cornered boxes. Subroutines and functions are colour coded to indicate the source file.

4.3 Changes to the respiration model

In its original form the respiration box model provided only daily estimates of respiration [*Williams, et al.*, 2005]. To calculate the current respiration, the previous daily respiration estimate was disaggregated using a sinusoidal term and an offset term.

4.4 CAB model structure overview

The CAB model is a (relatively) complex model; as such it contains many files, functions and subroutines. The main program is called 'PBLDRV' and is contained within the CAPS104CV8.f file. The PBLDRV program directly or indirectly calls all the other program files. The subroutine 'SPINTERFACE' is call point within PBLDRV for the biosphere component. We provide a calls map of CAB (Figure 2) and briefly describe each function/subroutine; listing the subroutine/function calls and the modules used. The programs usage of common blocks is not dealt with here, but these are almost entirely confined to the PBL code (i.e. the F77 code), please refer to the OSU1DPBL model manual for a detailed description of the common blocks.

5 SPA model files, subroutines and functions

5.1 All_declarations.f90

This file contains modules that define the global/commonly used variables. Two modules have been added for use in the coupled model; the module *COUPLE* and the module *DALEC*. The variables in COUPLE start with PS if the variable is passed from the PBL model (OSU1DPBL) to the biosphere model (SPA), and SP if they are passed the other way.

5.2 Scale declarations.f90

Defines the number of soil and canopy layers to use in the biosphere model.

5.3 Canopy.f90

5.3.1 SUBROUTINE DAY

- *CALLS SUBROUTINES*: ASSIMILATE, SET_LEAF, SOILDAY
- *USES MODULES:* CLIM, COUPLE, ERROR, HOURSCALE, IRRADIANCE_SUNSHADE, METAB, METEO, SOIL_STRUCTURE, VEG

The subroutine DAY controls the daily runs of SPA leaf-level and soil processes. First the subroutine initiates calculations of the soil energy balance, infiltration of precipitation, heat and water transfer between the soil layers and water uptake by the roots. Then the subroutine works through each canopy layer in turn. For each layer, sunlit and shaded areas are calculated, with shaded regions only receiving diffuse radiation. If the foliage is sunlit then the respiration, transpiration and assimilation rate of CO_2 are calculated (see the subroutine ASSIMILATE). This process is performed for both directly lit and shaded leaves.

5.3.2 SUBROUTINE SET_LEAF

- *USES MODULES:* METAB, METEO, VEG

The SET_LEAF subroutine sets the parameters V_{cmax} and J_{max} and hydraulic parameters (*rplant* and *rsoil*) for each canopy layer. The hydraulic parameters for the stem conductance are calculated on the assumption that the hydraulic conductivity is constant at all heights. If instead you wish to maintain a constant hydraulic conductance for all layers, the switch in the VEG input file should be set so *conductivity*=0.

5.4 Leaf.f90

5.4.1 SUBROUTINE ASSIMILATE

- *CALL SUBROUTINE*: DELTAPOTENTIAL
- *CALLS FUNCTIONS*: EVAP, LEAFTEMP, STOMDIFF, ZBRENT
- *USES MODULES:* C13, ERROR, METAB, METEO, VEG

Determines the assimilation of carbon, the dark respiration and evapotranspiration of the leaves.

5.4.2 SUBROUTINE DELTAPOTENTIAL

- *CALL SUBROUTINES*: ODEINT, LWP, RKQS
- *USES MODULE:* LWPINTEGRATOR

Calculates the change in leaf water potential using a Runge-Kutta ordinary differential equation integrator.

5.4.3 SUBROUTINE LWP

- *USES MODULES:* CANOPY, LWPINTEGRATOR, METAB, METEO

Determines the change in leaf water potential (LWP) for a given supply/demand.

5.4.4 FUNCTION ARRHENIOUS

Determines Arrhenious relationship; a temperature response function dependant on the activation energy for reaction.

5.4.5 FUNCTION CDIFF

- *CALLS FUNCTIONS*: DIFFUSION, FARQUHAR,
- *MODULES*: CUP, METAB, METEO

Determines the difference between metabolic assimilation rate of CO_2 and the CO_2 diffusion between inside and outside the leaf. at a given internal CO_2 concentration (C_i).

5.4.6 FUNCTION DIFFUSION

- *USES MODULE:* VEG

Determines the diffusion limited assimilation rate.

5.4.7 FUNCTION EVAP

- *USES MODULE:* VEG

Determines evapotranspiration rate using the Penman-Montieth equation (see 3.2.3 Evapotranspiration).

5.4.8 FUNCTION FARQUHAR

- *USES MODULES:* METEO, VEG

Calculates the metabolic carboxylation rate.

5.4.9 FUNCTION LEAFTEMP

- *USES MODULES:* COUPLE, ERROR, VEG, METEO

Solves the energy balance of the leaf to determine the leaf temperature.

5.4.10 FUNCTION STOMDIFF

- *CALLS FUNCTION*: STOMATA, MODULES: METAB, METEO, VEG

Determines if the criteria for stopping the incrementing of stomatal conductance has been satisfied (Chapter 3.2.5, Stomatal dynamics).

5.4.11 FUNCTION STOMATA

- *CALL SUBROUTINE*: DELTAPOTENTIAL
- *CALLS FUNCTIONS*: ARRHENIOUS, CDIFF, DIFFUSION, EVAP, FARQUHAR, LEAFTEMP, TEMPMET, ZBRENT
- *USES MODULES:* CUP, METAB, METEO, VEG

This routine determines the stable internal CO_2 concentration (C_i) for a given stomatal conductance (g_s) and updates the change in leaf water potential.

5.4.12 FUNCTION TEMPMET

An alternative temperature response function.

5.5 Light.f90

5.5.1 SUBROUTINE ATTENUATE_NIR

- *USES MODULE:* CANOPY

Calculates NIR attenuation.

5.5.2 SUBROUTINE ATTENUATE_PAR

- *USES MODULE:* CANOPY

Calculates PAR attenuation for shaded and sunlit canopy fractions.

5.5.3 FUNCTION FRACDIFF

- *USES MODULES:* CLIM, COUPLE

See 4.2.2 Calculation of diffuse radiation

5.5.4 SUBROUTINE LONGWAVE

- *USES MODULE:* CANOPY

Calculates the long-wave (LW) radiation attenuation.

5.5.5 SUBROUTINE SOLAR

- *CALLS SUBROUTINE*: ATTENUATE_NIR, ATTENUATE_PAR, LONGWAVE
- *CALLS FUNCTION*: FRACDIFHOUR
- *USES MODULES:* CANOPY, CLIM, COUPLE, HOURSCALE, IRRADIANCE_SUNSHADE, VEG

Determines the near infrared (NIR), photosynthetically active radiation (PAR), shortwave (SW) and long-wave (LW) attenuation, absorption, transmittance and reflectance of radiation between the sky, the canopy layers and the soil surface.

5.6 Soil functions.f90

5.6.1.1 SUBROUTINE CANOPY_BALANCE

- *CALLS SUBROUTINES*: CANSTOR, ODEINT, RKQS
- *USES MODULES:* HOURSCALE, INTEGRATOR, SOIL_STRUCTURE

Calls the Runge-Kutta ODE integrator to determine the leaf water runoff, storage and the evaporation from canopy elements (see SR CANSTOR).

5.6.1.2 SUBROUTINE CANSTOR

- *CALLS FUNCTION*: WETEVAP
- *USES MODULES:* CANOPY, HOURSCALE, INTEGRATOR, SOIL_STRUCTURE

Called by the Runge-Kutta ODE integrator to determine the leaf water runoff, storage and evaporation from the canopy.

5.6.1.3 SUBROUTINE CRANK_NICHOLSON

- *USES MODULES:* CANOPY, HOURSCALE, INTEGRATOR, SOIL_STRUCTURE

A finite difference partial differential equation solver for the soil temperature profile.

5.6.1.4 SUBROUTINE INFILTRATE

- *USES MODULES:* CLIM, HOURSCALE, HYDROL, METEO, SOIL_STRUCTURE

Determines the infiltration of surface water into the soil layers. Layers are saturated from the top down, until all layers are saturated. At this point the surface water is lost from the system.

5.6.1.5 SUBROUTINE SNOWCALC

- *USES MODULES:* CLIM, COUPLE, HOURSCALE, IRRADIANCE_SUNSHADE, SNOWINFO, SOIL_STRUCTURE, VEG

Determines the energy balance of the snow pack by calculating the evaporation/sublimation, melting and refreezing of the snow pack.

5.6.1.6 SUBROUTINE SNOWRUN

- *CALLS SUBROUTINE*: SNOWCALC
- *USES MODULES:* CLIM, HOURSCALE, IRRADIANCE_SUNSHADE, SNOWINFO, SOIL_STRUCTURE, VEG

Determines the dynamics of any snow pack, calculating snow height, snow weight and snow fall (if temperatures are below freezing). Snow falls if precipitation occurs at temperatures below freezing. The routine calculates the change the snow height and weight arising from new snowfall.

5.6.1.7 SUBROUTINE SOIL_BALANCE

- *CALLS SUBROUTINES*: ODEINT, RKQS, SOILSTOR
- *USES MODULES:* HOURSCALE, INTEGRATOR, ODEINT, SOILINFO, SOIL_STRUCTURE

This routine calculates the gravitational drainage using the Runge-Kutta ordinary differential equation (ODE) solver.

5.6.1.8 SUBROUTINE SOILDAY

- *CALLS SUBROUTINES*: CANOPY_BALANCE, CRANK_NICHOLSON, SNOWRUN, SOILFC, SOILFCVG, SWPSOILR, SWPSOILRVG, THAWDEPTH, WATERFLUXES, WATERTHERMAL, WATERUPTAKELAYER
- *CALLS FUNCTIONS*: ENERGY, THERMCOND, ZBRENT
- *USES MODULES:* CLIM, COUPLE, ERROR, HOURSCALE, IRRADIANCE_SUNSHADE, SNOWINFO, SOIL_STRUCTURE, VEG

Determine the canopy interception, direct evaporation and canopy runoff, as well as the soil infiltration, drainage and limit to the water uptake by root. The subroutine also solves the soil surface energy balance.

5.6.1.9 SUBROUTINE SOILSTOR

- *CALLS FUNCTIONS*: SOILCOND, SOILCONDVG
- *USES MODULES:* CANOPY, HOURSCALE, INTEGRATOR, SOILINFO, SOIL_STRUCTURE

Used to determine the gravitational water drainage. Gravitational drainage occurs when liquid water content is above field capacity.

5.6.1.10 SUBROUTINE THAWDEPTH

- *USES MODULES:* HOURSCALE, SOIL_STRUCTURE

Determines layer ice fraction, and depth of thaw.

5.6.1.11 SUBROUTINE WATERFLUXES

- *CALLS SUBROUTINES*: INFILTRATE, SOIL_BALANCE, SWPSOILR, SWPSOILRVG, WETTINGLAYERS
- *USES MODULES:* CLIM, HOURSCALE, HYDROL, SOIL_STRUCTURE, METEO

Calls other routines to determine the water gain/loss from each soil layer. Fluxes can be due to evaporation, dew fall, precipitation, runoff from leaves, gravitational drainage and uptake by roots.

5.6.1.12 SUBROUTINE WATERTHERMAL

- *USES SUBROUTINES*: CLIM, HOURSCALE, HYDROL, SOIL_STRUCTURE

Determines the transport of energy in the soil layers due to water fluxes between the soil layers.

5.6.1.13 SUBROUTINE WETTINGLAYERS

- *USES SUBROUTINES*: CLIM, HOURSCALE, HYDROL, METEO, SOIL_STRUCTURE

Determines the spread of dry/wet layers from the top soil layer down.

5.6.1.14 SUBROUTINE WATERUPTAKELAYER

- *USES SUBROUTINES*: CANOPY, HOURSCALE, METAB, METEO, SOIL_STRUCTURE, VEG

Determines which layer water withdrawn from

5.6.1.15 REAL FUNCTION ENERGY

- *CALLS FUNCTIONS*: EXCO, QEFLUX, THERMCOND
- *USES SUBROUTINES*: COUPLE, ENERGY_CONSTANTS, HOURSCALE, SOIL_STRUCTURE, VEG

Determines the surface temperature of the surface soil by solving the energy balance.

5.6.1.16 REAL FUNCTION EXCO

- *USES SUBROUTINES*: ENERGY_CONSTANTS, HOURSCALE, METEO, SOIL_STRUCTURE, VEG

Estimates the heat or moisture exchange coefficients with neutral buoyancy.

5.6.1.17 REAL FUNCTION HEATCAP

- *USES SUBROUTINE:* SOIL_STRUCTURE

Determines the volumetric heat capacity of soil.

5.6.1.18 REAL FUNCTION QEFLUX

- *CALLS FUNCTION*: EXCO
- *USES MODULES:* CLIM, ENERGY_CONSTANTS, HOURSCALE, METEO, SOIL_STRUCTURE, VEG

Determines the latent energy lost from soil surface.

5.6.1.19 REAL FUNCTION THERMCOND

- *USES SUBROUTINES*: HYDROL, SOIL_STRUCTURE

Determines the thermal conductivity of soil (see 4.2.6 Soil thermal conductivity).

5.6.1.20 REAL FUNCTION WETEVAP

- *USES SUBROUTINES*: ENERGY_CONSTANTS, HOURSCALE, VEG

Determines the rate of evaporation from surface of wet leaves.

5.7 SOIL AIR.f90

5.7.1 SUBROUTINE BOUNDARY

- *USES MODULES*: CLIM, METEO, VEG

Determines the boundary layer conductance for each canopy layer.

5.7.2 FUNCTION SOILCOND

- *USES MODULES*: CLIM, HOURSCALE, HYDROL, METEO, SOILINFO, SOIL_STRUCTURE

Determines the soil hydraulic conductivity using the equations from [*Saxton, et al.*, 1986].

5.7.3 FUNCTION SOILCONDVG

- *USES MODULES*: CLIM, hourscale, HYDROL, METEO, soilinfo, SOIL_STRUCTURE

Alternative to the SUBROUTINE SOILCOND. **(not used)**

5.7.4 SUBROUTINE SOILFC

- *USES MODULES*: HOURSCALE, HYDROL, METEO, SOIL_STRUCTURE

Determines the porosity using the algorithms of [*Saxton, et al.*, 1986] and the relationships in [*Nemati, et al.*, 2002] for organic soils.

5.7.5 SUBROUTINE SOILFCVG

- *USES MODULES*: CLIM, HOURSCALE, HYDROL, METEO, SOIL_STRUCTURE

Alternative to the SUBROUTINE SOILFC. **(not used)**

5.7.6 SUBROUTINE SWPSOILR

- *USES MODULES*: CLIM, hourscale, HYDROL, METEO, SOIL_STRUCTURE

Determines the soil water potential (SWP) for the plant uptake of water [*Saxton, et al.*, 1986]. Soil-root resistance is determined from separation of the root from the soil (increases with dry soils) and the resistance of the root to water flow.

5.7.7 SUBROUTINE SWPSOILRVG

- *USES MODULES*: CANOPY, METAB, METEO, SOILINFO, SOIL_STRUCTURE

Alternative to the SUBROUTINE SWPSOILR. **(not used)**

5.7.8 SUBROUTINE WATER_RETENTION

- *USES MODULES*: HYDROL, SOIL_STRUCTURE, SOILINFO

Calculates the field capacity.

5.8 RUNGE_KUTTA.f90

5.8.1 SUBROUTINE ODEINT

Integrator of ordinary differential equations [*Press*, 1986].

5.9 ZBRENT.f90

5.9.1 FUNCTION ZBRENT

This is a bisection routine which finds the root of a given function [*Press*, 1986].

5.10 IO.f90

5.10.1 SUBROUTINE DATOUT

- *USES MODULES*: CLIM, COUPLE, ENERGY_CONSTANTS, HOURSCALE, IRRADIANCE_SUNSHADE, METEO, SOIL_STRUCTURE, VEG

Generates the model output.

5.10.2 SUBROUTINE INIT

- *CALLS SUBROUTINE*: WATER_RETENTION
- *USES MODULES*: C13, CLIM, COUPLE, DALEC, HOURSCALE, HYDROL, METAB, METEO, SNOWINFO, SOIL_STRUCTURE, VEG

Opens up a files, for reading (parameters and in the offline biosphere model drivers) and for writing output files.

5.10.4 SUBROUTINE IO_DAILY2

- *USES MODULES*: COUPLE,CLIM, HOURSCALE, SOIL_STRUCTURE , VEG

Replaced the SUBROUTINE IO_DAILY in the original SPA. Reads in the phenology for each day.

5.11 SUBROUTINE Main.f90

This is the main subroutine in the SPA model. This is the subroutine that is called by the interface between the SPA model and the OSU1DPBL model.

6 OSU1DPBL model file, subroutines and functions

(The following subroutines are no longer used in OSU1DPBL due to being replaced by SPA: DFKT, HFLX, HRT, HSTEP, KTSOIL, SEC, SEDIR, SET, SFLX, SHFLX, SMFLX, SRC, SRT, SSHEAT, SSTEP, THSAT.)

OSU1DPBL also extensively uses COMMON BLOCKS, for information on these please refer to the OSU1DPBL manual.

6.1 caps104cV8.f

6.1.1 PROGRAM PBLDRV

- *CALLS SUBROUTINES:* CHACHA, CLOUD, ERR1, HFAK, PBLL, PRINT, SIGTOZ, SP, SPINTERFACE, SUN, SVP, ZTOSIG
- *USES MODULE:* COUPLE

This is the main program in both the original OSU1DPBL model, and the CAB model. This program controls all other subroutines, and subsequently is responsible for both the dynamics of the atmosphere and the biosphere. The biosphere subroutines are called at two points in this program.

6.1.2 SUBROUTINE CHACHA

This subroutine is responsible for the rescaling piecewise linear functions from grid to another. CHACHA does this rescaling using least squares.

6.1.3 SUBROUTINE CLOUD

- CALLS SUBROUTINE: SVP
- *USES MODULE:* COUPLE

This subroutine used to calculate the fractional cloud cover but has been bypassed (4.1.2 Cloud formation).

6.1.4 SUBROUTINE ERR1

Error message associated with CHACHA; passes out the array dimensions.

6.1.5 SUBROUTINE HFAK

Determines values for use in the integration of the hydrostatic equations

6.1.6 SUBROUTINE LCL

- CALLS SUBROUTINE: TDEW

Finds the lifting condensation level (LCL), the level at which a parcel of rising unsaturated air reaches its dew point and condensation occurs.

6.1.7 SUBROUTINE PBLL

- *CALLS SUBROUTINES*: CLOUD, ROSR12

Determines the turbulent mixing in the PBL and free atmosphere.

6.1.8 SUBROUTINE PRINT

- *CALLS SUBROUTINES*: FPSIM, SP, SVP, TDEW, TOPQ, T2M

Generates the model output for the atmospheric component of the model.

6.1.9 SUBROUTINE ROSR12

Inverts a tri-dimensional matrix.

6.1.10 SUBROUTINE SIGTOZ

Determines the height (m) of the sigma levels. Where the sigma levels are defined as fractions of the surface atmospheric pressure (from 1.000 to 0.616). Inverse of the SR ZTOSIG.

6.1.11 SUBROUTINE SFCXCH

Determines the bulk Richardson number and the surface exchange coefficients of heat and momentum.

6.1.12 SUBROUTINE SP

Determines geo-potential height of the LCL (see 6.1.6 SR LCL)

6.1.13 SUBROUTINE SUN

- *USES MODULE:* COUPLE

Determines the atmospheric radiation information.

6.1.14 SUBROUTINE SVP

Determines the saturation vapour pressure

6.1.15 SUBROUTINE TDEW

Determines the dew point temperature.

6.1.16 SUBROUTINE TOPQ

- *CALLS SUBROUTINES*: DQSDT, SVP

Determines the second model layer temperature and saturation mixing ratio by assuming the layer has the same potential temperature as the first model layer.

6.1.17 SUBROUTINE ZTOSIG

Determines sigma as a function of the height. Inverse of the SR SIGTOZ.

6.1.18 FUNCTION DQSDT

Determines the change in the saturation mixing ratio due to temperature.

6.1.19 FUNCTION FPSIH

Determines the stability correction to the temperatures in the surface layer.

6.1.20 FUNCTION FPSIM

Determines the stability correction to the winds in the surface layer.

6.1.21 FUNCTION T2M

- *CALLS FUNCTION*: FPSIH

Determines potential temperature at 2 m.

7 SPA-OSU1DPBL interface file and subroutines

7.1 SPinterface.f90

7.1.3 SUBROUTINE RESPIRATION

- *USES MODULE:* DALEC

Determines the respiration flux by partitioning GPP, and calculating the carbon pool dynamics (see 3.3.2 Respiration model structure).

7.1.1 SUBROUTINE SPINTERFACE

- *CALLS SUBROUTINES:* INIT, IO_DAILY2, SVP, MAIN_SPA, SURFTEMP, SFCXCH, RESPIRATION
- *USES MODULES:* CANOPY, CLIM, VEG, HOURSCALE, COUPLE, DALEC

This subroutine acts as the gateway between the OSU1DPBL model and the SPA model. The interface provides the biosphere model (SPA) with the correct time of day, initial parameterisations and the meteorology for the current time-step. The routine then calls the SPA model for that time step and calculates fluxes of respiration and evaporation into the atmosphere.

7.1.2 SUBROUTINE SURFTEMP

Solves the surface energy balance explicitly (see 4.2.7 Solving the surface energy balance).

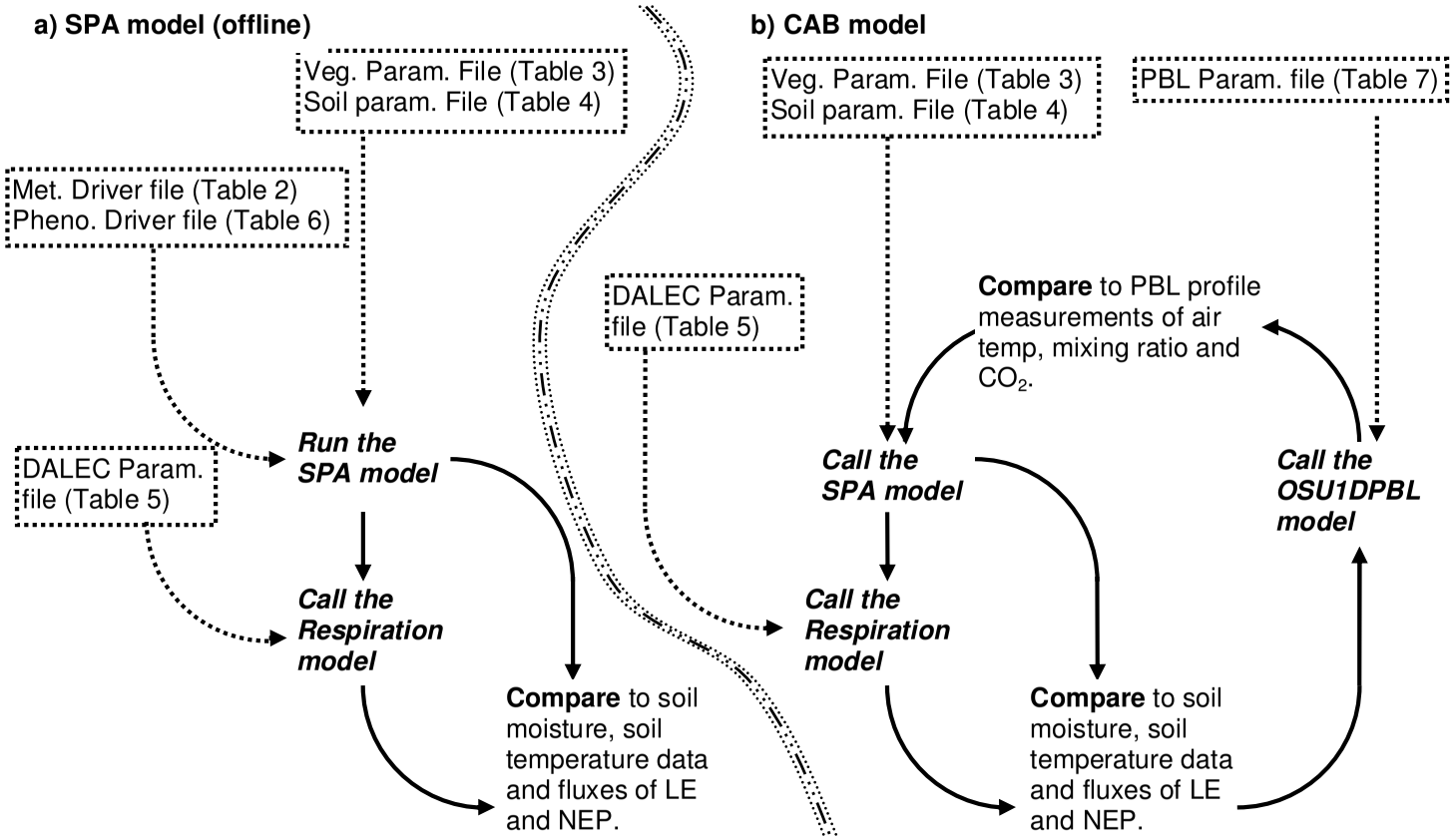

Figure 3: The biosphere model is run in two parts: 1) The biosphere component (SPA) is run in an offline mode. The SPA model is run for the whole study period. The respiration model is called by the SPA model to convert the GPP into NEE. Fluxes of NEE and LE are then compared to eddy covariance data. 2) Once the biosphere model and the parameterisations it uses have been corroborated, the same parameterisations are used in the fully coupled CAB model. In this model, the OSU1DPBL model generates the meteorology (corroborated with PBL measurements), which drives the SPA model, and subsequently the respiration model. The SPA model and the respiration model provide the land-surface conditions needed to drive turbulence in the PBL.

8 Running the model

The model is run in two stages:

STAGE 1: Verify the biosphere parameterisations (Figure 3a)

I. Compile the meteorological driver file (Table 9). In use the file will look like (Table 2):

Day	Air temp	CO_2	Wind Speed	RAD	VPD	PPFD	Precip.
250	13.18	365	2.29	0	0.52	0	0
250.02	12.94	365	2.07	0	0.49	0	0
250.04	12.56	365	1.56	0	0.46	0	0
250.06	12.32	365	2.11	0	0.45	0	0
250.08	11.89	365	2.94	0	0.41	0	0
250.1	10.92	365	2.84	0	0.40	0	0
250.12	10.46	365	2.62	0	0.42	0	0
250.15	9.94	365	2.96	0	0.38	0	0

Table 2: The general form of the meteorological driver file.

The file will start at midnight on the day in question (in this case day 250) and run the full length of the intended model run. Each row is represents a 30min period. The file should be saved as a comma-separated-value (.csv) file.

II. Compile the vegetation input file (Table 10). The file should look like (Table 3):

la_frac	0.1	0.15	0.2	0.15	0.1	0.1	0.05	0.05	0.05	0.05
nit_frac	0.1	0.15	0.2	0.15	0.1	0.1	0.05	0.05	0.05	0.05
ht	10	9.25	8.5	7.75	7	6.25	5.5	4.75	4	3.25
LAI	4.4		Total leaf area index							
Total_N	1.67		Total foliar nitrogen							
Gplant	10		Stem conductivity (or conductance if CONDUCTIVITY=0 see below)							
MinLWP	-1.5		Minimum leaf water potential							
Iota	1.005		Stomatal efficiency parameter							
Capac	2000		Leaf capacitance							
Lat	53.9		Latitude of site							
Outt	1		Detailed layer by layer output (1=ON, 0=OFF)							
Dimen	0.08		Characteristic dimension of leaf (i.e. ~width of leaf m)							
Rootress	100		Root resistivity							
Towerht	27		Height of tower with sensors							
Conductivity	1		Is tree conductivity defined (=1) is is tree conductance defined (=0)?							
KappaC	11		Rate coefficient for Vcmax							
KappaJ	31.31		Rate coefficient for Jmax							
resp_cont	0.088388		Rate coefficient for dark respiration							
Altitude	579.27		Altitude (m) for estimating pressure if these data are not supplied							

Table 3: The general form of the vegetation parameter file.

'ht' represents the heights of the individual canopy layers, and 'la_frac'/'nit_frac' the fraction of the total leaf area/nitrogen levels respectively. The file should be saved as a comma-separated-value (.csv) file.

III. Compile the soil input file (Table 11). The file should look like (Table 4):

Layers	layer 1	layer 2	layer 3	…	layer 19	layer 20	Core
Layer_thickness	0.1	0.1	0.1	…	0.1	0.1	0.1
Organic_fraction	0.5	0.15	0.09	…	0	0	0
Mineral_fraction	0.00001	0	0.4	…	0.4	0.4	0.4
Initial_water_fraction	0.0992	0.2558	0.4132	…	0.4	0.4	0.4
Initial_soil_temp	285.2491	285.5186	284.2713	…	273.15	273.15	274.05
Initial_ice_proportion	0	0	0	…	1	1	1
root_frac	0	0.01	0.54	…	0	0	0
rootl	5			…			
rootbiomass	597			…			
sand%	90	75	64	…	65	65	65
clay%	10	10	10	…	15	15	15
rootrad	0.0001	root radius, m					
snowweight	0	intial snow weight, kg m-2					
snowheight	0	initial snow height, m					

Table 4: The general form of the soil parameter file.

The soil file contains the composition and state of 20 soil layers (not all shown) and the core. The file should be saved as a comma-separated-value (.csv) file.

IV. Compile the DALEC (respiration) input file (Table 12). The DALEC file should look like (Table 5):

t1	4.4E-06
t2	0.5
t3	0.08
t4	0.47
t5	0.001
t6	0.00015
t7	0.0005
t8	0.001
t9	0.000023
Cf	556
Cw	5985
Cr	591
Clit	363.6
Csom	20616

Table 5: The general form of the respiration parameter file.

The file should be saved as a comma-separated-value (.csv) file.

V. Compile the phenology input file (Table 13). The phenology file should look like (Table 6):

day	lai	rootmass	totn
250	4.4	300	6.6
251	4.4	300	6.6
252	4.4	300	6.5
253	4.4	300	6.5
254	4.4	300	6.4
255	4.4	300	6.4
256	4.4	300	6.3

Table 6: The general form of the phenology driver file.

The driver file should start on the first day of the run and cover the whole intended study period at 1-day intervals. The file should be saved as a comma-separated-value (.csv) file.

VI. Check that the file locations/names match those in the modified SPA source code (SR 'INIT', file IO.f90).

VII. In the Program 'MAIN_SPA' (offline-SPA file 'main.f90') set the number of days to the require study length (i.e. if SPA is required to run for a year, set: 'DO j=1,365').

VIII. Run the offline biosphere model.

IX. Verify the parameterisations using comparisons against available data (see Table 15 for output files, e.g. eddy covariance, soil, biomass accumulation, respiration and leaf level data).

STAGE 2: Run the CAB model (Figure 3b)

I. Use the vegetation/soil/phenology files from the biosphere verification run. See STAGE 1 for file forms

II. Copy the output file '*Daily_DALEC.csv*' from the biosphere verification run. The file is generated automatically and should be copied over from the offline-biosphere output directory. This file includes DALEC parameters, and fluxes for each day.

III. Compile the PBL input file (Table 14). The file should look like (Table 7):

Control file for the PBL model						
IFCRI (cloud radiation interaction flag)	IFCLD(Flag for cloud diffusivity)					
1	1					
DELTAT(Timestep (s))	TEND (model run length (hrs))					
240	24					
250	Day of the year					
Latitude	Longitude	Timezone	Momentum	Heat	Displacement height	

			Roughness length	roughness length	of vegetation	
53.9	-105.3	-7	0.8	0.08	0	
Month	Day	Start time (hrs)				
9	7	0				
Surface pressure (Pa)						
95700						
Fractional cloud cover						
0.45						
Number of precipitation events						
1						
9	13	0	Start of precipitation event (hrs)	Duration (hrs)	Rate (kg m-2 s-1)	
Number of Geostrophic wind observations						
2						
u component	v component	Observation time				
-1.001	1.001	0				
0.301	-0.301	24				
Number of input levels	To use "m/s" unit for input "w", set "iwunit"=1					
24	1					
Height (m)	U component (m s-1)	v component (m s-1)	Vertical velocity (mb hr-1)	Air temp. (C)	Water mixing ratio (g kg-1)	CO2 (ppm)
0	-2.6	0	0	13.5	7.22	355.53
20	-2.49	0.51	0	13.16	6.44	357.86
145	-1.95	1.88	0	12.1	5.59	359.84
196	-1.66	2.27	0	13.36	5.99	360.51
280	-1.14	2.86	0	14.78	6.01	361
340	-0.72	3.23	0	15.15	6.03	361.14
500	0.66	4.41	0	15.04	6.01	362.26
630	2.06	5.55	0	14.64	5.62	362.18
750	3.16	6.44	0	13.96	5.73	361.81
800	3.36	6.64	0	11.84	5.13	360.81
850	3.56	6.64	0	10.64	5.13	360.81
900	3.76	6.64	0	9.44	5.13	361.21
1000	4.23	6.64	0	12.17	5.39	360.64
1250	5.39	6.43	0.01	10.39	5.25	360.72
1400	5.39	3.73	0.01	9.89	5.25	360.72
1500	5.87	2.85	0.01	9.3	4.9	361.1
1850	4.61	0.26	0.01	6.88	4.61	365
2150	3.49	-0.32	0.01	3.92	4.62	365
2600	6.32	-1.07	0.01	-0.17	4.44	365
3100	9.29	-2.4	0.01	-4.06	3.41	365
4800	11.74	-2.68	0.01	-11.84	0.54	365
5500	13.74	-2.09	0.01	-17.85	0.59	365
7500	15.95	-4.62	0.01	-32.49	0.47	365
9250	20.54	-6.81	0	-46.41	0.13	365

Table 7: The general form of the planetary boundary layer parameter file.

Extra precipitation events will be added as in the example for 2 precipitation events (Table 8):

Number of precipitation events					
2					
9	13	0.000001	Start of precipitation event (hrs)	Duration (hrs)	Rate (kg m-2 s-1)
15	18	0.0000005	Start of precipitation event (hrs)	Duration (hrs)	Rate (kg m-2 s-1)

Table 8: Inclusion of multiple precipitation events into the planetary boundary layer file (Table 7)

Extra geostrophic wind observations and input levels are added in the same manner.

IV. Check the phenology/ Daily_DALEC input files commence at the same day of year as the PBL input file, and cover the full range of dates.

V. Run the CAB model

VI. Verify the model using comparisons against available data (e.g. eddy covariance, soil, biomass accumulation, respiration, leaf level, radiosonde/aircraft data).

9 Overview of input and output files.

The offline SPA model and the fully coupled CAB model require a number of input parameter/driver files. These files are summarised here, with their typical value ranges and units.

Parameter	explanation	units	Typical values
daytime	Decimal time	Days	1-365
temptop	Air temperature above canopy	^{o}C	-
coa	Atmospheric CO_2 concentration	$\mu mol\ mol^{-1}$	0+
windsp	Wind-speed	$m\ s^{-1}$	n/a
swrad	Short-wave radiation	$W\ m^{-2}$	0+
vpdtop	Vapour pressure deficit	kPa	0+
partop	Photosynthetically active radiation	$\mu mol\ m^{-2}\ s^{-1}$	0+
ppt	precipitation	mm water equivalent	0+

Table 9 Meteorological drivers (used by the offline SPA model and CAB model)

Parameter	Explanation	Units	Typical values
(lafrac(i),i=1,numl)	Fraction of total leaf area in each canopy layer	Fraction	0—1
(nla(i),i=1,numl)	Fraction of total foliar nitrogen in each canopy layer	Fraction	0—1
(layerht(i),i=1,numl)	Height of each canopy layer	m	1—50
totla	Total LAI	$m^2\ m^{-2}$	0.1—10.0
totn	Total foliar N	$gN\ m^{-2}$	0.1—20.0
gplant	Stem conductivity or stem conductance	$mmol\ m^{-1}\ s^{-1}\ MPa^{-1}$ $mmol\ m^{-2}\ s^{-1}\ MPa^{-1}$	1—20 0.1—5.0
minlwp	Minimum leaf water potential	MPa	-2 — -4
iota	Stomatal efficiency	N/a	1.01-1.0007
capac	Leaf capacitance	$mmol\ m^{-2}\ MPa^{-1}$	1,000—10,000
lat	Latitude	^oN or ^oS	0—70
outt	Detailed layer by layer output?	0=no, 1=yes	0 or 1
dimen	Leaf characteristic dimension	m	0.01—0.2
rootresist	Root resistivity	MPa s g mmol-1 (biomass based)	10—500
towerht	Height of measurement tower	m	3—50
conductivity	Does conductance vary with stem length?	0=NO, 1=YES	0 or 1
kappac	Rate constant for V_{cmax}	$\mu mol\ g^{-1}\ s^{-1}$	10—50
kappaj	Rate constant for J_{max}	$\mu mol\ g^{-1}\ s^{-1}$	20—100

Table 10 Vegetation properties (used by the offline SPA model and CAB model)

Parameter	Explanation	Units	Typical values
thickness(i),i=1,core	Thickness of soil layer	m	0.1─0.5
organicfrac(i),i=1,core	Organic fraction of each soil layer	Fraction	0.0─0.5
mineralfrac(i),i=1,core	Mineral fraction of each soil layer	Fraction	0.0─0.5
waterfrac(i),i=1,core	Initial water fraction of each soil layer	Fraction	0.0─0.5
soiltemp(i),i=1,core	Initial temperature of each soil layer	K	270─300
iceprop(i),i=1,core	Initial proportion of water in each layer in ice	Fraction	0-1
rootfrac(i),i=1,core	Fraction of total root biomass in each soil layer	Fraction	0-1
rootl	Number of rooted layer (starting from the top)	N/A	1─20
rootbiomass	Total root biomass	g biomass m^{-2} ground	100─2000
Sandpc	% sand in soil layers	%	10─50
claypc	% sclay in soil layers	%	10─50
rootrad	Fine root radius	m	0.0005
draincheck	Fraction of porosity above which gravitational drainage occurs	Fraction	0.5─0.7
snowweight	Initial total snow weight	Kg m^{-2}	0+
snowheight	Initial snow height	m	0+

Table 11 Soil parameters (used by the offline SPA model and CAB model)

Parameter	Explanation	Units	Typical values
t1	Decomposition rate constant	-	$1x10^{-6}$ – 0.01
t2	Autotrophic respiration as a fraction of GPP	-	0.2 – 0.7
t3	Fraction of NPP allocated to foliage	-	0.01 – 0.5
t4	Fraction of NPP allocated to fine roots	-	0.01 – 0.5
t5	Turnover rate of foliage	-	$2x10^{-4}$ – 0.02
t6	Turnover rate of woody matter	-	$2x10^{-6}$ – 0.02
t7	Turnover rate of fine roots	-	$2x10^{-4}$ – 0.02
t8	Mineralization rate of fresh litter	-	$5x10^{-5}$ – 0.05
t9	Mineralization rate of soil organic matter and woody debris	-	$1x10^{-6}$ – 0.05
Cf	Foliage	g C m^{-2}	30 - 70
Cw	Wood (stems and coarse roots)	g C m^{-2}	750 – 900
Cr	Fine roots	g C m^{-2}	50 – 300
Clit	Fresh foliar and fine root litter	g C m^{-2}	20 – 3000
CSOM	Soil organic matter plus woody debris	g C m^{-2}	6000 - 10000

Table 12: DALEC (respiration) parameters (used by the offline SPA model and CAB, which uses the file generated automatically by the offline SPA model)

	Explanation	**Units**	**Typical values**
daynum	Decimal time	Days	1 - 365
laitree	Total LAI	$m^2 m^{-2}$	0 - 10
rootbiomass	total root biomass	g m-2 GA	0+
totn	total canopy N	g N m-2 GA	0 - 20

Table 13:: Phenology parameters (used by the offline SPA model and CAB model)

Parameter	Explanation	Units	Typical values
IFCRI	Cloud radiation interaction flag	-	0 - 1
IFCLD	Flag for cloud diffusivity	-	0 - 1
DELTAT	Base time step	sec	60 - 480
TEND	Model run length	hr	24 - 168
PSdoy	Day of the year	-	1 - 365
SLA	Latitude		-90 - 90
SLO	Longitude		-180 - 180
TZONE	Timezone		-12 - 12
ZO	Momentum Roughness length	m	0 - 2
Z0H	Heat roughness length	m	0 – 0.2
ZDO	Displacement height of vegetation	m	0 - 20
MO	Month	-	1 - 12
DY	Day	-	1 - 31
TIMEIS	Start time	hrs	0
PSFC	Surface pressure	Pa	< ~101,325
CLC	Fractional cloud cover	-	0 - 1
PRECIP_EVENTS	Number of precipitation events	-	0 -
PRST	Start of precipitation event	hrs	0 -
PREND	Duration	hrs	0 -
PRCIP	Rate	kg/m2/s	0 - 0.002
NUG	No. of Geostropic wind obs.	-	2
UGI	u component	m/s	-10 – 10
VGI	v component	m/s	-10 - 10
TGI	Observation time	hr	-
MZ1	Number of input levels	-	20 - 24
IWUNIT	To use "m/s" (instead of mb/hr) unit for input "w", set "iwunit"=1	-	1 or 0
DZ	Height (m)	m	Range (0-10000)
UNM	U component (m s-1)	m/s	-40 - 40
VNM	v component (m s-1)	m/s	-40 - 40
VERTM	Vertical velocity ()	m/s or mb/hr	-0.02 – 0.02
RNM	Air temp.	C	-50 - 40
QNM	Water mixing ratio	g/kg	0 – 8
TRNM	CO2	ppm	300 – 400

Table 14: PBL model input parameters (used by the CAB model).

File name	Called in SR	Time step	Output	Model
Daily.csv	DATOUT	daily	Daily GPP, water fluxes, hydraulic parameters	SPA
Daily_DALEC.csv	DATOUT	Daily	The respiration parameter file for the CAB model	SPA
Drivers.csv	DATOUT	daily	Summarises meteorological and vegetation drivers	SPA
Hourly.csv/ Hourly CAB.csv	DATOUT	SPA: 60 or 30 min CAB: every call of SPA	Photosynthesis, leaf respiration, evaporation and transpiration	SPA/CAB
Energy.csv	SOILDAY ('outt' switch)	SPA: 60 or 30 min CAB: every call of SPA	Soil surface energy balance and soil surface temperature	SPA/CAB
Solar.csv	SOLAR	60 or 30 minutes	Radiation absorption in each leaf layer	SPA
Soilwater.csv	SOILFUNCTIONS	Daily (default) or 60 or 30 minutes ('outt' switch)	Water fraction in top 15 soil layers, weighted soil water potential	SPA/CAB
Upfrac.csv	SOILFUNCTIONS	Daily	Fraction of total plant water uptake removed from each of top 15 soil layers	SPA
Iceprop.csv	SOILFUNCTIONS	SPA: 60 or 30 min CAB: every call of SPA	Ice proportion of water content in each of top 15 soil layers	SPA/CAB
Parcheck.csv	DATOUT ('outt' switch)	60 or 30 minutes	Checks that calculations in SOLAR match radiation assigned to each leaf in CANOPY	SPA
Soiltemp.csv	SOILFUNCTIONS	SPA: 60 or 30 min CAB: every call of SPA	Soil temperature in each of top 15 soil layers	SPA/CAB
Waterfluxes.csv	DATOUT	Daily	Water fluxes, and water budget closure calculations	SPA
Soilstatus.csv	SOILDAY ('outt' switch)	SPA: 60 or 30 min CAB: every call of SPA	Detailed water fluxes and water budget closure calculations	SPA/CAB
l1.csv (…l10.csv)	ASSIMILATE ('outt' switch)	60 or 30 minutes	Detailed leaf level diagnostics – stomatal conductance, photosynthesis, leaf water potential, absorbed radiation, temperature, for each canopy layer (numbered by file name)	SPA
PBL_met_data.csv	SPinterface	every call of SPA	The meteorology generated for the SPA model. Including NEE, LE CO_2 (ppm) and GPP	CAB
Pbl_out.csv	PRINT	Hourly	Characteristics of the PBL	CAB

Table 15: Output files from the offline SPA model and the CAB model.

10 References

Brost, R. A., and J. C. Wyngaard (1978), A Model Study of the Stably Stratified Planetary Boundary-Layer, *Journal of the Atmospheric Sciences*, *35*, 1427-1440.

Buck, A. L. (1981), New Equations for Computing Vapor-Pressure and Enhancement Factor, *Journal of Applied Meteorology*, *20*, 1527-1532.

Businger, J. A., et al. (1971), Flux-Profile Relationships in Atmospheric Surface Layer, *Journal of the Atmospheric Sciences*, *28*, 181-&.

Campbell, G. S. (1985), *Soil physics with BASIC : transport models for soil-plant systems*, xvi,150p. pp., Elsevier, Amsterdam ; Oxford.

Deardorf.Jw (1966), Counter-Gradient Heat Flux in Lower Atmosphere and in Laboratory, *Journal of the Atmospheric Sciences*, *23*, 503-&.

Deardorf.Jw (1972), Parameterization of Planetary Boundary-Layer for Use in General Circulation Models, *Monthly Weather Review*, *100*, 93-&.

Jones, H. G. (1992), *Plants and microclimate : a quantitative approach to environmental plant physiology*, 2nd ed., xxiv, 428 p. pp., Cambridge University Press, Cambridge [England] ; New York.

Mahrt, L., and H. Pan (1984), A 2-Layer Model of Soil Hydrology, *Boundary-Layer Meteorology*, *29*, 1-20.

Mailhot, J., and R. Benoit (1982), A Finite-Element Model of the Atmospheric Boundary-Layer Suitable for Use with Numerical Weather Prediction Models, *Journal of the Atmospheric Sciences*, *39*, 2249-2266.

Nemati, M. R., et al. (2002), Determining air entry value in peat substrates, *Soil Science Society of America Journal*, *66*, 367-373.

Pan, H. L., and L. Mahrt (1987), Interaction between Soil Hydrology and Boundary-Layer Development, *Boundary-Layer Meteorology*, *38*, 185-202.

Press, W. H. (1986), *Numerical recipes : the art of scientific computing*, xx,818p. pp., Cambridge University Press, Cambridge.

Priestley, C. H. B., and W. C. Swinbank (1947), Vertical Transport of Heat by Turbulence in the Atmosphere, *Proceedings of the Royal Society of London Series a-Mathematical and Physical Sciences*, *189*, 543-561.

Saxton, K. E., et al. (1986), Estimating Generalized Soil-Water Characteristics from Texture, *Soil Science Society of America Journal*, *50*, 1031-1036.

Troen, I., and L. Mahrt (1986), A Simple-Model of the Atmospheric Boundary-Layer - Sensitivity to Surface Evaporation, *Boundary-Layer Meteorology*, *37*, 129-148.

Williams, M. (2005), The Soil-Plant-Atmosphere model: Manual, version 1.2, April 2005, edited, p. 32, University of Edinburgh.

Williams, M., et al. (1996), Modelling the soil-plant-atmosphere continuum in a Quercus-Acer stand at Harvard forest: The regulation of stomatal conductance by light, nitrogen and soil/plant hydraulic properties, *Plant Cell and Environment*, *19*, 911-927.

Williams, M., et al. (2005), An improved analysis of forest carbon dynamics using data assimilation, *Global Change Biology*, *11*, 89-105.